July 2007
Research Report: UCPRC-RR-2007-12

Acoustical Absorption of Open-Graded, Gap-Graded, and Dense-Graded Asphalt Pavements

Authors:

A. Ongel and E. Kohler (UCPRC) and J. Nelson (WIA)

Work Conducted Under the Quiet Pavement Research Program as Part of Partnered Pavement Research Center Strategic Plan Element No. 4.16: Investigation of Noise, Durability, Permeability and Friction Performance Trends for Asphaltic Pavement Surface Types

PREPARED FOR:

California Department of Transportation
(Caltrans)
Division of Research and Innovation

PREPARED BY:

University of California
Pavement Research Center
Davis and Berkeley

DOCUMENT RETRIEVAL PAGE	**Research Report No.:** UCPRC-RR-2007-12

Title: Acoustical Absorption of Open-Graded, Gap-Graded, and Dense-Graded Asphalt Pavements

Authors: A. Ongel and E. Kohler (UCPRC) and J. Nelson (WIA)

Prepared for:	**FHWA No.:**	**Date Work Submitted:**	**Date:**
California Department of Transportation, Division of Research and Innovation, Office of Roadway Research	CA111200A	October 31, 2007	July 2007

Strategic Plan Element No.:	**Status:**	**Version No.:**
4.16	Stage 6 final	1

Abstract:
This report presents results of acoustical absorption measured on asphalt pavement samples. The tests were performed on 76 highway pavement sections and characterized the acoustical absorption at the center of the lane and under one of the wheelpaths (nontrafficked and trafficked areas of the lane, respectively). This document presents the absorption coefficients and resonance frequencies for different types of pavements, an analysis of the measured absorption coefficients, and the correlation of the absorption coefficients with measured tire/pavement noise levels. The acoustical absorption of the asphalt cores was measured with an impedance tube that allowed measurement between 200 and 1,700 Hz. The pavement in the study consists of mostly four types of asphalt concrete: dense graded, open graded, rubberized open graded, and gap graded. The study also included a limited number of sections with other asphalt mixes.

The study confirmed that greater acoustical absorption is obtained from pavements with high air-void content. It showed that the open-graded mixes have higher absorption values than gap- and dense-graded mixes. For both the center and wheelpath, the open-graded mixes showed an average absorption coefficient of about 0.20; this parameter for gap- and dense-graded mixes was approximately 0.04. Average absorption is an increasingly better predictor of tire/pavement noise levels at higher frequencies, with a correlation coefficient of 66 percent at 1,600 Hz.

Keywords: quiet pavements, tire/pavement noise, asphalt mixes, acoustical impedance, impedance tube, On-Board Sound Intensity

Proposals for Implementation:
None

Related Documents:

- Surface Condition and Road-Tire Noise on Caltrans Experimental Noise-Reducing Pavement Sections, UCPRC-RR-2006-10.
- Investigation of Noise, Durability, Permeability, and Friction Performance Trends for Asphaltic Pavement Surface Types: First- and Second-Year Results, UCPRC-RR-2007-03.

Signatures

A. Ongel **First Author**	E. Kohler **Technical Review**	D. Spinner **Editor**	J. T. Harvey **Principal Investigator**	T. J. Holland **Caltrans Contract Manager**

DISCLAIMER

The contents of this report reflect the views of the authors who are responsible for the facts and accuracy of the data presented herein. The contents do not necessarily reflect the official views or policies of the State of California or the Federal Highway Administration. This report does not constitute a standard, specification, or regulation.

PROJECT OBJECTIVES

This research project is part of the California Department of Transportation (Caltrans) Quieter Pavement Research (QPR) Work Plan. The central purpose of this research is to support the QPR program with goals and objectives that address identification of asphalt pavement surfaces that are both quieter and safer.

The research conforms with Federal Highway Administration (FHWA) guidance provided to state departments of transportation (DOTs) that conduct tire/pavement noise research. Results from this research are intended to identify best practices for selecting asphaltic surfaces on the basis of performance trends identified from field measurements for noise, permeability, friction, and durability.

The objective of the work described in this document was to determine the acoustic absorption of pavement samples and correlate the results with tire/pavement noise measurements conducted at exactly the same sections from which the samples were obtained

ACKNOWLEDGMENTS

The work included in this report was funded by the California Department of Transportation, Division of Research and Innovation. The technical advisor from the Pavement Standards Team was Bill Farnbach, from the Office of State Pavement Design. The authors would like to thank Bruce Rymer, from the Caltrans' Division of Environmental Analysis and Linus Motumah, project coordinator of Caltrans Quieter Pavement Research. The laboratory work was conducted with assistance of personnel from Wilson, Ihrig & Associates, in Oakland, California, under the supervision of Dr. James Nelson, who developed the testing capability of sound absorption on pavement cores.

EXECUTIVE SUMMARY

This report presents results of acoustical absorption measured on asphalt pavement samples. This work was performed as part of Partnered Pavement Research Center (PPRC) Strategic Plan Element 4.16, titled "Investigation of Noise, Durability, Permeability, and Friction Performance Trends for Asphaltic Pavement Surface Types." The tests were performed on 76 highway pavement sections and characterized the acoustical absorption at the center of the lane and under one of the wheelpaths (nontrafficked and trafficked areas of the lane). The samples were four-inch diameter cores obtained by the University of California Pavement Research Center (UCPRC) as part of the project aimed at characterizing the durability and surface properties of the flexible pavements used by the California Department of Transportation (Caltrans) on the state highway network.

This document presents the absorption coefficients and resonance frequencies for different types of pavements, an analysis of the measured absorption coefficients, and the correlation of the absorption coefficients with measured tire/pavement noise levels. The acoustical absorption of the asphalt cores was measured with an impedance tube developed jointly by Wilson Ihrig & Associates, Inc. (WIA), and the UCPRC. The experimental setup allowed for reliable measurement of absorption at frequencies between 200 and 1,700 Hz. The maximum (peak) absorption coefficients are reported for each pavement core, as well as average absorption over the range of frequencies evaluated.

Acoustical absorption results were correlated with tire/pavement noise levels obtained as part of the larger project using the California On-Board Sound Intensity (OBSI) method. The pavements in the study are mostly four types of asphalt concrete: dense graded (DGAC), open graded (OGAC), rubberized open graded (RAC-O), and rubberized gap graded (RAC-G). A limited number of sections with other asphalt mixes were also included, and they are part of a list of experimental sections set up by the Caltrans Division of Environmental Analysis. The age of most of the pavement sections ranged between 1 and 8 years. The sections are generally balanced with respect to traffic and rainfall levels and come from various regions of the state.

The study confirmed that greater acoustical absorption is obtained from pavements with high air-void content. It showed that the open-graded mixes have higher absorption values than the gap and dense-graded mixes. For both the center and wheelpath, the open-graded mixes showed an average absorption coefficient of about 0.20; this parameter for gap- and dense-graded mixes was approximately no more than 0.04. In terms of peak absorption, that is, the maximum over the range of frequencies as opposed to the average coefficient, only about one-third of the measured samples showed peak absorption greater than 0.10. Many sections did not show a peak at all, meaning that the curve of absorption coefficient versus frequencies was flat.

The relationship between sound absorption at the wheelpath and the overall tire/pavement noise levels was investigated. The study found that increased absorption reduces the sound intensity levels for dense- and gap-graded mixes, but for open-graded mixes overall tire/pavement OBSI noise levels do not seem to be affected by changes in the absorption values. The study of the effect of absorption on tire noise at specific frequencies revealed that higher average absorption is correlated with reduced tire/pavement noise levels starting at 630 Hz for gap- and dense-graded mixes. For both open-graded mixes, a higher absorption does not reduce noise levels at low frequencies, but for frequencies above 1,000 Hz the noise levels become lower if absorption increases, and this correlation becomes increasingly stronger for the third-octave bands at 1,000, 1,250, and 1,600 Hz. This finding is interpreted to mean that absorption reduces high-frequency tire noise, but does not benefit low-frequency noise. In fact, low-frequency noise is greater on those pavements that offer greater absorption because they are open graded and therefore have surface textures that are responsible for higher levels of low-frequency noise.

TABLE OF CONTENTS

LIST OF TABLES

LIST OF FIGURES

ABBREVIATIONS AND TERMS USED IN THE TEXT

BWC	Bonded wearing course
Caltrans	California Department of Transportation
CSV	Comma-separated values
DGAC	Dense-graded asphalt concrete
DOT	Department of transportation
ES	Environmental section
FHWA	Federal Highway Administration
MPD	Mean profile depth
NMAS	Nominal maximum aggregate size
OBSI	On-board Sound Intensity
OGAC	Open-graded asphalt concrete
QP	Quieter pavements section
QPR	Quieter Pavement Research
RAC-G	Rubberized asphalt concrete, gap gradation
RAC-O	Rubberized asphalt concrete, open gradation
UCPRC	University of California Pavement Research Center
WIA	Wilson Ihrig & Associates, Inc.

1 INTRODUCTION

This report presents results of a study of acoustical absorption measured on asphalt pavement samples. This work was performed as part of Partnered Pavement Research Center (PPRC) Strategic Plan Element 4.16, titled "Investigation of Noise, Durability, Permeability, and Friction Performance Trends for Asphaltic Pavement Surface Types." This study was conducted as part of the Quieter Pavement Research (QPR) Program of the California Department of Transportation (Caltrans). The pavement cores were collected from the field as part of PPRC SPE 4.16. The purpose of PPRC SPE 4.16 is to provided a preliminary characterization of the durability and surface properties of the flexible pavements used by Caltrans on the state network.

Pavement cores were collected by the University of California Pavement Research Center (UCPRC), and the acoustical absorption data was measured at the laboratory of Wilson, Ihrig & Associates, Inc. (WIA). This document presents the maximum absorption coefficients and resonance frequencies for different types of pavements, an analysis of the measured absorption coefficients, and the correlation of the absorption coefficients with measured tire/pavement noise levels. The acoustical absorption of the asphalt cores was measured at the WIA laboratory in Oakland using an impedance tube developed jointly by WIA and UCPRC. Initial testing was conducted by WIA, which established the measurement procedure; subsequent tests and analysis of the results were conducted by UCPRC.

The tests were performed on a total of 75 highway pavement sections and characterized the acoustical absorption using two drilled cores: one from the center of the lane, where little wheel traffic is expected, and the other from directly under one of the wheelpaths.

Acoustical absorption results are correlated in this report with tire/pavement noise levels obtained as part of the larger project. The California On-Board Sound Intensity (OBSI) method was used to measure tire/pavement noise.

The specific objectives of this study are to:

- Determine and compare the absorption coefficients of different asphalt pavement types
- Correlate the acoustical absorption values with the tire/pavement noise

Two sets of pavement sections are included in this work.

2 METHODOLOGY

2.1 Background on Acoustical Absorption

When a sound wave strikes an acoustical material, it causes the particles that make up the material to vibrate, and this vibration results in friction, generating a small amount of heat, which the material absorbs. Therefore, when a wave hits an acoustical material, some of the acoustic energy is reflected, and the rest is converted to heat and absorbed. Sound absorption is defined as the energy that is not reflected by the material.

When sound waves hit a porous material, the waves travel through the air paths in the material, and sound energy is dissipated by frictional and viscous losses in the pores and the vibration of the small particles of the material (1).

The acoustic absorption coefficient of a material represents the proportion of acoustic energy not reflected by the surface of the material for a normal incidence plane wave. The absorption coefficient, α, can be calculated from the acoustic impedance, Z, of the surface using Equation 1 (2).

$$\alpha = 1 - \frac{|Z - \rho c|^2}{|Z + \rho c|^2}, \qquad (1)$$

where

ρc = characteristic air impedance,

c = speed of sound,

ρ = density of air, and

Z = ratio of sound pressure acting on the surface of the material to the particle velocity normal to the surface.

Acoustical properties of porous structures are characterized using either phenomenological or microstructural models. The microstructural model considers that sound propagation occurs in straight pores and then accounts for tortuosity of the pores using shape factors. The phenomenological model considers the porous medium to be a globally compressible fluid where dissipations occur (3). The microstructural model uses the specific air-flow resistance (R_s), porosity, tortuosity or shape factor, and viscous and thermal shape factors, while the phenomenological model uses only specific air-flow resistance, porosity, and tortuosity to characterize the porous medium. Berengier (4) showed that the two models are in close agreement for the case of porous pavements. However, the phenomenological model was found to provide a simpler description using specific air-flow resistance, porosity, and tortuosity for predicting the acoustical absorption properties of pavements (5).

Specific air-flow resistance is the frictional resistance to flow through the pores. Increasing specific air-flow resistance reduces the maximum absorption coefficient and tends to flatten the absorption curves. The total air-flow resistance (R_T) is calculated as indicated in Equation 2, where e is the thickness (in meters) of the pavement surface layer:

$$R_T = R_s \times e \qquad (2)$$

Thickness has an effect on both the shape of the absorption curve and the frequencies at which the maxima occurs. Increasing thickness increases the absorption coefficient and lowers the frequencies where the maxima occur. However, after a certain thickness, called superthickness, further increases in thickness have no effect on the absorption coefficient. The superthickness value depends on other parameters such as porosity, specific air-flow resistance, and shape factor. Berengier et al. (4) reported that for a porous medium with a porosity of 25 percent, shape factor of 3.5, and specific air-flow resistance of 20 rayls/cm, the superthickness would be 47 cm. Porosity is the ratio of the volume of connected pores to the total volume. For low values of $R_s \times e/2\rho c$, the porosity has no effect on the maximum absorption values and no effect on the frequencies at which the maxima occur. However, higher porosity increases the absorption values between the maximum values. For very large $R_s \times e/2\rho c$ values or at superthickness, increasing porosity increases the maximum absorption values. The shape factor, or tortuosity, takes into account the air paths not following the normal direction. For moderately high values of $R_s \times e/2\rho c$, the shape factor has almost no influence on the maximum values. An increase in the shape factor narrows the width of the curves and decreases the minimum values of absorption (4).

2.2 Measurement of Acoustical Absorption

Acoustical absorption measurements were conducted using a Bruel & Kjaer Type 4206A impedance tube with two Bruel & Kjaer Type 4187 ¼-inch condenser microphones and Bruel & Kjaer Type 2670 preamplifiers. This device has a 100-mm-diameter (internal diameter) tube with an acoustic driver and microphones and a 63.5-mm sample holder. For testing the pavement cores, the Bruel & Kjaer 100-mm-diameter impedance tube was fitted with custom sample holders ranging in diameter from 101.5 to 104.5 mm to accommodate cores of different diameters and long cores with irregular profiles.

An acoustic gel (a material also used as a surgical lubricant) was employed to fill the annulus between the core and the sample holder wall. The gel was chosen rather than an oil-based grease, Vaseline, or cold cream, because the gel could be easily washed off without leaving a residue, thus preserving the core for further testing. The bottom sections of the cores were considered to be impervious, so the piston seal at the end of the

impedance tube was not employed for testing. However, the rear surfaces of the cores were sealed with the gel as an added precaution. None of the cores tested appeared to conduct air.

The test was performed according to ASTM E-1050-98, for measuring acoustical absorption with an impedance tube using the two-microphone method. Transfer functions were measured with a Larson Davis Model 2900 analyzer, and results were transferred to a desktop computer with Larson Davis' software. The comma-separated values (CSV) files containing the transfer functions were imported into *Excel* spreadsheets, from which the transfer functions were copied and pasted into a custom spreadsheet for computation of absorption spectra. Figure 1 shows the impedance tube, microphones, analyzer, and speaker.

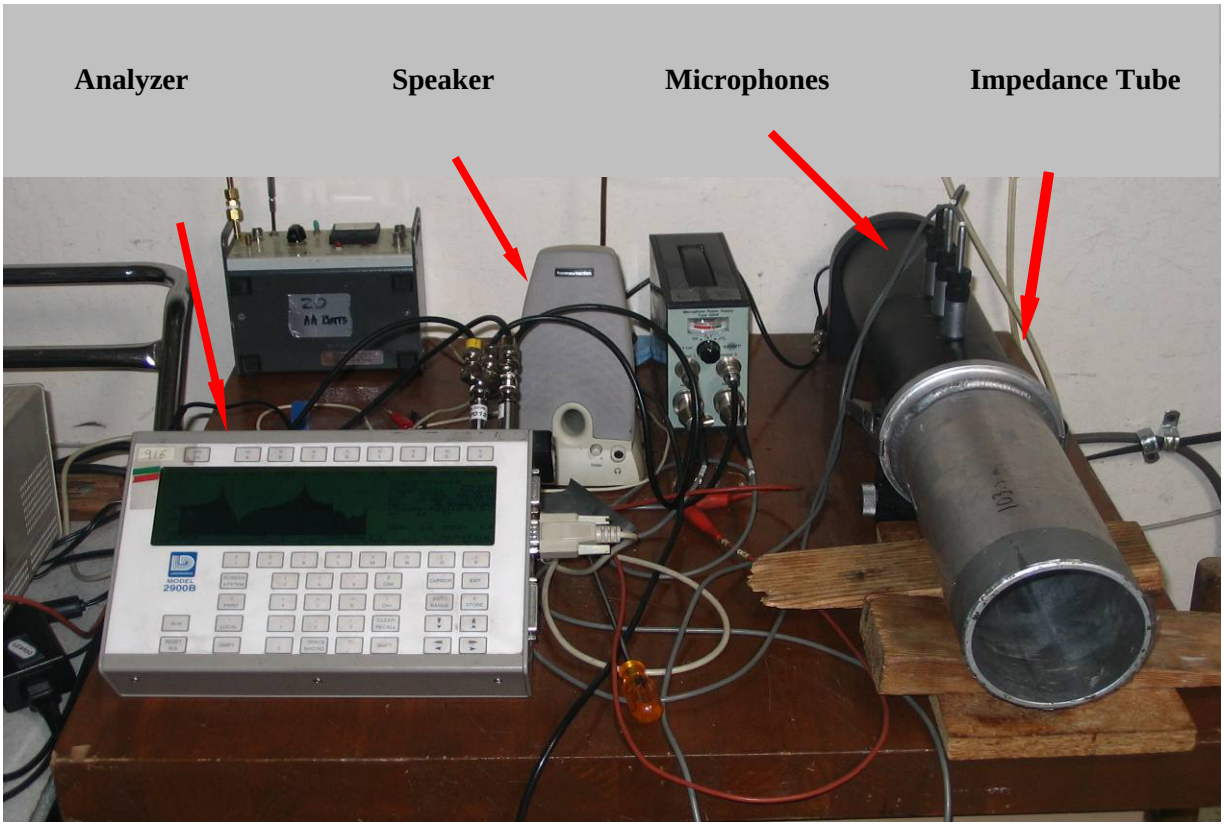

Figure 1: Impedance tube system.

Initially, a calibration sample was used to adjust the test system for each test specimen. Later, two transfer functions were obtained for each core: one for the forward microphone orientation, and the other for the reverse microphone orientation. These functions were then used to self-calibrate each test result, with the forward transfer function used to obtain the main data sample. Thus, temperature and barometric conditions were consistent during each test, and some minor improvement was obtained for the test results. The process still follows ASTM E-1050-98.

During each test, an acoustical absorptive material was placed between the acoustic driver and microphones to help reduce resonances within the tube. The absorptive material was too close to the microphones during some of the early tests and was later moved farther to the rear, toward the acoustic driver. This adjustment also improved the low-frequency performance of the tube.

Temperature and barometric pressure were collected during each test. Temperature was measured with a scientific mercury thermometer, and barometric pressure was measured with a Bruel & Kjaer barometer used during calibration of the microphones. Temperature and barometric pressure had only a marginal effect on absorption over the range considered. All tests were conducted at room temperature, ranging from about 68 to 75°F. Barometric pressures were reasonably constant, as is typical in the San Francisco Bay Area. The microphones were calibrated using a Bruel & Kjaer Piston Phone Type 4220.

2.3 Air-Void Content (Porosity)

Air-void content values were obtained by UCPRC for all the sections of the experiment, separately for the center of the lane and the wheelpath. The air-void content values reported in this document were obtained using approximately four cores from the center and four cores from the wheelpath from the same pavement sections where the absorption cores were obtained. The cores used for determination of air-void content were six-inch-diameter cores and had to be destroyed as part of the test, whereas for absorption testing the cores were four inches in diameter and were preserved. Air-void content was calculated using the bulk specific gravity (G_{bulk}) and maximum theoretical specific gravity ($G_{\max}$) values. The first value was obtained using the CoreLok® method, and the second was obtained by applying Caltrans test method CT 309. The air-void content was then calculated according to the formula in Equation 3:

$$AirVoid\_(\%\_by\_Volume) = \frac{G_{\max} - G_{bulk}}{G_{\max}} \times 100 \qquad (3)$$

Note that the calculated air-void content does not necessarily correspond to the connected air-void content. In addition to air-void content, the thicknesses of the pavement layers were measured in the laboratory. However, the other parameters, such as specific air-flow resistivity and tortuosity of the cores, are not known.

2.4 Tire/Pavement Noise

Tire/pavement noise measurements were conducted on the pavement sections from which the cores were taken. The measurements were conducted using the California OBSI method, which calls for a preferred test speed of 60 mph and uses microphones at the leading and trailing edges of the tire's contact patch. The sections were

almost 500 feet long. The test vehicle including the microphone setup is shown in Figure 2. The details of how the tire/pavement noise was collected are not included here but can be found elsewhere (5).

Figure 2: Instrumented vehicle and microphone setup for measuring tire/pavement noise.

3 PAVEMENT SECTIONS IN THE STUDY

3.1 Sections Evaluated for Sound Absorption

Absorption tests were performed on 76 highway pavement sections to characterize the acoustical absorption at the center of the lane and at one of the wheelpaths. A total of 71 sections (142 pavement cores) had tests performed on cores from the center and a wheelpath. In five other sections the results were obtained from cores that were either from the center of the lane or the wheelpath (6 pavement cores). This information is detailed in Table 1, along with records from replicate tests. As explained in the introduction, two sets of pavement sections are included in this work: environmental sections (ES) and quieter pavement (QP) sections (which include sections labeled N).

Table 1: Number of Absorption Tests on Center and Wheelpath Cores

	Source of Pavement Core		
	Center	**Wheelpath**	**Total Cores**
Number of typical ES sections	18	18	36
Number of typical QP and N sections	53	53	106
Total number of typical center and wheelpath cores tested			142
Additional results			
Section QP05	2	-	2
Section QP12	1	-	1
Section QP44	1	-	1
Section QP51	-	1	1
Section N467	-	1	1
Total number of original cores tested			148
Replicates			
Section QP11		1	1
Section QP13	4		4
Section QP20	2		2
Total tests reported			155

3.2 Properties of Pavement Sections

As mentioned before, two sets of pavement sections are included in this work: ES and QP sections. The pavement types in the ES sections were selected by the Caltrans Division of Environmental Analysis, and projects were especially built to compare the durability and noise properties of new pavement types with those of the pavement types commonly used in California, including open-graded, rubberized gap-graded, and dense-

graded mixes. The pavement types in the QP sections are what Caltrans typically uses in construction and rehabilitation of highways. They can be categorized as open-graded, gap-graded, and dense-graded asphalt mixes, depending on the intended levels of porosity. The naming conventions for mix types are as follows:

- OGAC: Open-graded asphalt concrete
- DGAC: Dense-graded asphalt concrete
- RAC-O: Rubberized asphalt concrete, open gradation
- RAC-G: Rubberized asphalt concrete, gap gradation

Other less conventional types of mixes are explained where necessary.

Table 2 provides some basic information about the pavement sections in the study:

- Section ID: Identifier given by UCPRC to each section
- Section location: District, county, route, direction, and post-mile
- Pavement type: Type of asphalt mixture
- Construction date: Approximate date of paving
- OBSI-Aquatred: On-Board Sound Intensity measured with an Aquatred tire
- MPD: Mean profile depth, used to express pavement macrotexture
- NMAS: Nominal maximum aggregate size, corresponding to 3/8, 1/2, and 3/4 inch

Additional information about the ES and QP sections is available from other related documents (5, 6), including information about traffic and rainfall levels, coring scheme, and measured pavement properties such as surface friction, permeability, and aggregate gradation. Only partial information is available for some of the sections, and not every section listed in Table 2 was evaluated for absorption, but all are included here for completeness of the table.

Table 2: Locations and Other Properties of the Pavement Sections in the Study

Section ID	Section Location	Pavement Type	Construction Date	OBSI-Aquatred in dB(A)	MPD (mm)	NMAS (mm)
ES01	07LA138E16.4	OGAC	5/2/2002	100.2	0.92	12.5
ES02	07LA138W17.2	OGAC	5/2/2002	102.1	0.80	9.5
ES03	07LA138E17.2	OGAC	5/2/2002	100.5	0.86	12.5
ES04	07LA138W18.9	OGAC	5/2/2002	102.4	0.79	12.5
ES05	07LA138E18.9	RAC-O	5/2/2002	101.6	0.70	12.5
ES06	07LA138W20.2	RAC-O	5/2/2002	102.5	0.61	12.5
ES07	07LA138E20.6	BWC	5/2/2002	103.8	0.58	12.5
ES08	07LA138W20.6	BWC	5/2/2002	103.8	0.69	12.5
ES09	07LA138W20.9	DGAC	5/2/2002	104.0	0.59	12.5
ES10	07LA19N3.4	EU GG	5/2/2005	101.9	0.82	12.5
ES11	03YOL80W4.8	OGAC	6/1/1998	105.1	1.02	9.5
ES12	06FRE33N71.1	RAC-G	6/4/2004	103.1	0.61	19
ES13	06FRE33N71.5	RAC-G	6/4/2004	103.2	0.65	12.5
ES14	06FRE33N71.7	RUMAC-GG	6/4/2004	103.9	0.53	19
ES15	06FRE33N72.6	RUMAC-GG	6/4/2004	103.7	0.65	12.5
ES16	06FRE33N72.8	Type G- MB	6/4/2004	104.4	0.36	19
ES17	06FRE33N73.7	Type G- MB	6/4/2004	104.3	0.30	19
ES18	06FRE33N73.9	Type D- MB	6/4/2004	104.4	0.45	19
ES19	06FRE33N74.8	Type D- MB	6/4/2004	104.7	0.51	19
ES20	06FRE33N74.9	DGAC	6/4/2004	103.8	0.49	19
ES21	04SM280N6.2	RAC-O	9/2/2002	102.0	1.21	12.5
ES22	03SAC5S17.7	RAC-O	6/4/2004	100.9	0.78	12.5
ES23	03SAC5N16.6	RAC-O	6/4/2004	101.8	0.85	12.5
QP01	07LA710S6.0	RAC-O	9/1/2003	102.8	0.78	12.5
QP02	04MRN101N20.2	RAC-G	10/1/2001	103.0	0.72	12.5
QP03	04MRN37W14.2	OGAC	10/1/2000	102.6	1.21	12.5
QP04	04SON121E4.2	OGAC	1/2/2002	100.8	1.18	12.5
QP05	04MRN101S7.9	RAC-G	7/1/1997	104.4	1.07	12.5
QP06	06FRE99N12.8	DGAC	10/5/2005	103.9	0.53	19
QP07	06KER99S31.0	DGAC	10/1/2001	106.1	0.69	12.5
QP08	03SAC50E16.3	RAC-O	3/1/2001	101.0	1.22	12.5
QP09	04SM280S10.0	DGAC	10/2/2000	103.8	0.76	12.5
QP10	07VEN34W5.9	RAC-G	11/1/2000	104.3	0.89	19
QP11	07LA60E26.3	DGAC	3/1/1999	104.5	0.65	19
QP12	08SBD58E4.2	RAC-O	12/1/2000	102.3	1.35	9.5
QP13	08SBD38E2.2	OGAC	7/1/2001	102.5	1.29	12.5
QP14	08RIV15S33.7	RAC-G	6/1/2001	103.6	0.85	12.5
QP15	07LA138E61.3	DGAC	9/5/2005	103.3	0.64	12.5
QP16	04ALA92E7.7	DGAC	10/1/1992	104.9	1.06	12.5
QP17	10AMA49S16.4	RAC-O	11/2/2002	104.2	1.29	9.5
QP18	10CAL4W15.6	RAC-G	1/1/2000	105.3	1.47	12.5
QP19	05SLO46W21.0	RAC-G	10/1/2001	102.3	0.76	12.5

Section ID	Section Location	Pavement Type	Construction Date	OBSI-Aquatred in dB(A)	MPD (mm)	NMAS (mm)
QP20	05SCr152E7.9	OGAC	10/5/2005	104.2	1.25	12.5
QP21	03ED50W17.3	DGAC	10/4/2003	105.0	1.01	19
QP22	04SCl237E2.2	OGAC	10/1/1998	104.8	1.62	12.5
QP23	04SCl237E3.8	OGAC	5/1/2001	103.0	1.30	12.5
QP24	04SCl85N4.0	RAC-O	5/1/1998	103.3	0.96	12.5
QP25	04CC680S24.3	DGAC	10/1/1998	106.1	0.77	19
QP26	04SCl280N1	RAC-G	10/5/2005	101.7	0.80	12.5
QP27	03PLA80E21.7	DGAC	5/6/2006	103.1	0.63	19
QP28	04MRN101S2.2	OGAC	3/2/2002	101.6	1.05	12.5
QP29	03SAC16E13.0	OGAC	11/1/1998	103.8	1.30	9.5
QP30	03ED50W20.1	DGAC	10/2/2002	106.2	0.83	9.5
QP31	04SON1N1.0	RAC-G	1/1/2001	103.9	0.63	12.5
QP32	04NAPA128E6.1	RAC-O	3/1/1998	103.0	1.07	12.5
QP33	06TUL63N20.2	RAC-G	10/1/2005	100.7	0.72	19
QP34	06TUL63N22.6	RAC-O	10/1/2005	101.3	0.89	12.5
QP35	06TUL99S42.8	RAC-O	9/5/2005	103.3	1.02	12.5
QP36	04CC680S23.3	RAC-O	11/3/2003	100.9	0.99	12.5
QP37	01MEN1E38.4	RUMAC-GG	9/1/2005	103.4	0.77	12.5
QP38	01MEN1E39.1	Type D MB	9/1/2005	104.6	0.43	19
QP39	01MEN20E39.8	RAC-G	9/1/2005	102.9	0.80	12.5
QP40	01MEN20E40.7	DGAC	9/1/2005	104.4	0.41	19
QP41	01MEN20E41.0	RAC-O	9/1/2005	101.6	0.95	12.5
QP42	01LAK29E37.5	RAC-O	10/1/2005	104.8	1.19	12.5
QP43	04SOL113N18.1	DGAC	4/5/2005	103.5	0.57	12.5
QP44	03PLA80E2.8	OGAC	12/1/2005	103.6	1.51	12.5
QP45	03YOL80W0.2	OGAC	11/1/2005	101.0	1.24	9.5
QP46	011SD8E0.7	RAC-G	10/1/2000	102.8	0.82	12.5
QP47	01MEN101N50.8	RAC-O F-mix	9/1/2003	103.6	1.81	19
QP48	01MEN20W21.6	OGAC F-mix	6/1/1998	*	1.64	19
QP49	01MEN20W22.3	OGAC F-mix	6/1/1998	*	1.77	19
QP50	01HUM101N111.7	RAC-O F-mix	8/1/2002	105.6	1.50	19
QP51	03PLA80W16.2	RAC-O	9/19/2006	101.2	1.16	12.5
QP52	01MEN101N40.3	RAC-O F-mix	9/10/2005	104.4	1.54	19
N103	01MEN1N1.5	OGAC	10/4/2000	*	*	9.5
N104	01MEN1N3.6	OGAC	10/4/2000	102.0	*	9.5
N105	01MEN1N3.8	OGAC	10/4/2000	*	*	12.5
N114	01MEN1N22.8	DGAC	10/1/1998	101.6	*	12.5
N121	01MEN1N28.7	DGAC	10/1/1998	101.4	*	12.5
N434	06Kern65N0.3	DGAC	10/1/1999	104.7	0.71	12.5
N436	06Kern65N1.8	DGAC	10/1/1999	*	0.74	12.5
N466	06Tul65S26.5	RAC-O	10/1/2002	100.4	*	9.5
N467	06Tul65S27.4	RAC-O	10/1/2002	101.0	*	9.5
N468	06Tul65S29.1	RAC-O	10/1/2002	*	*	9.5

4 TEST RESULTS AND ANALYSIS OF ACOUSTICAL ABSORPTION VALUES

4.1 General Information on Sound Absorption Results

The result of each sound absorption test is a vector containing the absorption coefficient at frequencies from 0 to 2,000 Hz in 3.125-Hz increments. That is 640 values, each ranging from 0 to 1 depending on the fraction of the sound energy that at any given frequency is reflected back ($\alpha = 0$) or absorbed ($\alpha = 1$). A typical plot of absorption coefficients is shown in Figure 3. This particular plot, which comes from section QP51, shows a clearly defined peak with $\alpha = 0.67$ at a frequency of 1,000 Hz. The frequency at which the maximum absorption occurs is known as the resonant frequency. In some cases the absorption plot is flat, meaning that there is no resonant frequency, while in other cases there are two peaks.

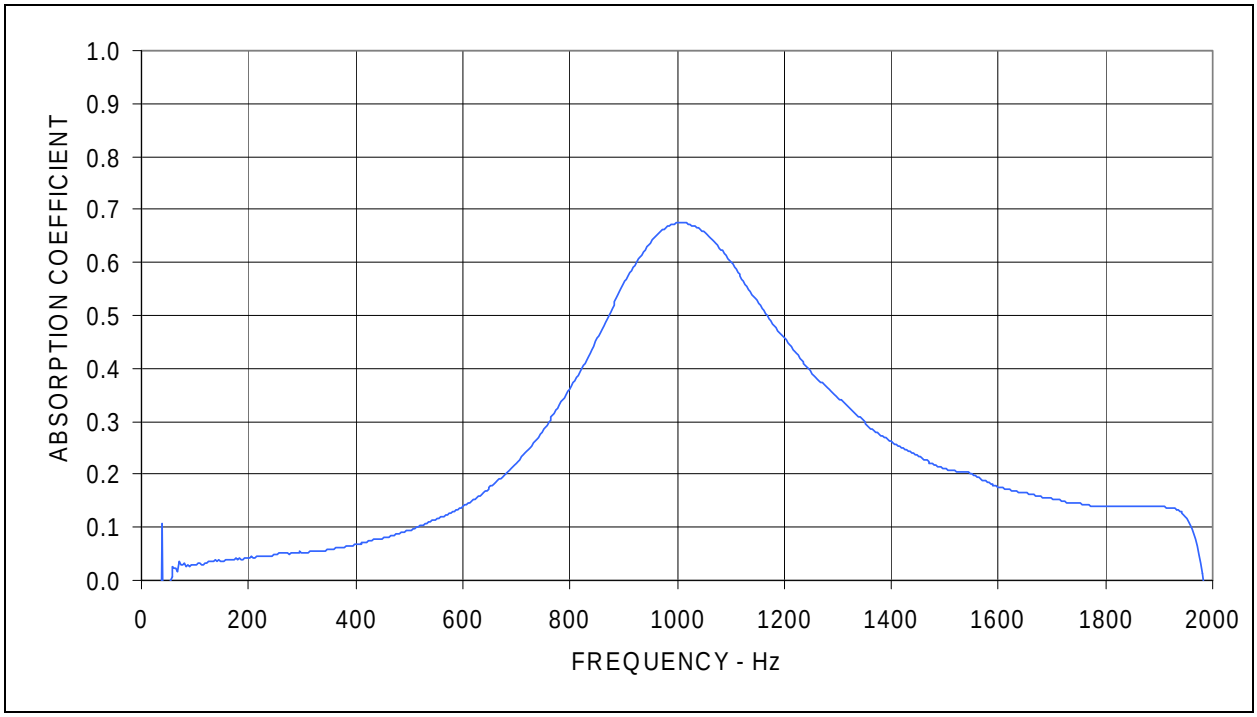

Figure 3: Example of acoustical absorption spectra.

Leakage through the annulus around the pavement core, or blow-by, may have affected some of the test results at frequencies below about 200 Hz, as indicated by an upturn in the absorption spectrum with decreasing frequency in this range. This frequency was below the main frequency range of interest, so this effect was considered acceptable in some cases. Absorption at frequencies below 200 Hz was not included in the calculation of average absorption values.

Given the geometry of the impedance tube used, the absorption results are accurate only up to frequencies around 1,700 Hz, because radial modes may be present beyond this frequency. Nevertheless, the plots were extended to above 2,000 Hz to see the test results at these higher frequencies, as there was some discussion within the research team about extending the procedure beyond the theoretical maximum frequency of the tube.

For the absorption value, the analysis presented here uses the average of the measured absorption between 200 and 1,700 Hz instead of the maximum absorption value, so that absorption effects can be considered at all frequencies.

The analysis of the absorption results presented in the following sections is separated into two parts: environmental sections (ES) and quieter pavement (QP) sections. The ES sites came from a number of long-term studies initiated by the Caltrans Division of Environmental Analysis and the QP sites were selected from several on-going studies being performed by the Office of Pavement Design.

4.2 ES Section Results

Acoustical absorption data for the ES series of cores is summarized in Table 3. The table includes the average and maximum absorption values, along with the resonant frequency, for the wheelpath and the center of the lane. Figure 4 shows the absorption at the center of the lane and at the wheelpath for all ES sections, indicating the first and third quartile and the maximum and minimum absorption values found in the 200 to 1,700-Hz frequency range.

Table 3: Summary of Absorption Results for ES Sections

Section	Center Average (%)	Center Maximum (%)	Center Resonant Frequency (Hz)	Wheelpath Average (%)	Wheelpath Maximum (%)	Wheelpath Resonant Frequency (Hz)
ES01	19	29	740	9	14	1,690
ES03	11	18	330	8	13	290
ES05	14	18	490	6	10	450
ES07	4	7	1,560	6	18	470
ES10	11	16	1,530	10	14	1,560
ES11	24	55	1,330	23	61	1,630
ES12	6	9	210	3	5	1,550
ES13	8	11	330	3	5	1,560
ES14	2	3	1,660	5	6	1,120
ES15	7	9	1,240	2	12	1,700
ES16	6	15	>1,700	2	2	300
ES17	5	14	>1,700	6	23	400
ES18	3	4	210	12	26	1,430
ES19	4	8	200	4	13	1,700
ES20	6	15	260	3	5	1,560
ES21	27	67	830	25	74	670
ES22	27	53	930	14	26	680
ES23	23	47	810	28	61	1,230

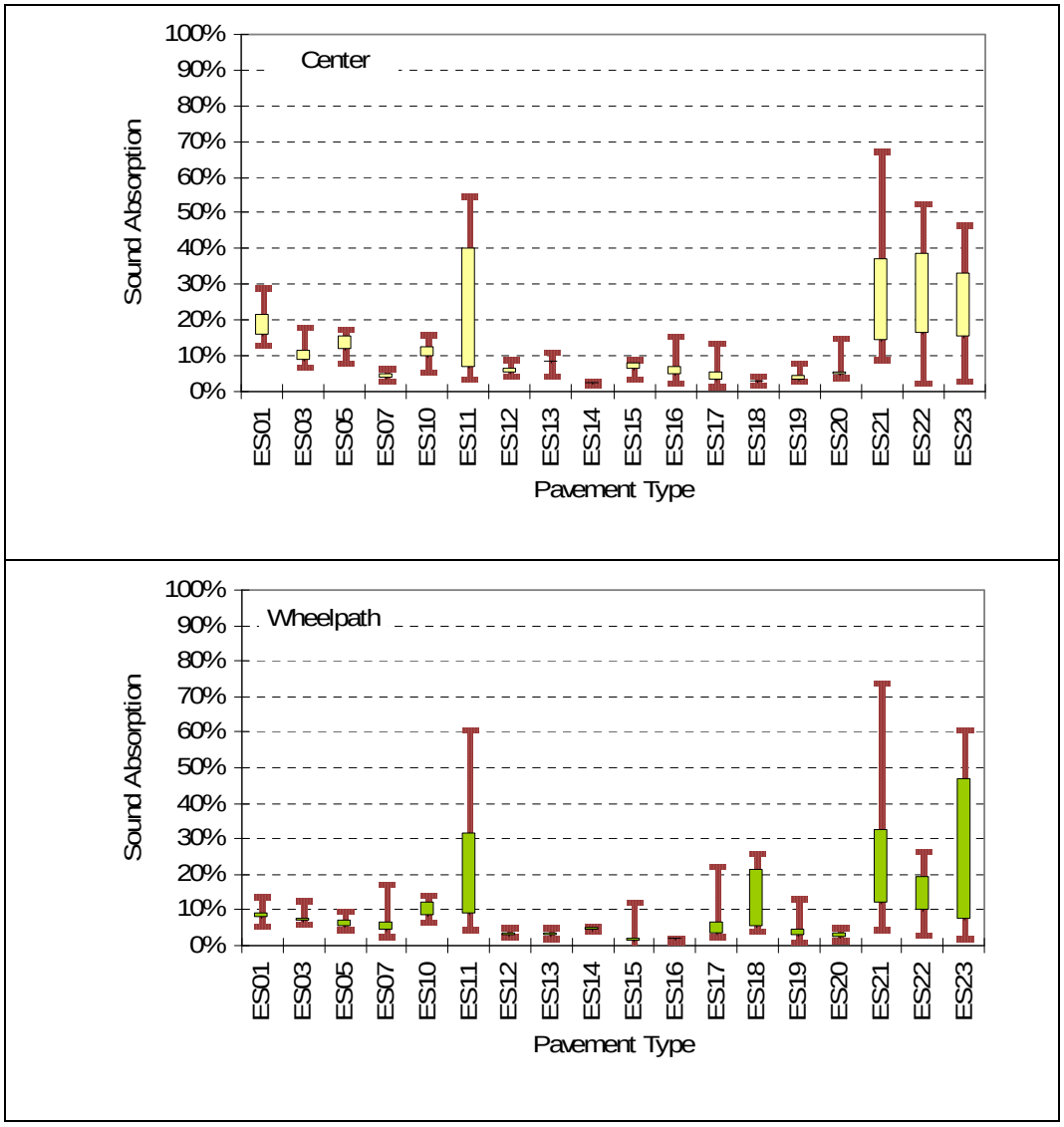

Figure 4: Sound absorption from cores at the center of the lane and at the wheelpath on ES sections.

Sections ES11, ES21, ES22, and ES23 were found to have the highest absorption. Additional information about the sample cores and test conditions is presented in Table 4. This information includes the overall thickness of the tested core and the thickness of the surface layer (the overall thickness includes at least part of the pavement layer below the surface). The table also presents the range of air-void content values measured on various cores from the same section and same location (either the lane center or wheelpath). The sample ID indicates the section type (in this case, ES), the section number, a core number for that section, and the suffix *C* for cores taken from the center of the lane or *W* for cores from the wheelpath. The same naming convention applies to the QP section data presented later. The core number within a section has been preserved in the ID for inventory purposes (other cores were used for other tests).

Table 4: Additional Specimen and Test Information for the ES Sections

Sample ID	Overall Thickness (mm)	Top-Layer Thickness (mm)	Air-Void Content (%)	Barometric Pressure (mm Hg)	Temperature (°C)	Specimen Mass (grams)
ES01-2C	100	100	10.7–14.1	758	22.8	1,814
ES01-1W	80	90	8.4–10.9	758	23.3	1,701
ES03-4C	40	96	12.7–16.8	758	23.3	1,814
ES03-3W	45	90	9.7–10.9	759	19.4	1,587
ES05-4C	30	95	9.6–14.5	759	19.4	1,701
ES05-3W	30	120	12.0–14.8	758	23.3	2,268
ES07-2C	82	147	7	758	20.6	2,721
ES07-1W	32	110	5.4–6.5	759	19.4	2,268
ES10-2C	62	82	11.3–12.2	758	21.1	1,361
ES10-1W	55	140	9.8–12.7	758	21.1	2,608
ES11-2C	90	20	15.9–20.3	766	20.0	1,472
ES11-3W	122	20	15.9–20.3	759	20.0	2,265
ES12-4C	132	80	5.7–10.5	765	21.1	2,265
ES12-1W	80	196	7.9	757	19.4	3,628
ES13-2C	143	41	8.2–8.6	761	21.1	2,492
ES13-1W	50	150	5.2–14.4	758	21.4	2,721
ES14-1W	134	34	4.0–5.2	763	21.1	2,378
ES14-2C	130	30	4.0–5.2	763	21.1	1,925
ES15-4C	170	95	5.0–13.8	762	20.6	3,171
ES15-3W	190	90	5.0–13.8	761	21.1	3,284
ES16-2C	137	50	2.3–5.7	759	20.0	2,492
ES16-3W	100	55	2.3–5.7	765	21.7	1,812
ES17-4C	150	50	3.6–5.0	759	20.0	2,718
ES17-3W	87	157	1.7–5.0	760	23.3	2,721
ES18-4C	136	85	3.6–5.5	765	21.1	2,537
ES18-3W	135	85	2.0–4.3	761	21.1	
ES19-2C	35	35	2.5–7.5	758	21.1	454
ES19-3W	135	40	3.4–7.4	759	20.0	2,492
ES20-2C	75	170	5.9–7.9	758	22.2	2,948
ES20-3W	57	146	5.2–6.9	758	21.7	2,494
ES21-2C	45	45	12.7–14.0	758	21.7	698
ES21-1W	175	50	12.5–15.0	763	20.0	3,398
ES22-2C	30	83	15.8–18.5	759	23.9	1,587
ES22-3W	30	78	17.2–18.4	760	23.9	1,361
ES23-2C	35	73	18.8–21.3	759	21.7	1,361
ES23-3W	25	80	17.9–19.7	760	22.8	1,361

Some of the ES sections are located in close proximity to each other along a stretch of road, which exposes them to the same level of traffic loading and traffic speed and to the same climate conditions. What follows is an analysis for two groups of sections: one located on State Route 138 in Los Angeles County (LA 138) where sections ES01 to ES09 are located, and the other on State Route 33 in Fresno County (Fresno 33), where sections ES12 to ES20 are located.

4.2.1 LA 138

Figure 5 compares the absorption values of three LA 138 sections with open-graded asphalt mixes for both the center and wheelpath cores. Table 5 shows the surface type, air-void content, and thickness of these three sections.

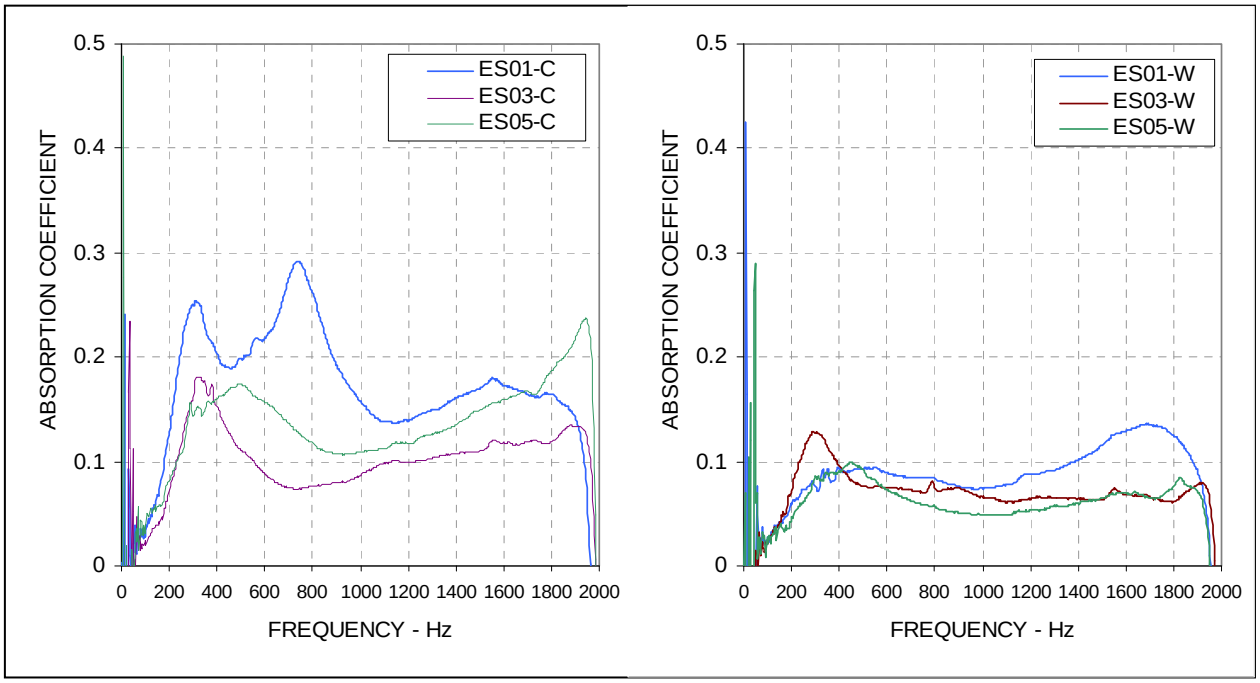

Figure 5: Acoustical absorption spectra for LA 138 open-graded mixes (center in left plot, wheelpath in right plot).

Table 5: Properties of LA 138 Sections

Section	Core Location	Surface Type	Air-Void Content (%)	Thickness (mm)
ES01	Center	OGAC	12.40	75
	Wheelpath	OGAC	9.40	75
ES03	Center	OGAC	15.16	30
	Wheelpath	OGAC	10.32	30
ES05	Center	RAC-O	11.82	30
	Wheelpath	RAC-O	13.00	30

The figure shows that the center cores have more pronounced peaks than the wheelpath cores at lower frequencies. A related investigation (6) found that the center cores usually have higher air-void content and pores that are less clogged at the top compared to the wheelpath cores. On the basis of this information, it may

be inferred that the reason for the difference in absorption between center and wheelpath cores is that the center cores may have larger pore sizes than those from the wheelpath. The larger pore sizes shift the thermal relaxation frequencies to lower values, resulting in peak absorption values at lower frequencies as seen for center cores.

The center cores of sections ES01 and ES03 have higher air-void content and absorption values than the wheelpath cores, while the center cores of ES05 have lower air-void content but higher absorption values than the wheelpath cores. The lower absorption values of the wheelpath core from ES05 may be due to clogging by fine particles at the top part of the core and higher tortuosity. Note that the absorption measurements were conducted on 1 wheelpath and 1 center core out of a total of 12 cores taken from each section. Air-void content was determined using the remaining cores. The actual air-void content of the cores where the sound absorption was measured may be slightly different than that from the cores that were used for air-void determination.

4.2.2 Fresno 33

Figure 6 compares the absorption spectra of the Fresno 33 RAC-G sections. Even though the sections have very similar air-void contents, the cores from the center present higher absorption values than those from the wheelpath. This difference can be again explained by the higher air-void content at the top part of the cores. Also, the air-void content of the wheelpath cores of open-graded mixes, as shown in Table 6, is higher than that of the gap- and dense-graded mixes, and the absorption values are close to those of the gap-graded mixes. These results occur because the wheelpath cores of open-graded mixes are clogged at the top, resulting in a reduction in absorption values, while the air-void contents stay relatively constant.

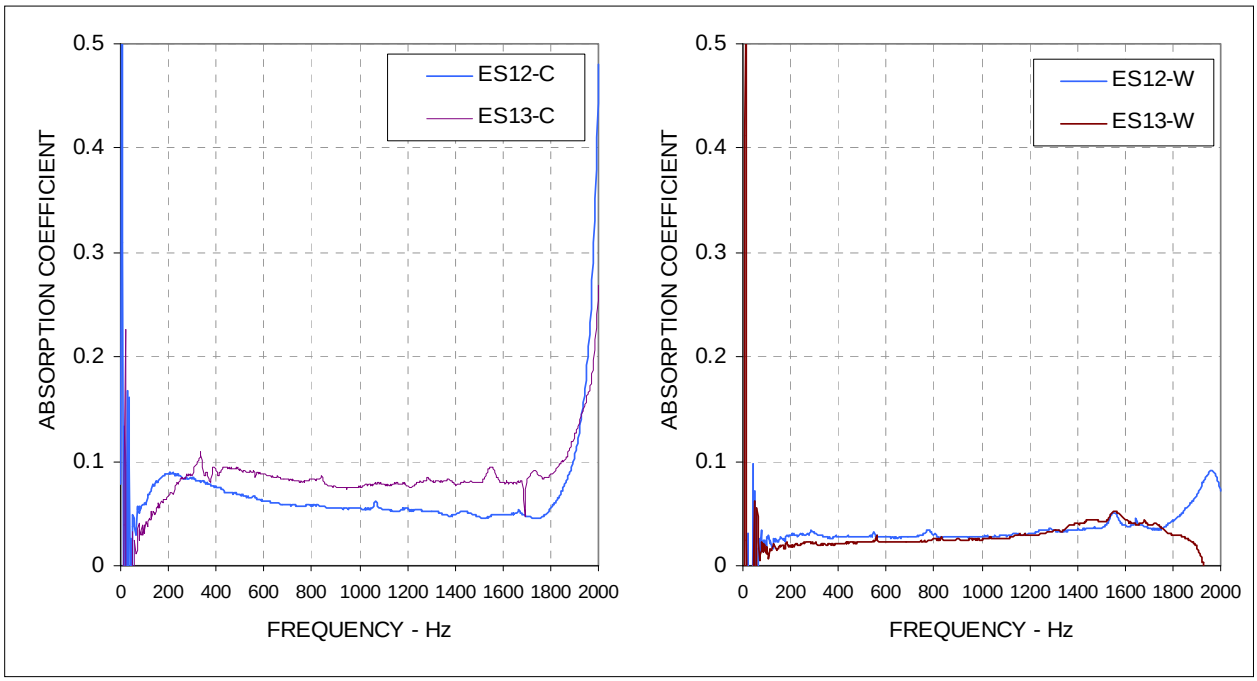

Figure 6: Acoustical absorption spectra for Fresno 33 RAC-G mixes (center in left plot, wheelpath in right plot).

Table 6: Properties of Fresno 33 RAC-G Sections

Section	Core Location	Surface Type	Air-Void Content (%)	Thickness (mm)
ES12	Center	RAC-G	8.37	75
	Wheelpath	RAC-G	7.87	75
ES13	Center	RAC-G	8.42	30
	Wheelpath	RAC-G	8.71	30

Figure 7 compares the absorption spectra of another type of mix at the same location. Instead of RAC-G, these sections use a material called rubber-modified asphalt concrete gap-graded (RUMAC GG). Table 7 presents the surface type, air-void content, and thickness of two sections of this type. Note that the thickness of one of the sections is twice as great as that of the other, and that the absorption values as well as the air-void content of the wheelpath and center are close to each other.

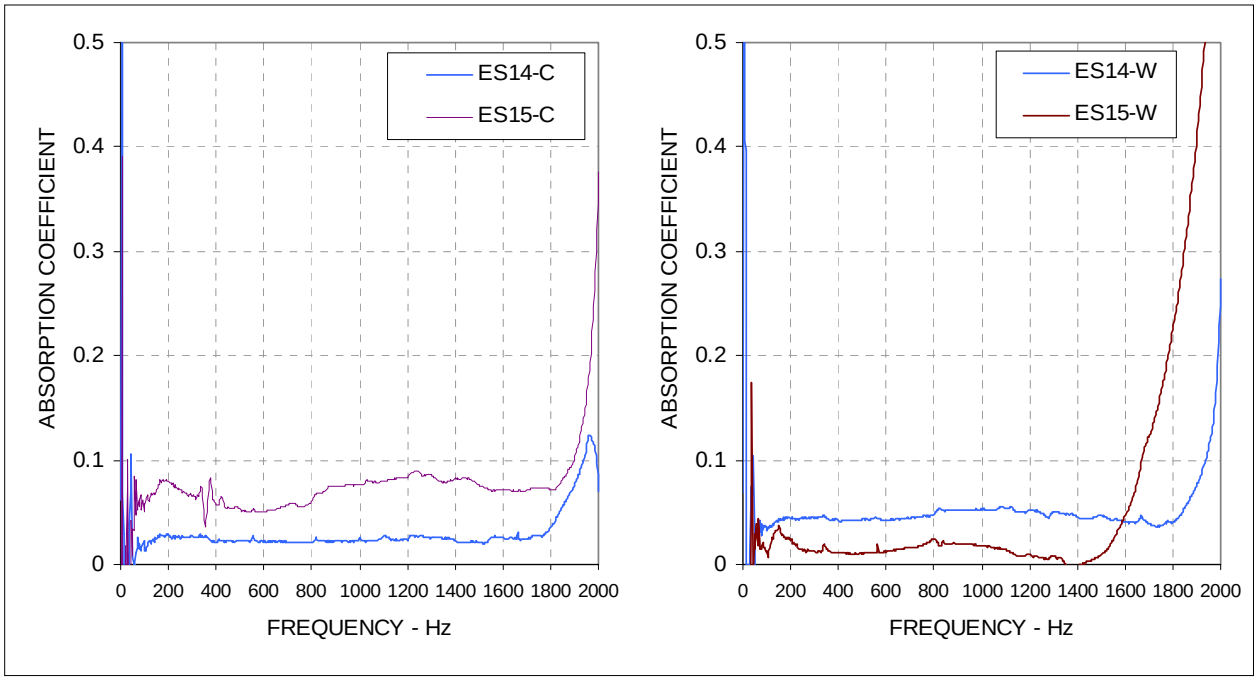

Figure 7: Acoustical absorption spectra for Fresno 33 RUMAC GG mixes (center in left plot, wheelpath in right plot).

Table 7: Properties of Fresno 33 RUMAC GG Sections

Section	Core Location	Surface Type	Air-Void Content (%)	Thickness (mm)
ES14	Center	RUMAC GG	4.67	45
	Wheelpath	RUMAC GG	4.52	45
ES15	Center	RUMAC GG	5.15	90
	Wheelpath	RUMAC GG	5.10	90

4.3 QP Section Results

Acoustical absorption data for the QP series of cores is summarized in Table 8, using the same format as was used for the ES data. Figure 8 through Figure 10 show the absorption at the center of the lane and at the wheelpath, indicating the first and third quartile and the maximum and minimum absorption found in the 200 to 1700-Hz frequency range. Additional information about the sample cores and test conditions is presented in Table 9.

Table 8: Summary of Absorption Results for the QP Sections

Section	Center Average (%)	Center Maximum (%)	Center Resonant Frequency (Hz)	Wheelpath Average (%)	Wheelpath Maximum (%)	Wheelpath Resonant Frequency (Hz)
QP02	14	15	1,240	10	12	1,250
QP03	28	77	730	21	48	590
QP04	17	44	520	15	34	360
QP06	7	8	1,160	7	12	340
QP07	3	4	>1,700	1	2	>1,700
QP08	24	46	1,030	18	36	870
QP09	2	4	>1,700	7	11	>1,700
QP10	4	8	>1,700	2	3	>1,700
QP11	1	4	>1,700	1	3	>1,700
QP12	26	53	820	N/A	N/A	N/A
QP13	8	20	>1,700	11	20	>1,700
QP14	4	8	>1,700	10	12	>1,700
QP15	4	7	>1,700	4	7	>1,700
QP16	2	5	>1,700	2	4	>1,700
QP17	3	6	>1,700	5	15	>1,700
QP18	10	13	>1,700	6	8	>1,700
QP19	5	11	>1,700	6	17	>1,700
QP20	36	97	1,430	30	79	980
QP21	3	9	>1,700	2	10	>1,700
QP22	N/A	N/A	N/A	15	22	1,060
QP23	22	52	710 and >1,700	30	47	600 and >1,700
QP24	4	13	>1,700	5	14	>1,700
QP25	3	10	>1,700	2	10	>1,700
QP26	7	17	>1,700	8	13	>1,700
QP27	3	14	>1,700	11	13	560
QP28	16	28	>1,700	15	24	>1,700
QP29	16	31	1,680	10	25	>1,700
QP30	2	4	>1,700	2	3	>1,700
QP31	3	10	>1,700	4	6	>1,700
QP32	22	39	600	6	9	310
QP33	17	26	410	9	20	>1,700
QP34	8	18	>1,700	7	15	>1,700
QP35	32	67	1,230	30	56	1,160
QP36	16	25	610	6	11	300
QP37	5	8	820	4	5	1,610
QP38	4	5	430	3	5	1,550
QP39	10	13	>1,700	7	19	>1,700
QP40	4	8	1,570	2	4	1,560
QP41	35	72	1,010	32	75	980
QP42	31	52	900	30	63	1,360
QP43	4	6	1,560	4	7	1,560
QP44	12	24	>1,700	N/A	N/A	N/A
QP45	33	85	1,120	22	58	860
QP46	10	12	<200	9	14	<200
QP47	27	53	600 and >1,700	14	35	540 and >1,700
QP48	4	13	>1,700	5	14	>1,700

Section	Center Average (%)	Center Maximum (%)	Center Resonant Frequency (Hz)	Wheelpath Average (%)	Wheelpath Maximum (%)	Wheelpath Resonant Frequency (Hz)
QP49	3	14	>1,700	4	16	>1,700
QP50	14	22	430 and >1,700	11	18	450
QP51	29	68	1,010	N/A	N/A	N/A
QP52	14	24	>1,700	10	21	>1,700
N103	3	11	>1,700	3	10	320
N104	12	21	>1,700	11	16	250
N105	17	51	>1,700	43	73	1,100
N121	3	9	230	5	13	240
N434	2	3	1,550	6	14	630
N467	N/A	N/A	N/A	19	29	790

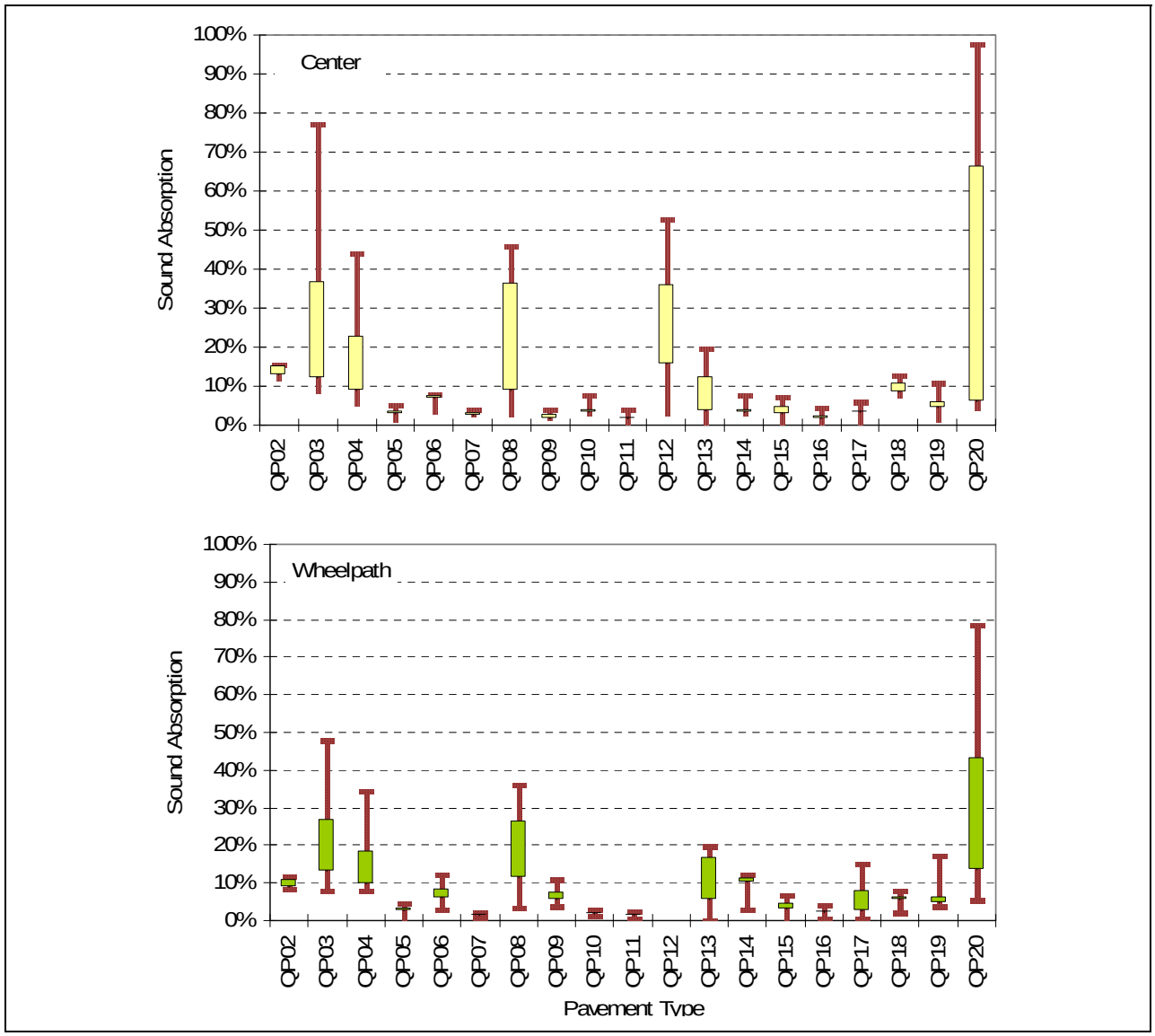

Figure 8: Sound absorption from cores at the center of the lane and at the wheelpath on sections QP02 to QP20.

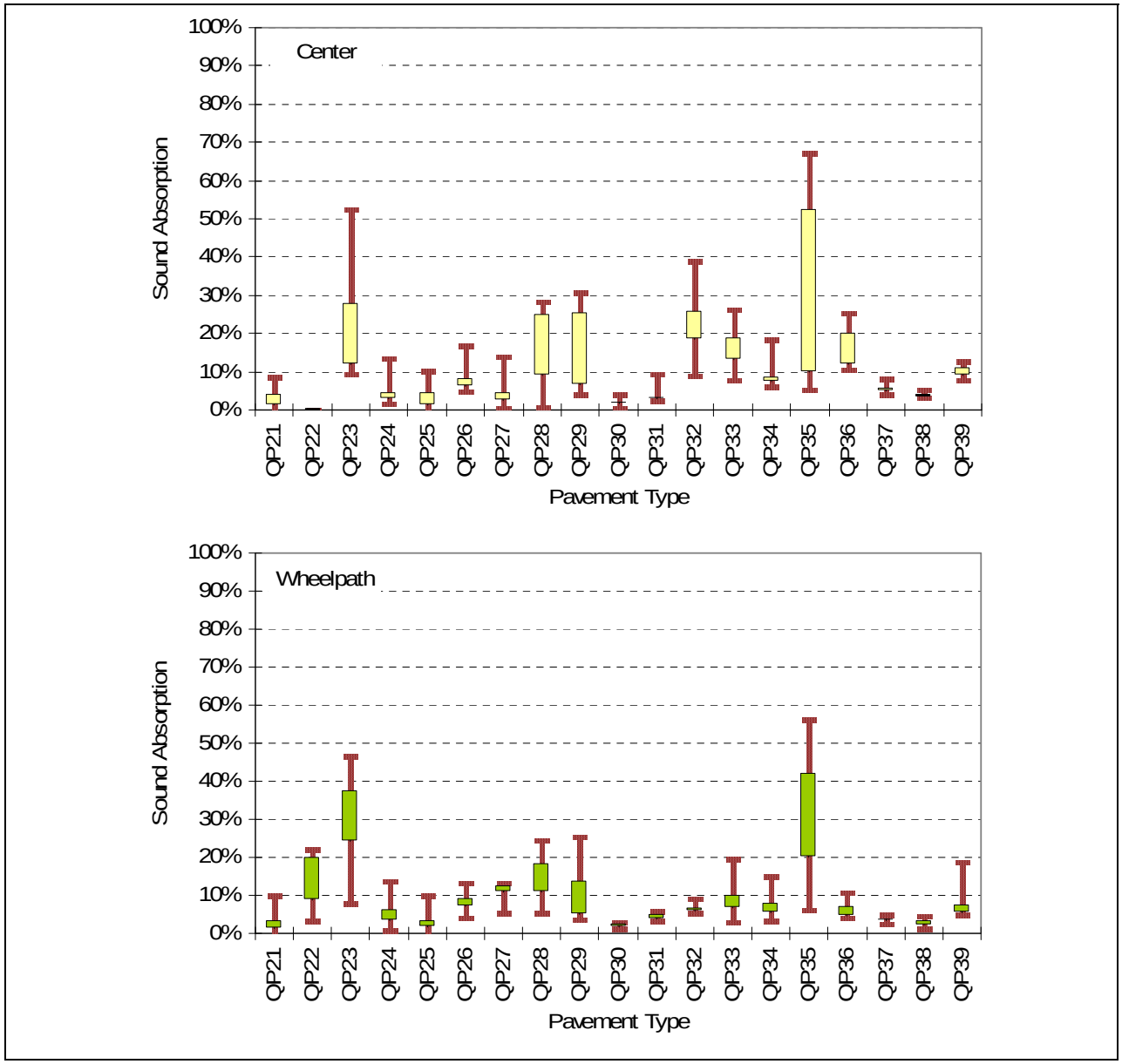

Figure 9: Sound absorption from cores at the center of the lane and at the wheelpath on sections QP21 to QP39.

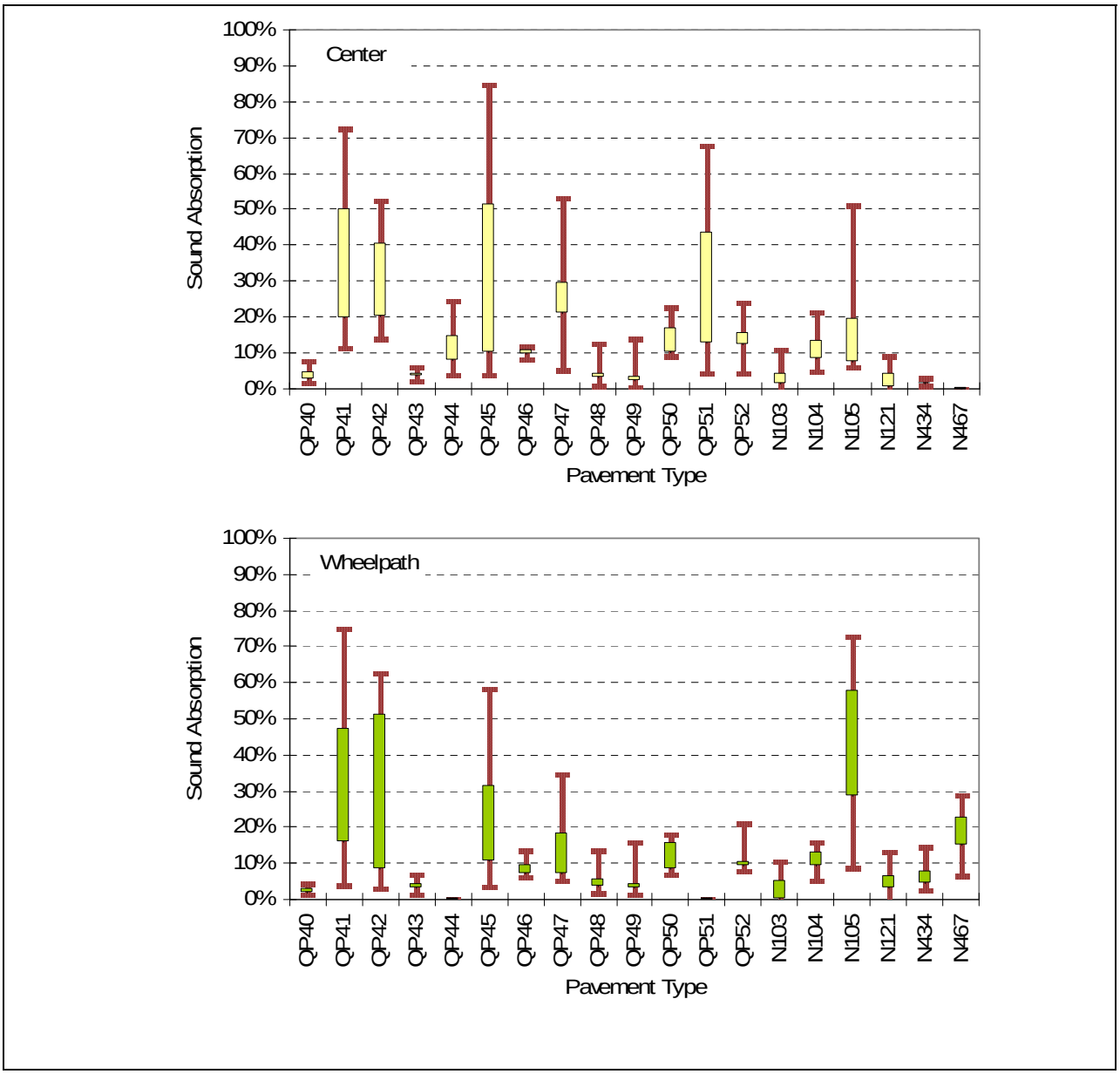

Figure 10: Sound absorption from cores at the center of the lane and at the wheelpath on sections QP40 to N467.

Table 9: Additional Specimen and Test Information for the QP Sections

Sample ID	Overall Thickness (mm)	Top Layer Thickness (mm)	Air-Void Content (%)	Barometric Pressure (mm Hg)	Temperature (°C)	Specimen Mass (grams)
QP02-4C	203	75	7.6–9.1	763	20.6	3628
QP02-3W	205	68	8.2–8.7	758	21.7	3855
QP03-4C	81	45	20.5–20.9	757	22.2	1020
QP03-1W	237	45	17.7–18.9	758	21.7	4649
QP04-3W	160	47	15.9–16.2	758	21.7	2948
QP04-4C	143	45	16.7–17.2	758	20	2608
QP05-1W	170	45	8.1–11.4	761	22.8	2993
QP05-2C	160	50	11–11.4	764	21.7	2812
QP05-4C	101		8.1–11.4	762	21.7	3175
QP06-4C	62	108	5.1–5.3	758	21.1	2041
QP06-3W	60	100	4.4–6.0	758	20.6	1814
QP07-4C	115	115	5.5–6.1	762	23.3	2154
QP07-1W	117	117	3.6–4.7	761	20	2381
QP08-2C	30	30	19.7	758	22.2	454
QP08-3W	30	30	16.4–19.3	758	22.2	454
QP09-3W	217	108	4.6–4.8	758	22.2	4308
QP09-4C	215	43	3.2–4.8	758	21.7	4308
QP10-2C	92	17	10.7–12.8	760	23.3	1587
QP10-3W	77	24	8.5–8.6	763	21.1	1360
QP11-9W	85	25	4.6–6.5	762	21.1	1451
QP11-2C	68	68	4.6–6.5	758	21.7	1361
QP11-3W	113	37	5.0–6.0	766	20	2041
QP11-3W	113	37	5.0–6.0	759	21.1	1814
QP12-2C	35	115	20–21.4	762	21.7	2177
QP13-1W	127	20	15.8–20.3	763	21.7	2,630
QP13-2C	146	18	15.8–20.3	763	22.8	2,630
QP13-2C-A	146	18	15.8–20.3	763	22.2	2,630
QP13-2C-B	146	18	15.8–20.3	762	23.3	2,630
QP13-2C	146	18	17.6–20.3	769	22.8	2,154
QP14-3W	125	30	10.5–13.3	762	21.1	3,067
QP14-4C	170	25	10.5–13.3	771	21.7	3,401
QP15-1W	178	28	6.1–7.1	773	22.8	3,289
QP15-2C	175	175	6.1–7.1	769	22.8	2,154
QP15-3W	115	115	6.1–7.1	769	22.2	3,289
QP15-4C	175	25	6.1–7.1	762.5	21.7	1,995
QP16-3W	101	25	6.1–11.1	769	22.2	2,154
QP16-4C	120	25	6.1–11.1	768	23.3	1,474
QP17-2C-B	83	53	18.0–18.5	761	20.6	2,494
QP17-3W	130	25	18.0	771	21.1	1,247
QP18-1W	72	30	8.4–10.0	758	21.1	4,082
QP18-2C	220	33	9.2–11.4	760	21.1	1,812
QP19-1W	100	40	9.3–10.0	761	20	2,265
QP19-2C	135	41	11.4–11.9	761	20	2,039
QP20-3W	105	32	20.3–21.2	761	20	1,699
QP20-4C	88	32	21.0–23.8	761	20	1,699
QP20-4C	88	32	21.0–23.8	761	20	2,718
QP21-1W	147	35	6.5	761	20	3,171
QP21-2C	164	35	7.9	761	20	2,492
QP22-1W	135	27	13.3–15.8	761	20	2,718
QP22-2C	145	26	13.2–13.6	760	21.1	2,492

Sample ID	Overall Thickness (mm)	Top Layer Thickness (mm)	Air-Void Content (%)	Barometric Pressure (mm Hg)	Temperature (°C)	Specimen Mass (grams)
QP23-1W	136	47	17.0–18.7	761	20	2,945
QP23-2C	157	35	18.0–19.5	761	20	3,398
QP24-1W	200	33	11.4–13.1	760	21.1	1,586
QP24-2C	91	30	10.8–12.6	760	21.1	1,042
QP25-1W	65	65	7.1–11.1	761	20	3,624
QP25-2C	200	70	7.8–8.2	761	20	2,809
QP26-1W	143	42	8.6–10.0	760	21.1	2,809
QP26-2C	150	47	6.1–9.9	761	20.6	4,077
QP27-1W	198	36	4.4–7.3	761	20	4,077
QP27-2C	205	37	4.5–9.3	758	21.7	2,812
QP28-1W	152	65	8.7–14.7	768	23.9	3,855
QP28-2C	220	65	8.7–14.7	762	23.3	3,175
QP29-3W	170	15	15.6–23.0	760	20.6	3,061
QP29-4C	165	17	15.6–23.0	760	20.6	3,855
QP30-1W	200	78	6.2–8.9	757	22.2	3,968
QP30-2C	212	33	6.2–8.9	758	21.1	1,247
QP31-1W	70	25	7.1–10.1	758	21.7	794
QP31-2C	44	44	7.1–10.1	758	22.8	1,020
QP32-1W	60	60	11.0–14.8	758	21.7	1,361
QP32-2C	55	55	16.9–20.7	759	20	2,945
QP33-1W	150	150	12.6–14.5	759	24.4	3,401
QP33-2C	60	182	13.5–14.6	759	20	1,812
QP34-1W	110	20	7.8–11.5	760	21.1	1,812
QP34-2C	110	60	12.5–15.2	758	21.4	1,361
QP35-1W	85	20	14.7–21.3	759	21.7	1,361
QP35-2C	80	20	17.3–20.9	758	21.7	2,721
QP36-3W	150	50	13.3–17.9	758	21.7	1,587
QP36-4C	90	36	13.6–14.6	758	25	906
QP37-1W	50	50	4.2–5.2	759	21.1	454
QP37-2C	50	50	4.2–5.5	759	24.4	3,628
QP38-1W	192	55	4.7–5.6	763	21.1	1,019
QP38-4C	51	51	4.7–7.4	760	21.1	4,077
QP39-1W	215	61	6.5–8.3	765	21.1	3,737
QP39-2C	207	56	6.6–9.0	759.5	21.7	4,989
QP40-1W	252	45	4.6–5.1	760	22.8	3,628
QP40-2C	195	45	6.3–7.6	758	20.6	4,649
QP41-1W	245	35	17.2–19.2	758	20.6	4,637
QP41-2C	240	35	19.0–19.1	759	23.9	1,814
QP42-3W	90	10	17.4–19.4	758	21.1	1,587
QP42-4C	90	30	18.5–20.1	758	21.7	2,268
QP43-1W	130	67	3.4–5.2	758	22.2	3,855
QP43-2C	220	80	4.6–6.3	758	21.7	2,268
QP44-4C	117	30	17.8–19.4	761	21.1	3,171
QP45-2C	180	30	20.2–21.1	761	21.1	2,265
QP45-3W	125	30	N/A	759	23.9	1,020
QP46-3	80	20	N/A	759	23.9	1,361
QP46-4C	100	20	11.0–13.2	761	21.1	4,757
QP47-2C	250	46	8.4–10.3	761	21.1	2,718
QP47-3W	145	44	11.6–15.0	760	21.1	2,039
QP48-1W	105	56	11.6–12.4	759	20	1,925
QP48-2C	100	50	11.2–14.3	761	21.1	1,359

Sample ID	Overall Thickness (mm)	Top Layer Thickness (mm)	Air-Void Content (%)	Barometric Pressure (mm Hg)	Temperature (°C)	Specimen Mass (grams)
QP49-1W	87	30	12.7–14.7	761	21.1	1,812
QP49-2C	95	30	11.9–16.3	758	21.7	2,041
QP50-1W	117	47	11.0–11.7	759	20	2,718
QP50-4C	152	50	12.4–13.8	758	22.2	4,082
QP51-1W	207	32	19.0–20.1	759	20	4,213
QP52-1W	230	50	7.2–8.4	760	21.1	4,304
QP52-2C	230	45	8.3–11.9	759.5	21.1	1,586
01-N103-1W	80	12		759.5	21.1	2,492
01-N103-2C	138	20		759.5	21.1	906
01-N104- 1W	50	10	15.2–15.7	759.5	21.1	1,019
01-N104-2C	50	17	17.1–18.0	759.5	21.1	1,133
01-N105-5W	65	40	21.0–21.2	759.5	21.1	3,398
01-N105-8C	178	20	21.2–22.4	759.5	21.1	1,133
01-N121-3W	58	58	8.2	759.5	21.1	1,812
01-N121-4C	90	55	6.7	758	20.6	2,041
06-N434-1W	98	62	N/A	758	20	2,721
06-N434-2C	135	70	4.1	758	20	2,494
06-N467-3W	135	25	18.9–24.4			

5 DESCRIPTIVE ANALYSIS OF ACOUSTICAL ABSORPTION VALUES

The results from both the environmental sections (ES) and the quieter pavement (QP) sections were studied to explore the sound absorption characteristics of the different asphalt mix types. The analysis uses the average of the measured absorption between 200 and 1,700 Hz. Figure 11 shows a comparison of absorption at the center of the lane for open-graded and non-open-graded pavements, distinguishing between those mixes with and without inclusion of rubber. Rubberized mixes were distinguished from nonrubberized mixes to evaluate any rubber-inclusion effect on acoustical absorption. The figure shows that open-graded mixes have higher absorption values than gap- and dense-graded mixes. RAC-G (rubberized gap-graded) mixes have slightly higher absorption values than dense-graded mixes, but this is believed to be the result of higher air-void content rather than the result of the presence of rubber. In this type of plot, the whiskers indicate the total range of absorption for the whole section in a given category, and the boxes represent the range between the 25th and 75th percentiles. The median is represented by the line inside the box, and the dot is the average value. Figure 12 shows the variation in wheelpath average absorption values for different pavement types. As in Figure 11, Figure 12 shows that open-graded mixes have higher wheelpath absorption values than gap- and dense-graded mixes. The center absorption was higher than the wheelpath absorption in 57% of the sections, and the average ratio of center absorption to wheelpath absorption was 1.2. The largest difference between center and wheelpath absorption was found in section QP32 (see Appendix A)

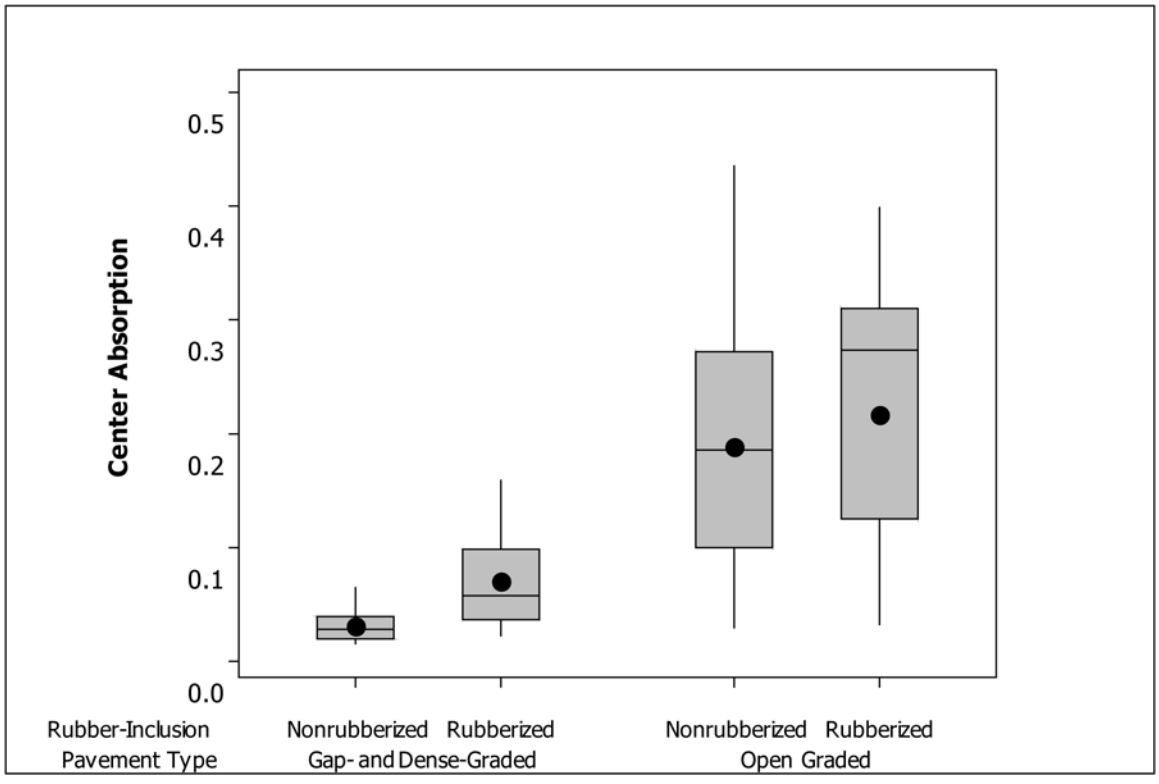

Figure 11: Comparison of center absorption values for different surface types.

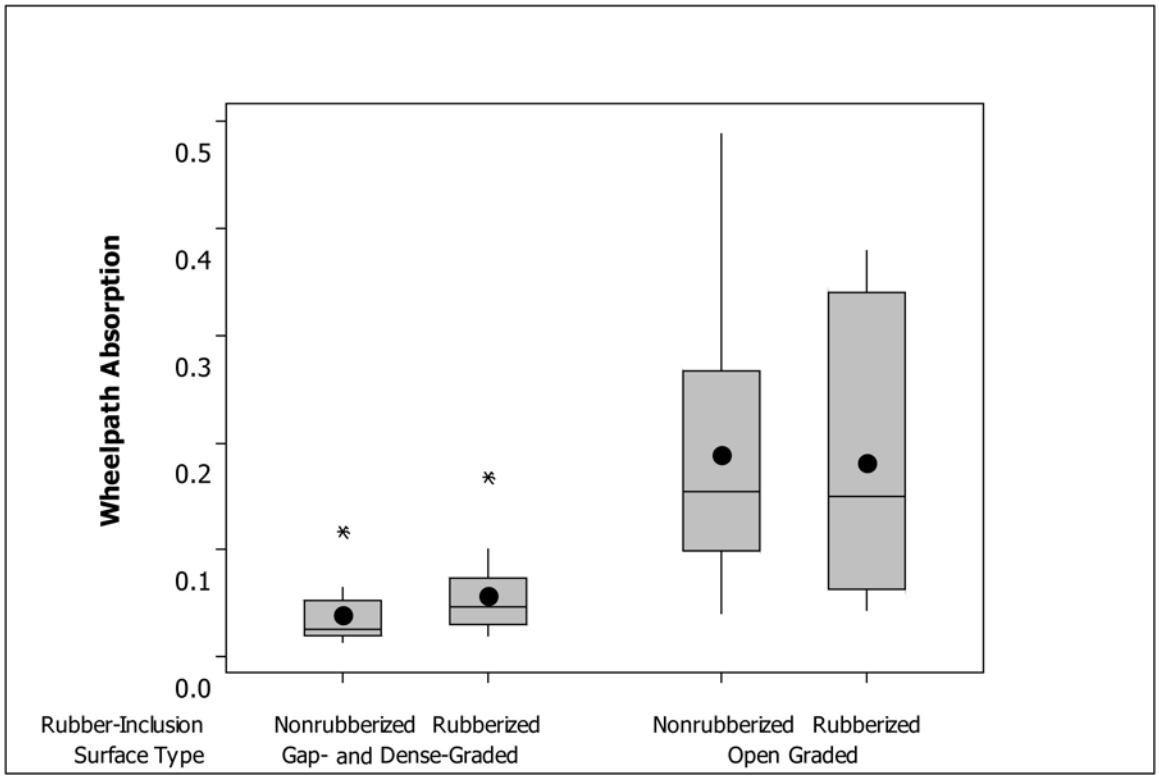

Figure 12: Comparison of wheelpath absorption values for different surface types.

Absorption values for all the surface types in the study are summarized in Figure 13. The absorption values in this case are the averages from the wheelpath and center locations. Table 10 presents the average air-void content and average pavement age of different surface types. The table shows that the open-graded (OGAC and RAC-O) mixes have the highest absorption values as well as the highest air-void content. On the other end, the gap-graded mixes, including RAC-G, bonded wearing course (BWC), RUMAC-GG, and Type G MB, and the dense-graded mixes, including DGAC and Type D MB, present the lowest absorption values. Although the OGAC F-mixes have high air-void content, their absorption values are very low, close to those of the dense-graded mixes. This unexpected result can be attributed to the age factor. The age of pavements in the OGAC F-mix category is greater than the age of the other open-graded mixes. Fine particles may have clogged the pores in the top part of the surface mix over time, hence reducing absorption. The sample size unfortunately does not allow more conclusive interpretation of the findings.

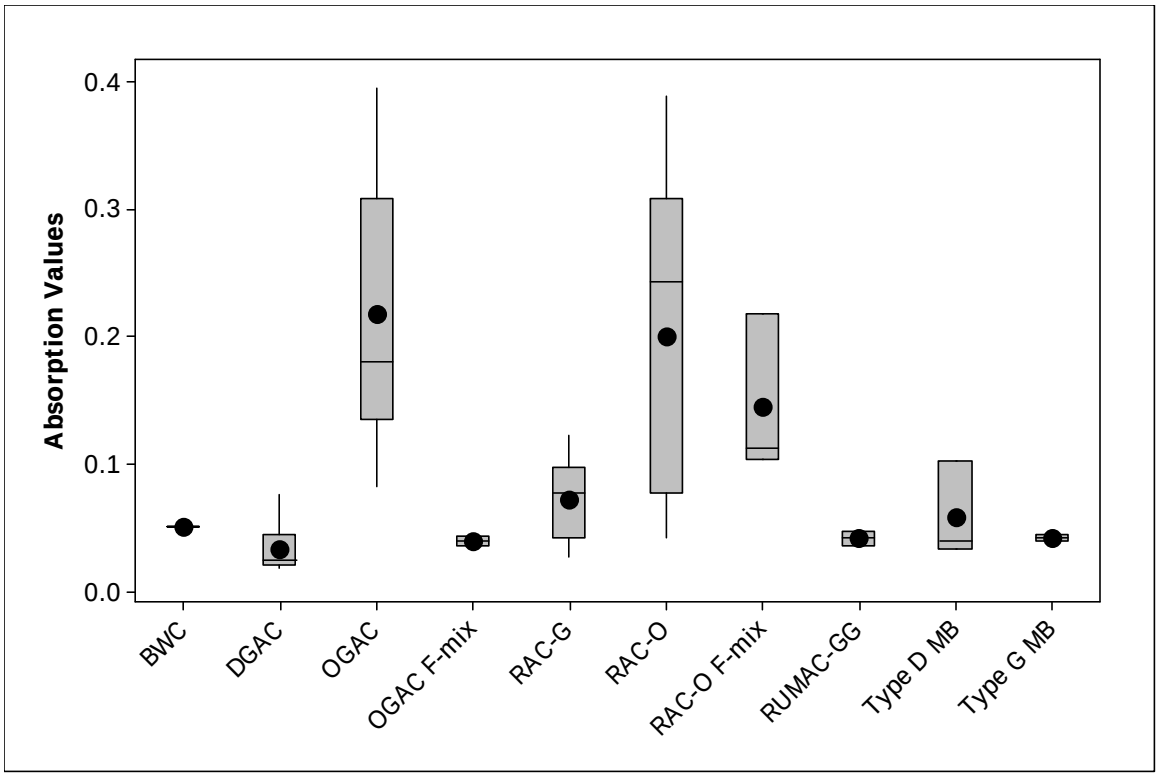

Figure 13: Comparison of absorption values for all surface types (average of center and wheelpath).

Table 10: Average Air-Void Content and Average Ages of Different Surface Types

Surface Type	Absorption Coefficient (%)	Air-Void Content (%)	Age (years)	Number of Sections
BWC	5	6.5	3.4	2
DGAC	4	6.7	4.3	18
OGAC	22	17.0	4.2	18
OGAC F-mix	5	13.4	8.2	2
RAC-G	7	9.9	3.9	13
RAC-O	20	15.9	2.9	20
RAC-O F-mix	14	11.2	2.7	3
RUMAC-GG	5	4.8	1.5	2
Type-D MB	7	5.3	1.5	2
Type-G MB	5	3.5	1.5	2

6 CORRELATION BETWEEN ABSORPTION AND AIR-VOID CONTENT AND THICKNESS

Figure 14 and Figure 15 show the correlation of absorption values with the air-void content for the wheelpath and center cores, respectively. There is a linear trend between the natural logarithm of absorption values and the air-void content: increasing the air-void content increases the average absorption values. However, this trend is stronger for wheelpath cores.

Figure 16 shows that increasing thickness does not have a significant effect on the absorption values for open-, dense- and gap-graded mixes.

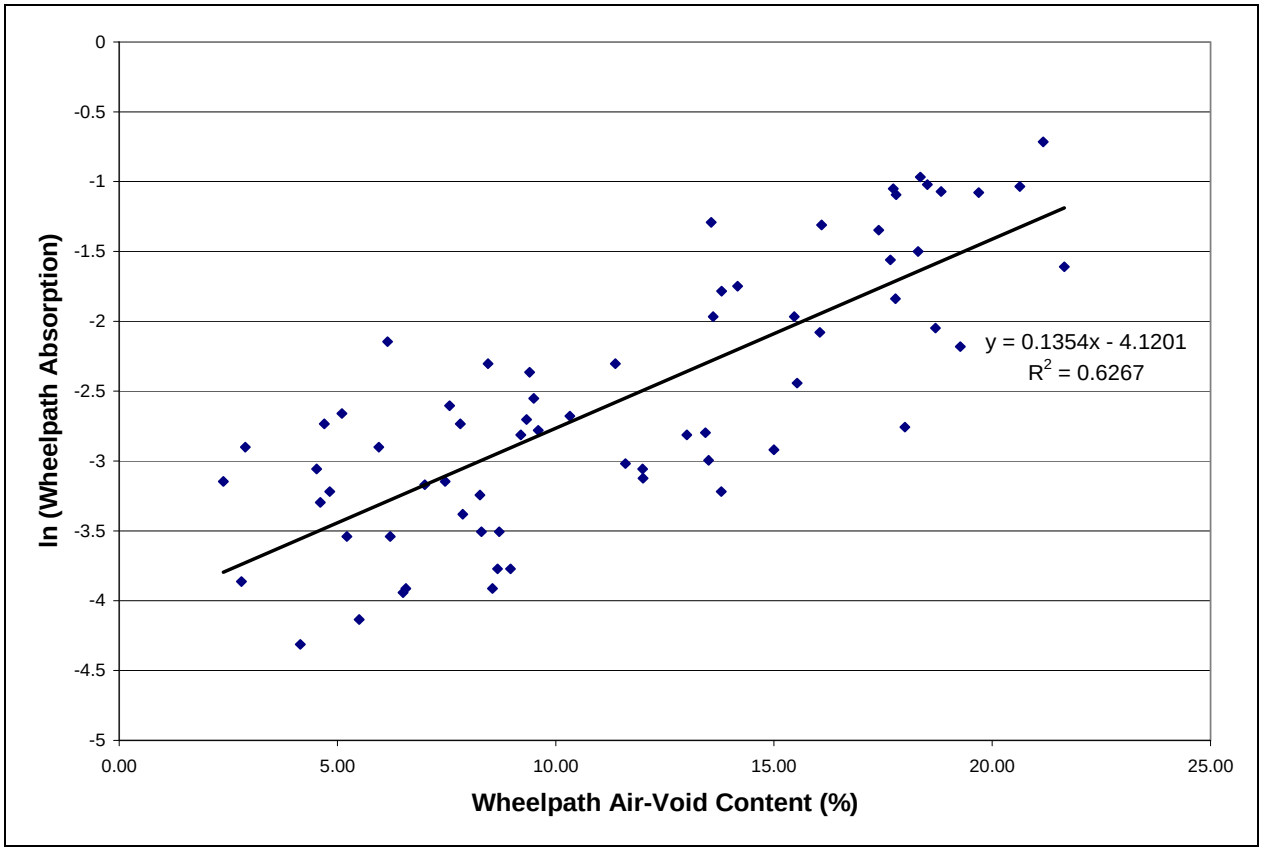

Figure 14: Correlation of wheelpath absorption values with air-void content (%).

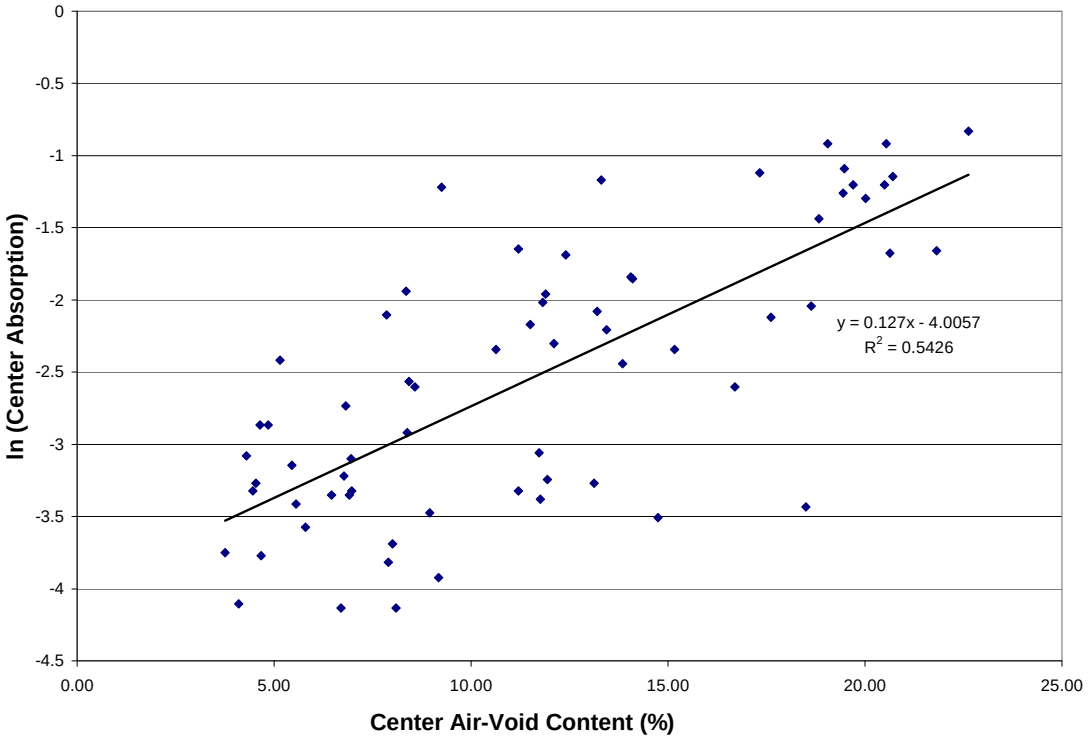

Figure 15: Correlation of center absorption values with air-void content (%).

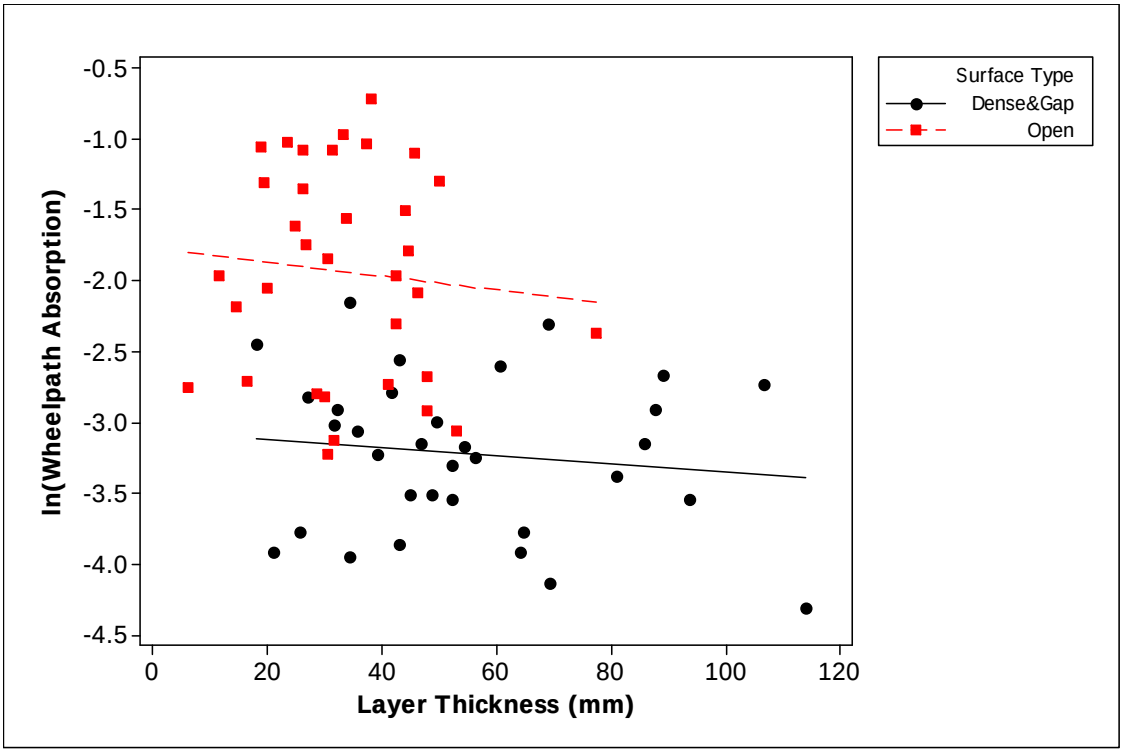

Figure 16: Correlation of absorption values with the surface layer thickness for different surface types.

7 CORRELATION BETWEEN ABSORPTION VALUES AND OBSI LEVELS

The relationship between sound absorption and tire/pavement noise levels was investigated. Only the wheelpath absorption is shown here because the tire/pavement measurements data comes from measurements at the wheelpath. Figure 17 shows this relationship for different surface types. The figure shows that increased absorption is correlated with decreased the sound intensity levels (OBSI) for dense- and gap-graded mixes. However, for open-graded mixes, the sound intensity levels do not seem to be correlated with the absorption values.

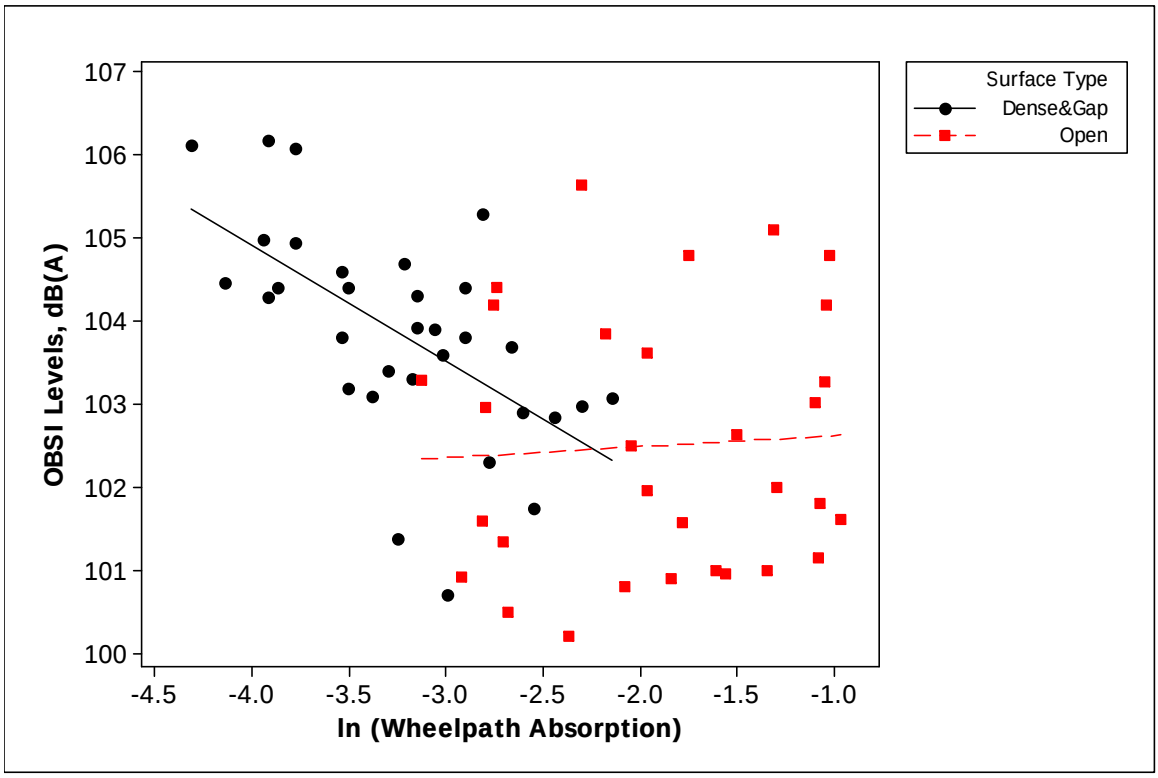

Figure 17: A-weighted sound intensity levels versus the absorption values for different surface types.

Figure 18 shows the A-weighted sound intensity levels for frequencies between 500 and 1,600 Hz compared to the absorption values. The absorption values were calculated using frequencies up to 1,700 Hz. The sound intensity levels were also calculated using the third-octave-band frequencies up to the same limit as for the absorption data (1,700 Hz) to see if they correlate better with the absorption values. However, this filtering of the OBSI data did not improve the correlation between absorption values and sound intensity, as it showed the same trend as in Figure 17.

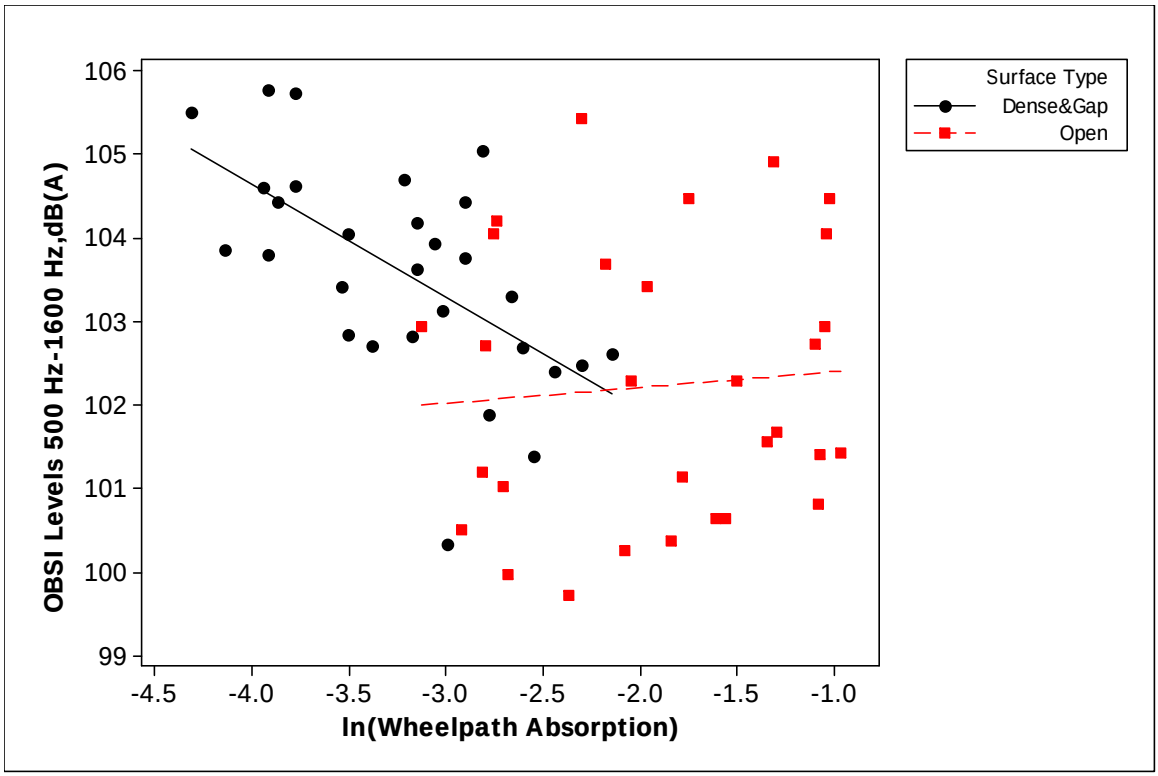

Figure 18: Partial A-weighted sound intensity levels versus the absorption values for different pavement types.

In the analysis that follows, the OBSI level at individual third-octave-band frequencies is plotted against absorption results. Figure 19 shows the sound intensity levels at 500 Hz, and Figure 20 shows the sound intensity levels at 630 Hz. The figures show that increasing absorption values reduce the sound intensity levels for dense- and gap-graded mixes. For open-graded mixes, however, greater absorption at these lower frequencies does not mean reduced sound intensity because less noise due to greater absorption is surpassed by more noise due to texture, which in turn is a consequence of the open structure that causes more absorption.

Figure 21 shows the sound intensity levels at 800 Hz, and Figure 22 shows the sound intensity levels at 1,000 Hz. The figures show that increasing absorption values reduce the sound intensity levels for dense- and gap-graded mixes. However, for open-graded mixes there is no strong correlation between sound intensity levels and absorption values at 800 and 1,000 Hz.

Figure 23 shows the sound intensity levels at 1,250 Hz compared to the absorption values, and Figure 24 shows the sound intensity levels at 1,600 Hz compared to the absorption values. The figures show that increasing absorption values reduces the noise levels for open-, dense-, and gap-graded mixes.

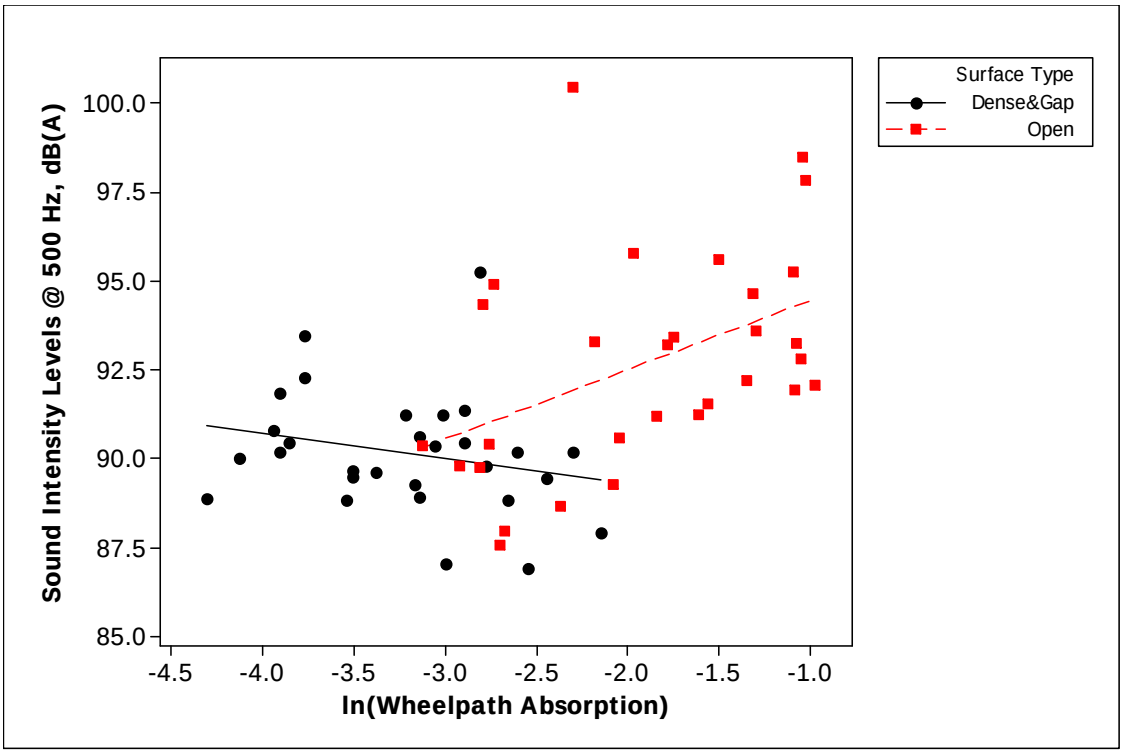

Figure 19: Sound intensity levels at 500 Hz versus the absorption values.

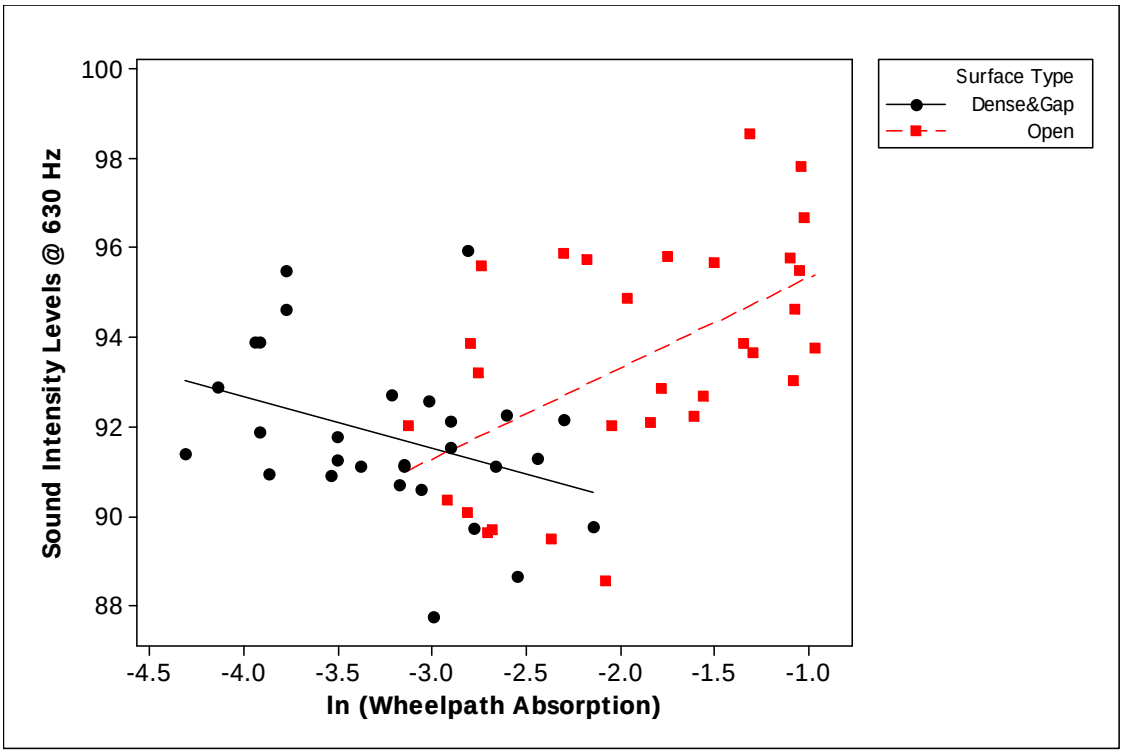

Figure 20: Sound intensity levels at 630 Hz versus the absorption values.

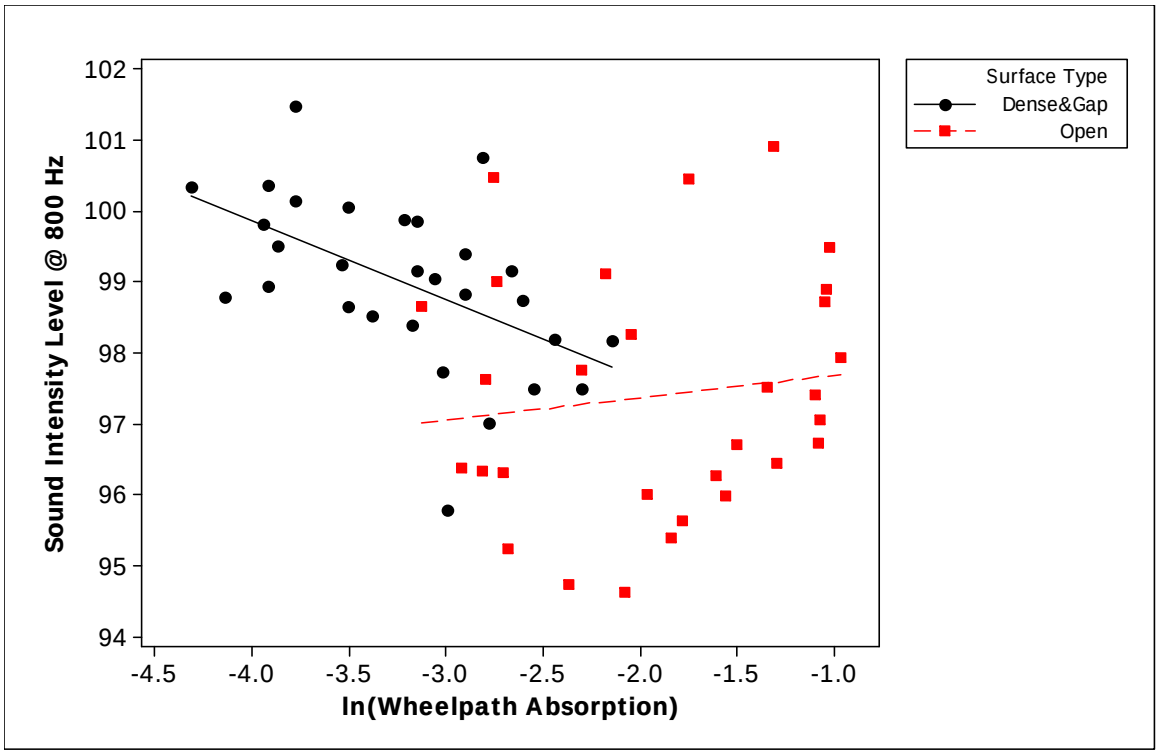

Figure 21: Sound intensity levels at 800 Hz versus the absorption values.

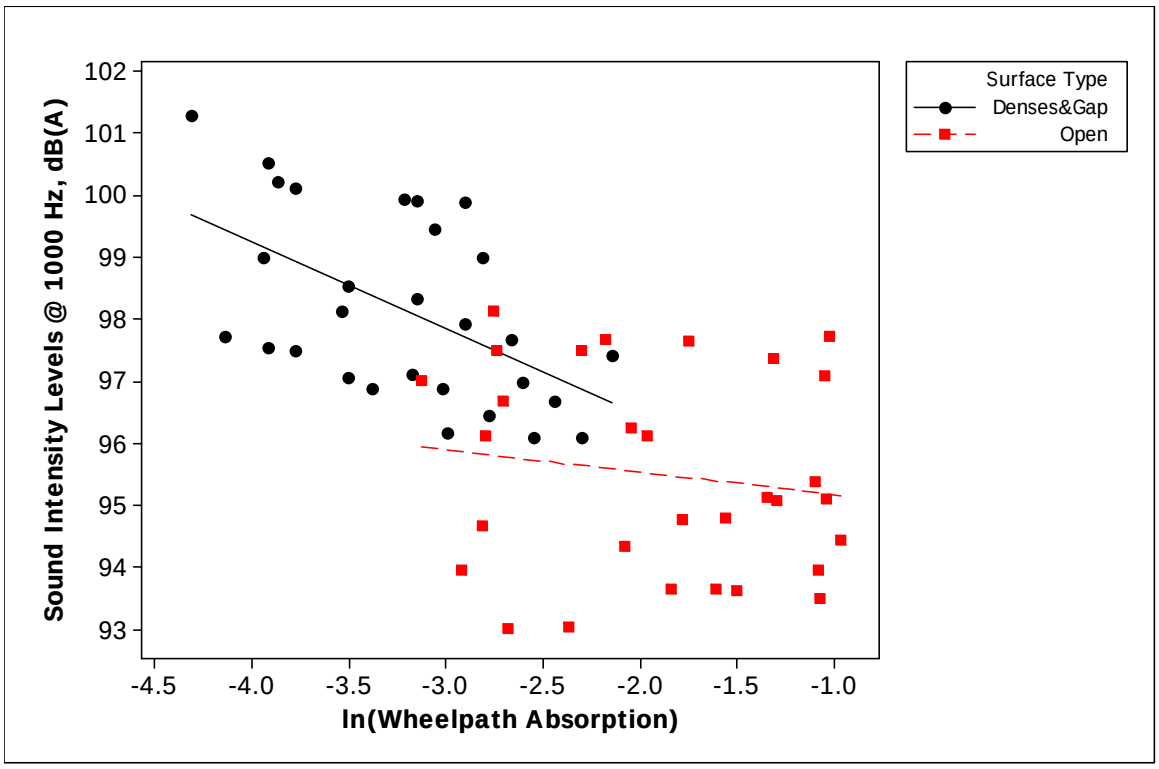

Figure 22: Sound intensity levels at 1,000 Hz versus the absorption values.

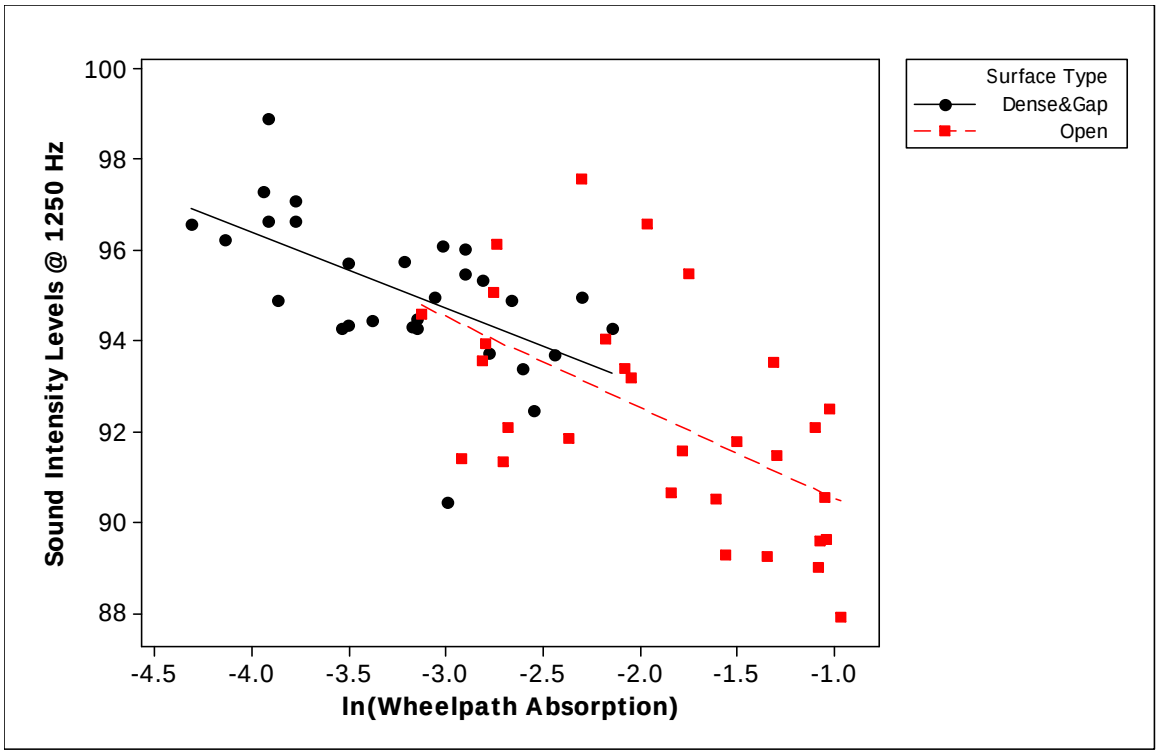

Figure 23: Sound intensity levels at 1,250 Hz versus the absorption values.

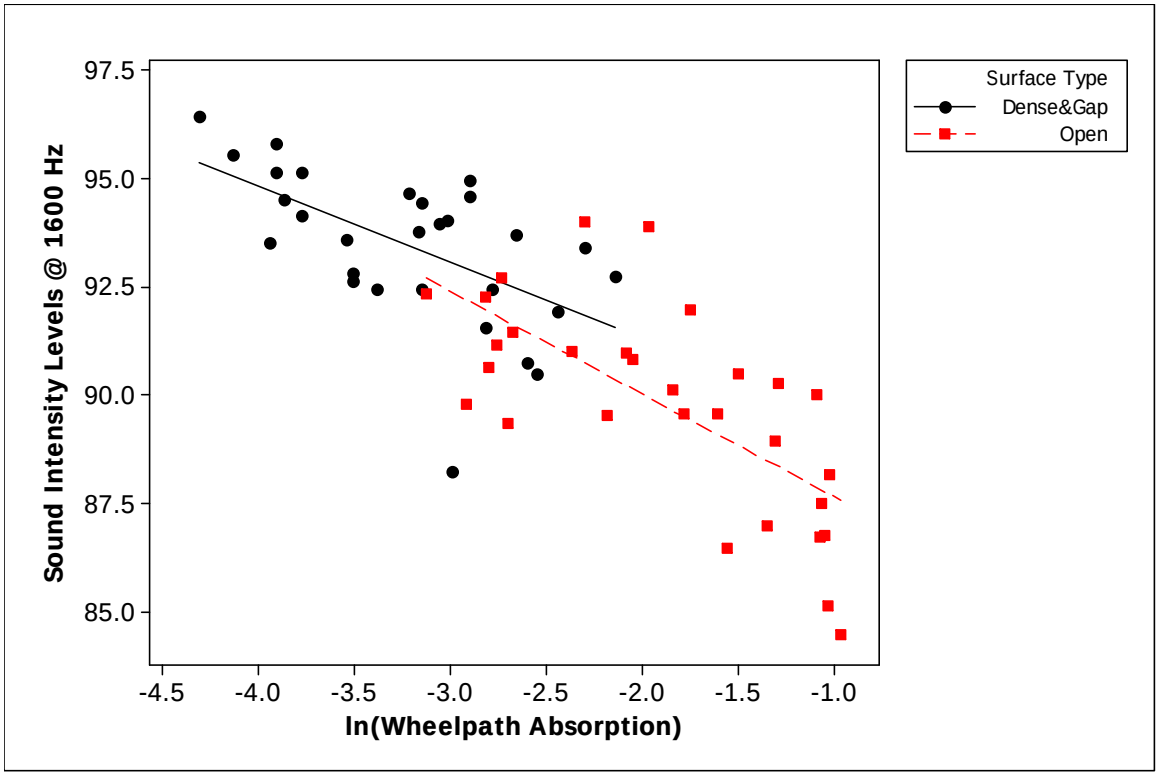

Figure 24: Sound intensity levels at 1,600 Hz versus the absorption values.

8 REGRESSION ANALYSIS FOR THIRD-OCTAVE BAND FREQUENCIES

To quantify the effects of absorption values on tire/pavement noise levels at different frequencies, regression analyses were conducted at third-octave-band frequencies from 500 to 1,600 Hz.

8.1 Regression Analysis for OBSI at 500 Hz

8.1.1 Combined Data Set

The 500-Hz sound intensity levels were explained by absorption and surface type. Surface type is coded as 1 for open-graded mixes and as 0 for gap- and dense-graded mixes. The regression equation is:

500 Hz = 93.0 + 0.892 ln(Wheelpath Absorption) + 1.37 Surface Type
S = 2.46298 R-Sq = 25.2% R-Sq(adj) = 22.6%

Surface type turned out to be insignificant when included with wheelpath absorption in the regression. Figure 19 showed that absorption affects open-graded mixes and dense-graded mixes differently. Therefore, separate regression analyses were conducted for different surface types.

8.1.2 Open-Graded Mixes

The regression equation is:

500 Hz = 96.4 + 1.95 ln(Wheelpath Absorption)
S = 2.81461 R-Sq = 19.2% R-Sq(adj) = 16.3%

8.1.3 Gap- and Dense-Graded Mixes

The regression equation is:

500 Hz = 87.9 - 0.694 ln(Wheelpath Absorption)
S = 1.71152 R-Sq = 5.3% R-Sq(adj) = 1.8%

According to the regression analysis, absorption was found to be significant for open-graded mixes but insignificant for dense- and gap-graded mixes. Increasing absorption at 500 Hz increases the noise levels for

open-graded mixes; however, this result likely occurs because the lower frequency levels are affected by texture, and open-graded mixes have higher texture and hence higher noise levels than gap- and dense-graded mixes.

8.2 Regression Analysis for OBSI at 630 Hz

8.2.1 Combined Data Set

The 630-Hz sound intensity levels were explained by absorption and surface type. The regression equation is:

630 Hz = 94.2 + 0.754 Surface Type + 0.751 ln(Wheelpath Absorption)
S = 2.20496 R-Sq = 17.6% R-Sq(adj) = 14.7%

Surface type and absorption were found to be insignificant in the regression, perhaps because surface type and absorption values are highly correlated. Therefore, separate regression analyses were conducted for different surface types.

8.2.2 Open-Graded Mixes

The regression equation is:

630 Hz = 97.4 + 2.03 ln(Wheelpath Absorption)
S = 2.20242 R-Sq = 29.6% R-Sq(adj) = 27.1%

8.2.3 Gap- and Dense-Graded Mixes

The regression equation is:

630 Hz = 88.0 - 1.17 ln(Wheelpath Absorption)
S = 1.71772 R-Sq = 13.7% R-Sq(adj) = 10.5%

According to the regression analysis, absorption was found to be significant for both surface types. Increasing absorption increases the sound intensity levels for open-graded mixes, and it reduces the noise levels for gap- and dense-graded mixes. Increasing absorption increases the noise levels at 630 Hz because the lower frequency levels are affected by texture, and open-graded mixes have higher texture and hence higher noise levels than gap- and dense-graded mixes.

8.3 Regression Analysis for OBSI at 800 Hz

8.3.1 Combined Data Set

The 800-Hz sound intensity levels were explained by absorption and surface type. The regression equation is:

800 Hz = 98.2 – 0.255 ln(Wheelpath Absorption) – 1.26 Surface Type
S = 1.48794 R-Sq = 24.0% R-Sq(adj) = 21.3%

Wheelpath absorption turned out to be insignificant when included with surface type in the regression. However, according to Figure 21 there is a strong correlation between absorption values and sound intensity levels for dense- and gap-graded mixes. Therefore, separate regression analyses were conducted for different surface types.

8.3.2 Open-Graded Mixes

The regression equation is:

800 Hz = 98.0 + 0.317 ln(Wheelpath Absorption)
S = 1.72579 R-Sq = 1.6% R-Sq(adj) = 0.0%

8.3.3 Gap- and Dense-Graded Mixes

The regression equation is:

800 Hz = 95.4 – 1.11 ln(Wheelpath Absorption)
S = 1.04034 R-Sq = 28.2% R-Sq(adj) = 25.5%

According to the regression analysis, absorption was found to be significant for gap- and dense-graded mixes but insignificant for open-graded mixes. Increasing absorption reduces the noise levels of gap- and dense-graded mixes.

8.4 Regression Analysis for OBSI at 1,000 Hz

The 1,000-Hz sound intensity levels were explained by absorption and surface type.
The regression equation is:

1,000 Hz = 95.7 – 0.777 ln(Wheelpath Absorption) – 1.63 Surface Type
S = 1.49278 R-Sq = 48.8% R-Sq(adj) = 46.9%

Increasing absorption reduces the sound intensity levels for open-, dense-, and gap-graded mixes at 1,000 Hz. At a given absorption value, open-graded mixes have lower sound intensity levels than gap- and dense-graded mixes.

8.5 Regression Analysis for OBSI at 1,250 Hz

According to Figure 23, increasing absorption values reduces the noise levels for open-, dense-, and gap-graded mixes. Therefore, only absorption values were used in the regression analysis. The regression equation is:

1,250 Hz = 88.6 – 1.99 ln(Wheelpath Absorption)
S = 1.69106 R-Sq = 54.5% R-Sq(adj) = 53.7%

Increasing absorption reduces the noise levels for open-, dense-, and gap-graded mixes.

8.6 Regression Analysis for OBSI at 1,600 Hz

According to Figure 24, increasing absorption values reduces the noise levels for open-, dense-, and gap-graded mixes. Therefore, only absorption values were used in the regression analysis. The regression equation is:

1,600 Hz = 85.3 – 2.47 ln(Wheelpath Absorption)
S = 1.64156 R-Sq = 66.1% R-Sq(adj) = 65.5%

Increasing absorption reduces the noise levels for open-, dense-, and gap-graded mixes.

9 SUMMARY AND CONCLUSIONS

This report presented the methodology and the results of a study of sound absorption measured on core samples from various pavement sections. It compared sound absorption values for different pavement types and correlated absorption values with the California On-Board Sound Intensity (OBSI) values. The findings of this study are as follows:

- Increasing air-void content increases the absorption values.
- Open-graded mixes have higher absorption values than gap- and dense-graded mixes.
- Increasing absorption reduces the noise levels at all frequencies for gap- and dense-graded mixes.
- For pavement types such as for open-graded mixes, where noise generation from surface texture is important, the effect of increased absorption changes gradually with frequency. At low frequencies (630 and 800 Hz), the sound intensity increases with higher absorption, but at high frequencies (1,000, 1,250, and 1,600 Hz), the sound intensity decreases with higher absorption. In other words, for open-graded mixes the expectation that increased sound absorption will reduce sound intensity is only true at high frequencies; for dense- and gap-graded mixes, however, the expected relationship between increased sound absorption and reduced sound intensity is true at all frequencies.
- Absorption values better explain the noise levels at higher frequencies. The average absorption values are the best predictors of OBSI levels at 1,600 Hz, with a correlation coefficient of 66 percent.

REFERENCES

1. Anderson, G. A. L. (December 1999). *An Investigation into the Factors Which Affect the Acoustical Characteristics of Bituminous Porous Road Surfaces*. PhD thesis. University of Ulster, Australia.
2. Hamet, J. F., and M. C. Berengier. (1993). "Acoustical Characteristics of Porous Pavements: A New Phenomenological Model." Proceedings: Inter-Noise 93: People Versus Noise. International Conference on Noise Control Engineering. Leuven, Belgium.
3. Berengier, M. C., M. R. Stinson, G. A. Daigle, and J. F. Hamet. (January 1997). Porous Road Pavements: Acoustical Characterization and Propagation Effects. *Journal of Acoustical Society of America*, Vol. 101, No. 1, pp. 155–162.
4. Berengier, M., J. F. Hamet, and P. Bar. (1990). Acoustical Properties of Porous Asphalts: Theoretical and Environmental Aspects. In *Transportation Research Record 1265*, Transportation Research Board, National Research Council, Washington, D.C., pp. 9–24.
5. Ongel, A., and E. Kohler. (November 2006). *Surface Condition and Road-Tire Noise on Caltrans Experimental Noise Reducing Pavement Sections*. University of California Pavement Research Center, UC Davis and Berkeley.
6. Ongel, A., J. Harvey, E. Kohler, Q. Lu, and B. Steven. (April 2007). *Investigation of Noise, Durability, Permeability, and Friction Performance Trends for Asphaltic Pavement Surface Types: First- and Second-Year Results,* University of California Pavement Research Center, UC Davis and Berkeley (in process).

APPENDIX

This appendix presents the spectral absorption for the sample cores at the center of the lane and in the wheelpath for each pavement section of the study. Readings outside the 200-to-1,700 Hz range are considered unreliable.

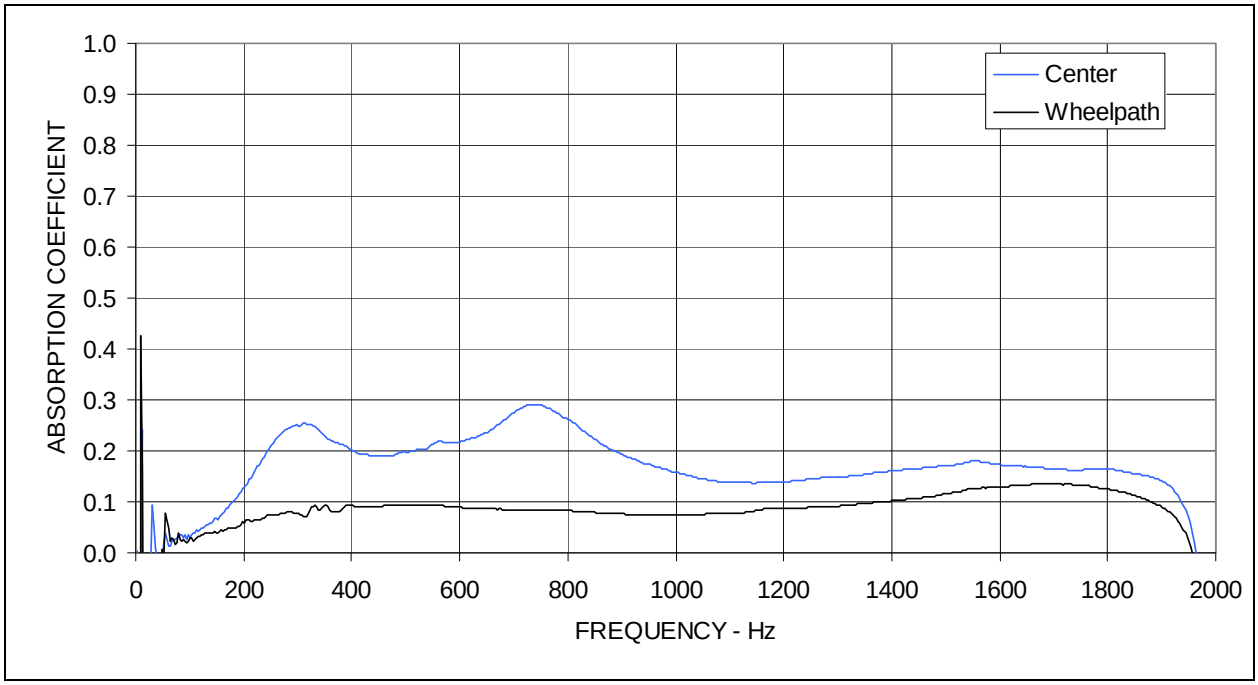

Figure A1: Sound absorption measured on cores from section ES01.

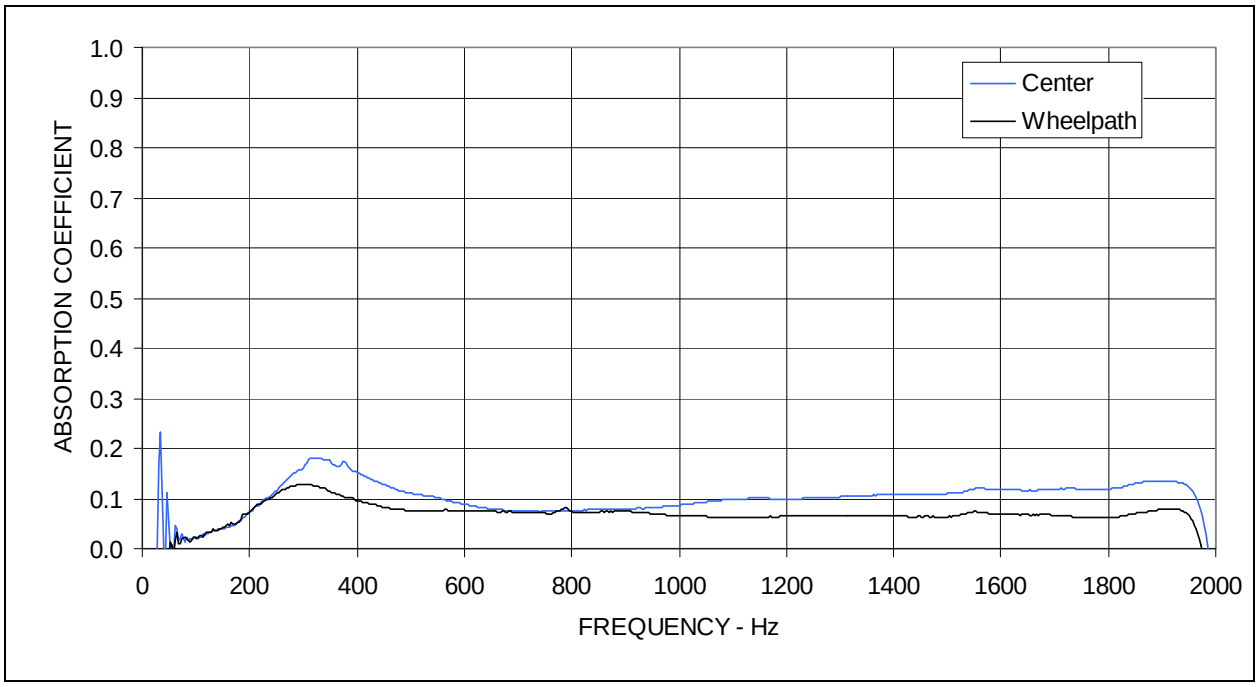

Figure A2: Sound absorption measured on cores from section ES03.

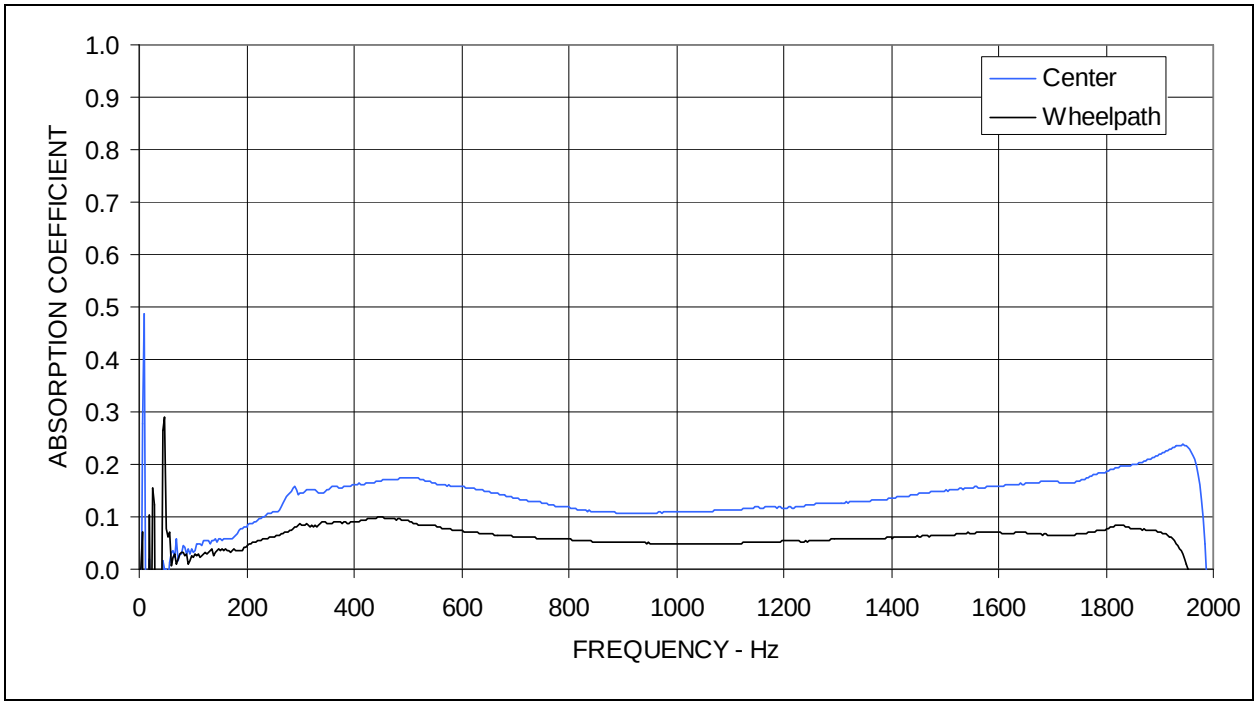

Figure A3: Sound absorption measured on cores from section ES05.

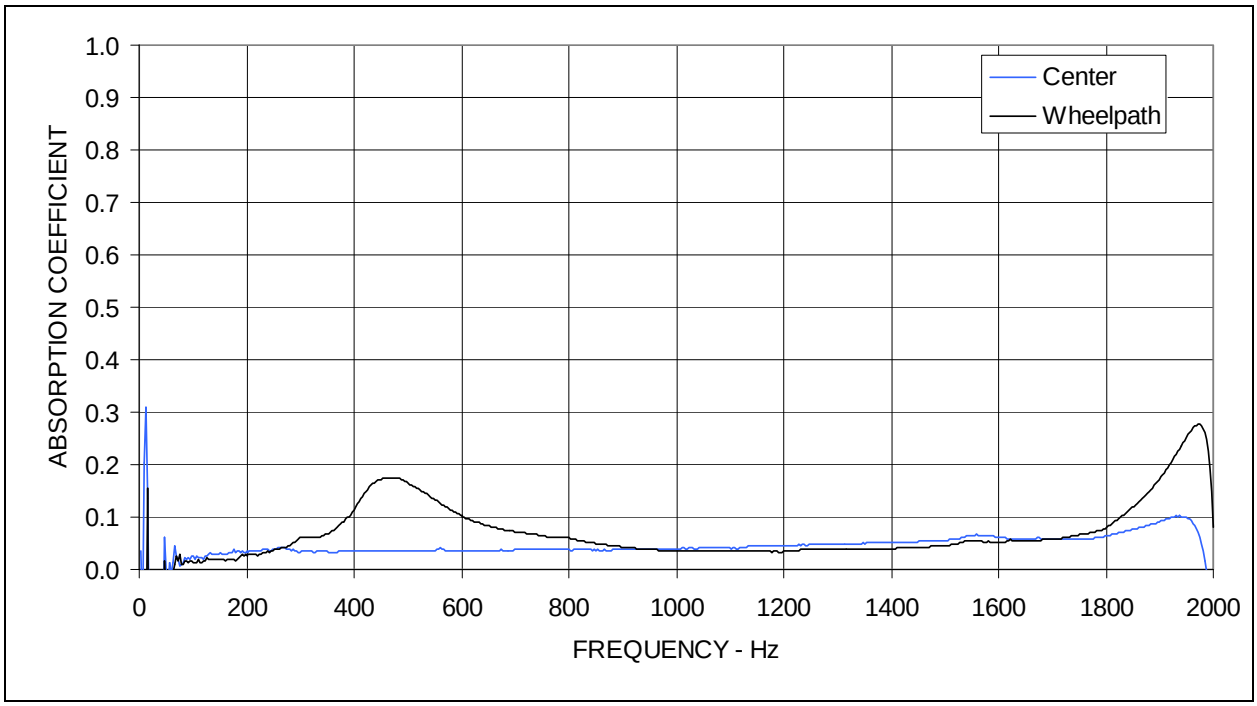

Figure A4: Sound absorption measured on cores from section ES07.

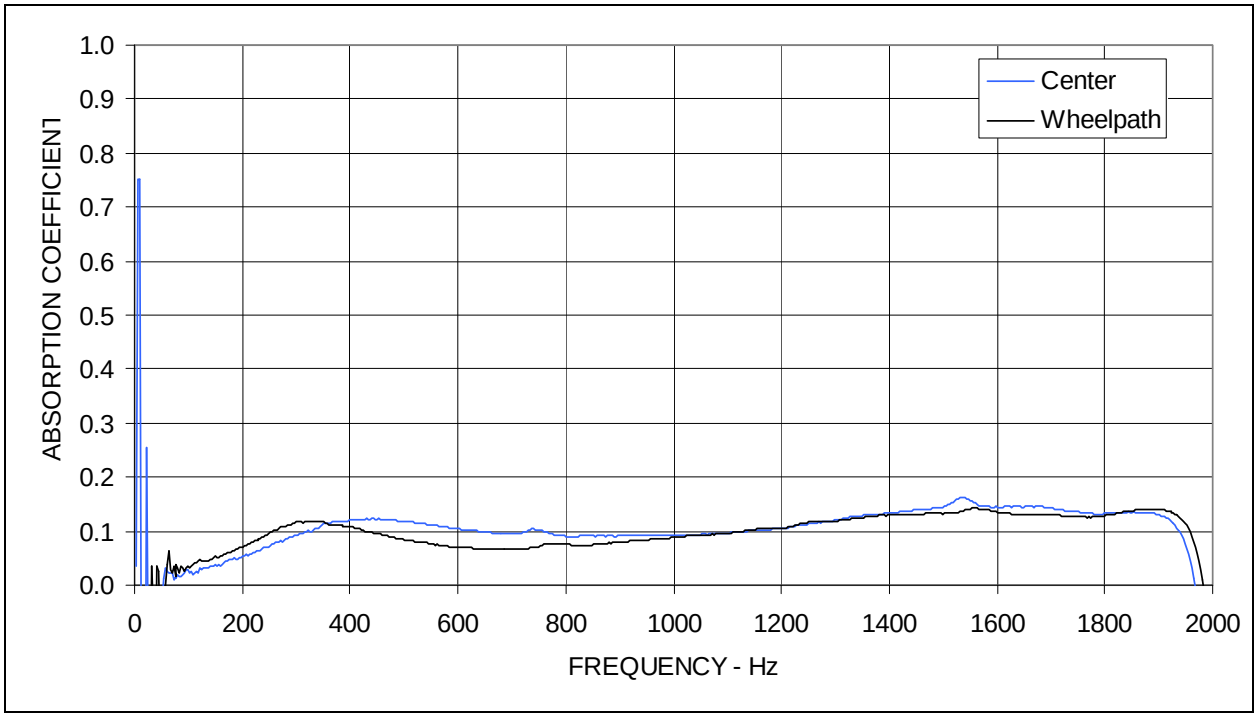

Figure A5: Sound absorption measured on cores from section ES10.

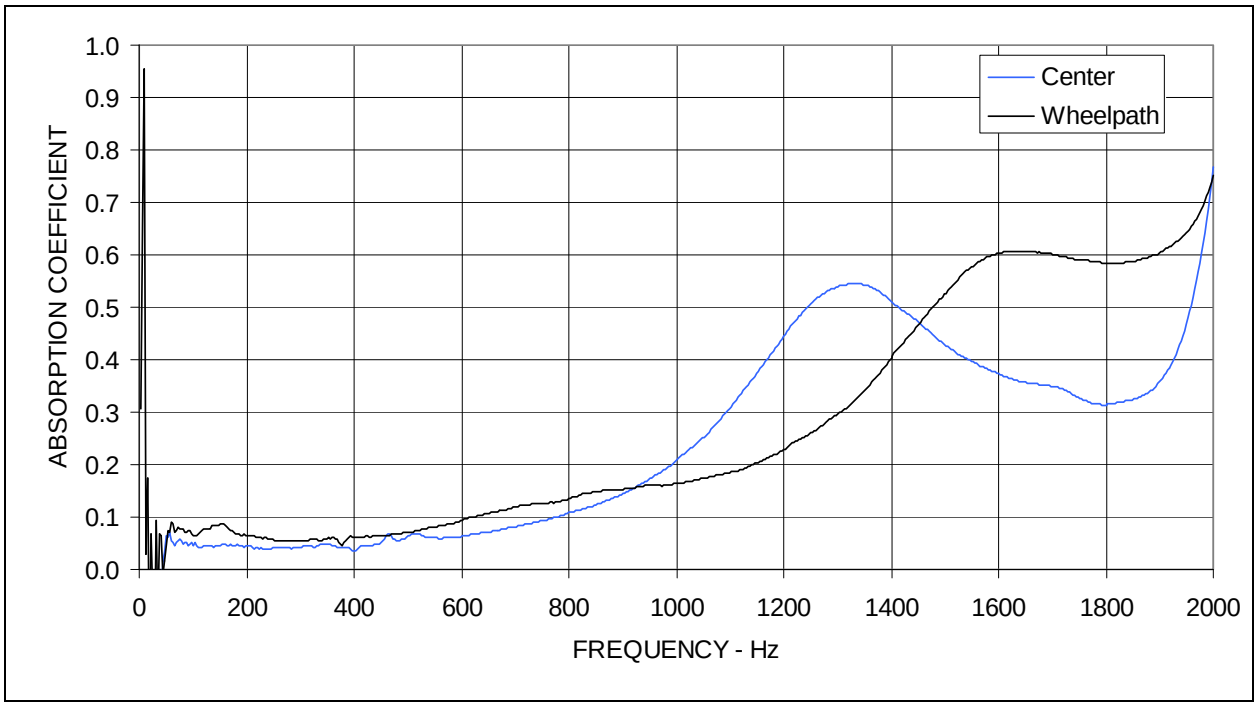

Figure A6: Sound absorption measured on cores from section ES11.

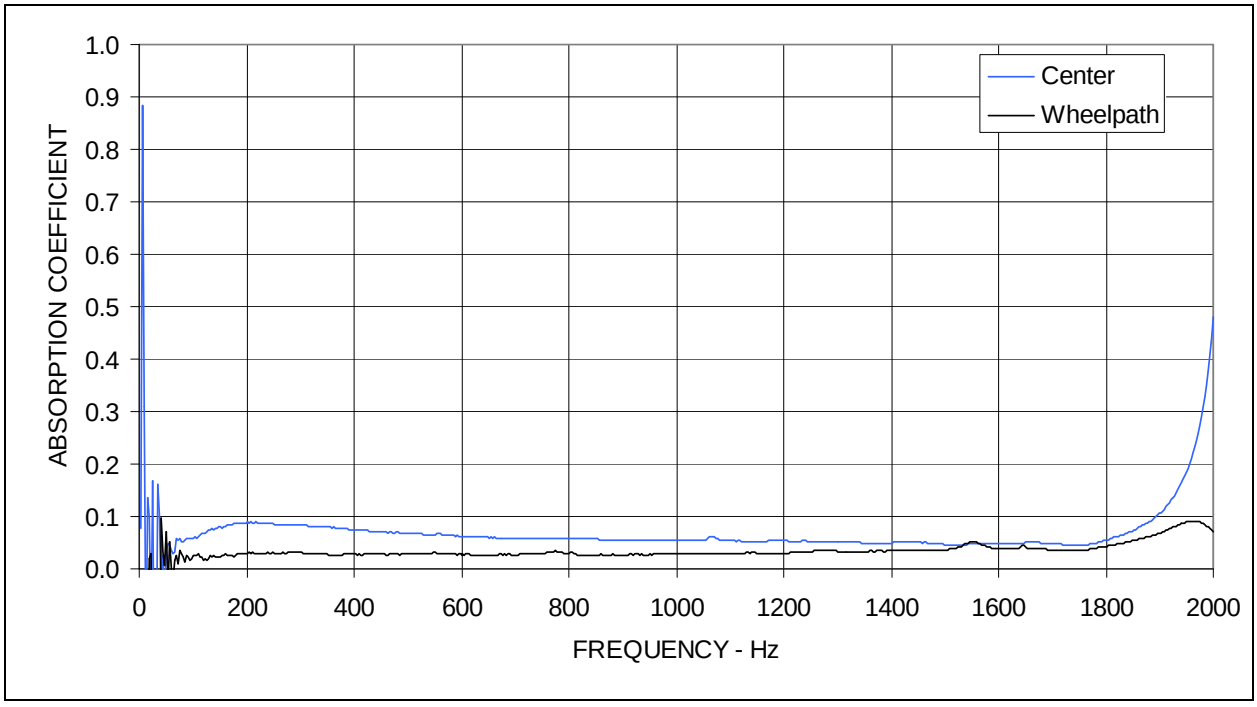

Figure A7: Sound absorption measured on cores from section ES12.

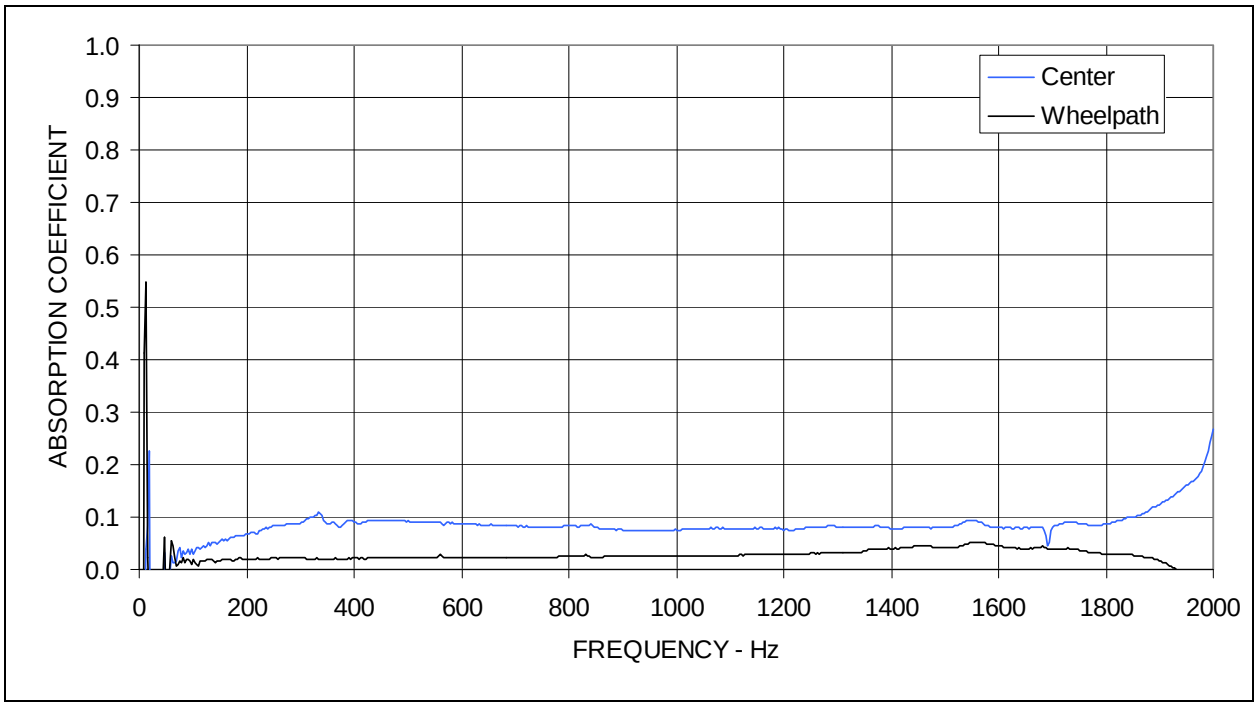

Figure A8: Sound absorption measured on cores from section ES13.

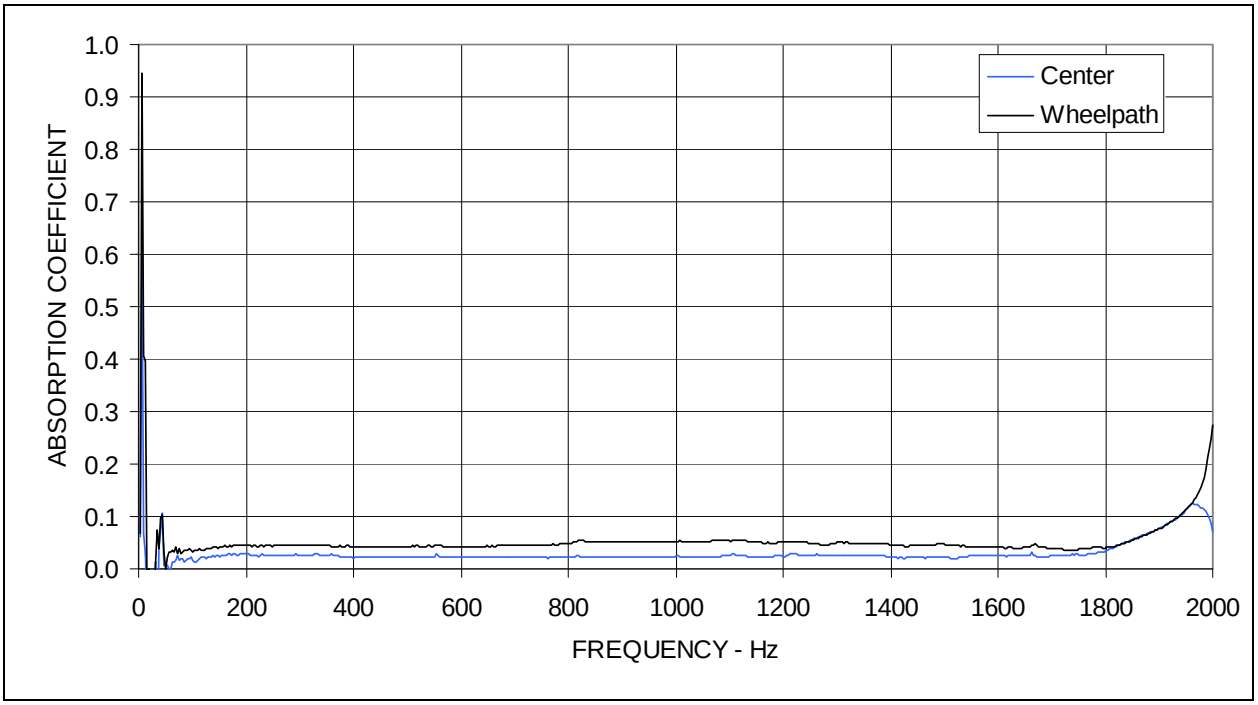

Figure A9: Sound absorption measured on cores from section ES14.

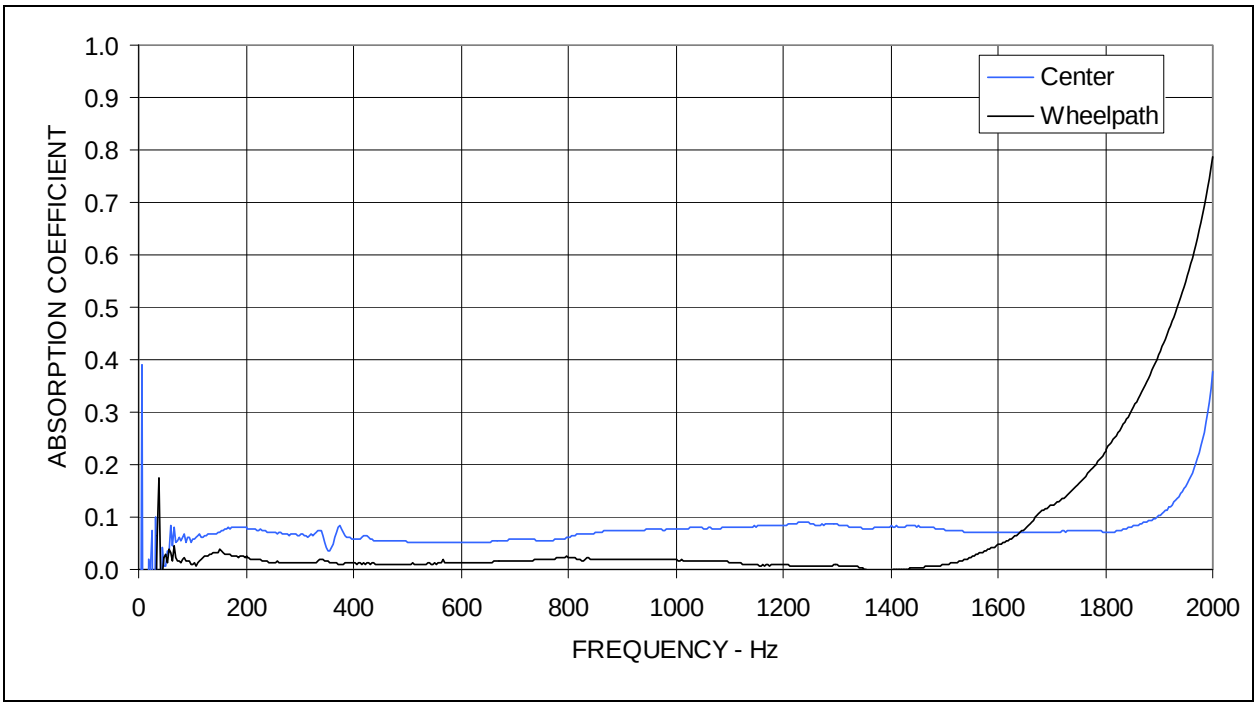

Figure A10: Sound absorption measured on cores from section ES15.

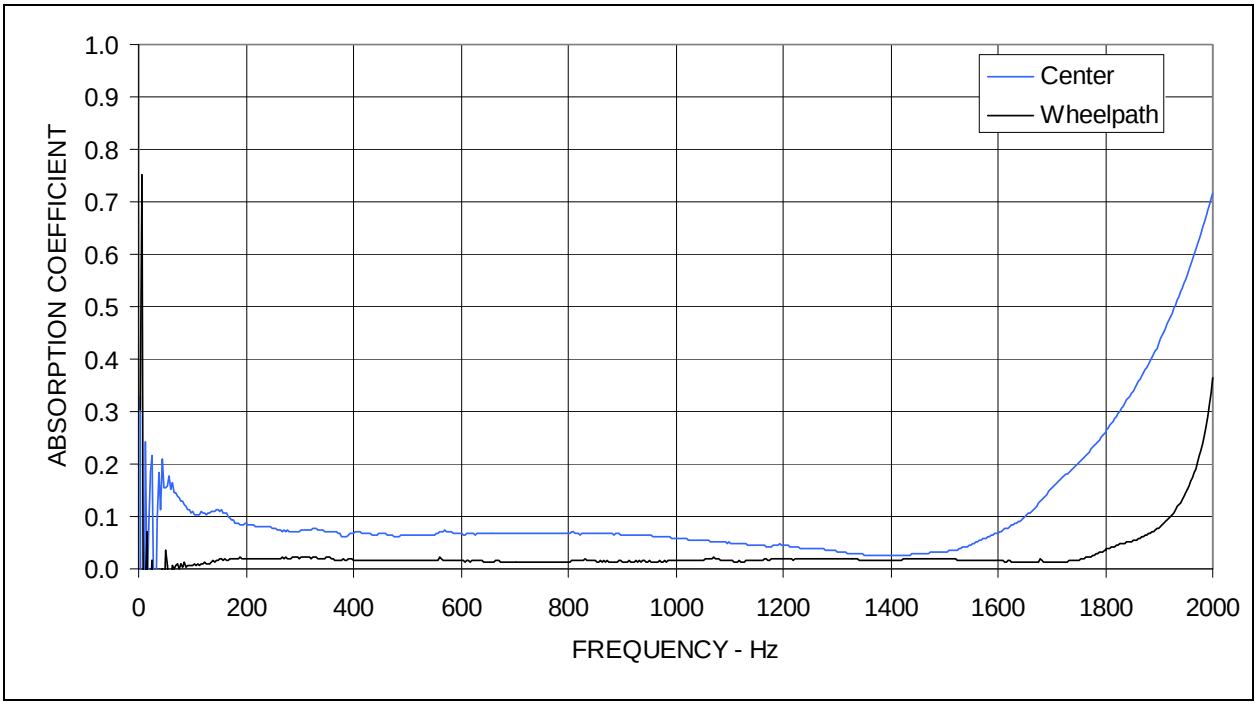

Figure A11: Sound absorption measured on cores from section ES16.

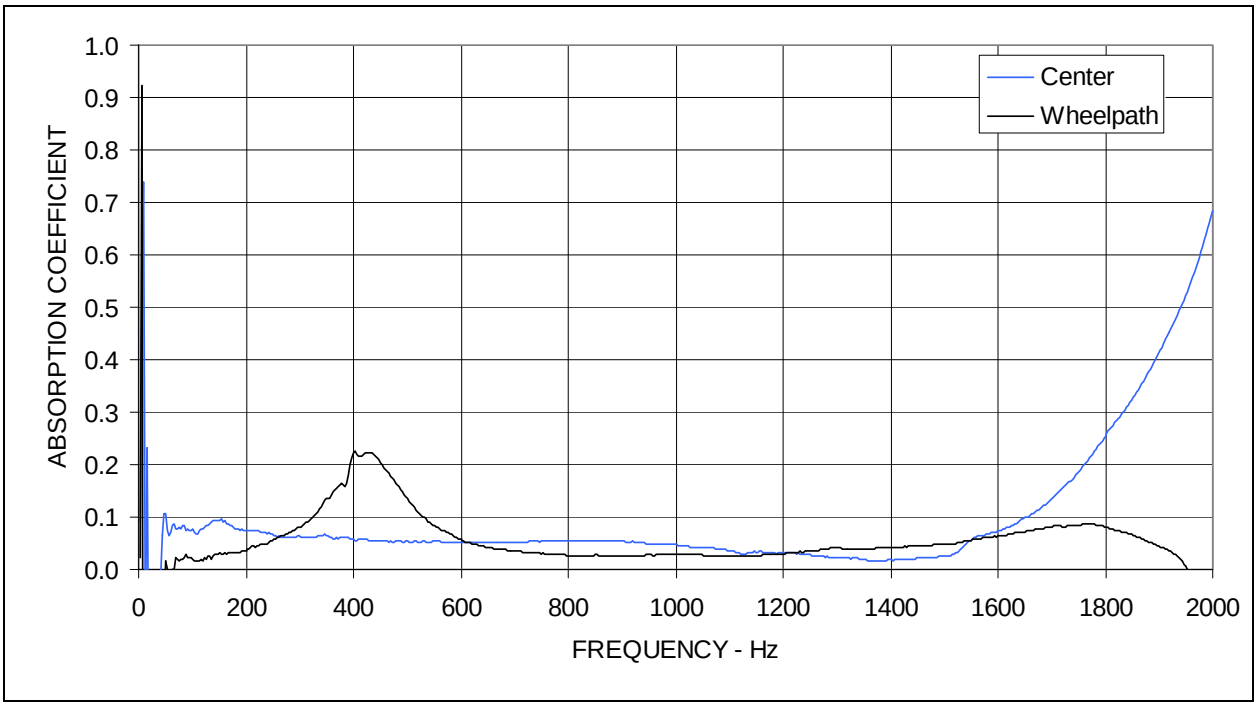

Figure A12: Sound absorption measured on cores from section ES17.

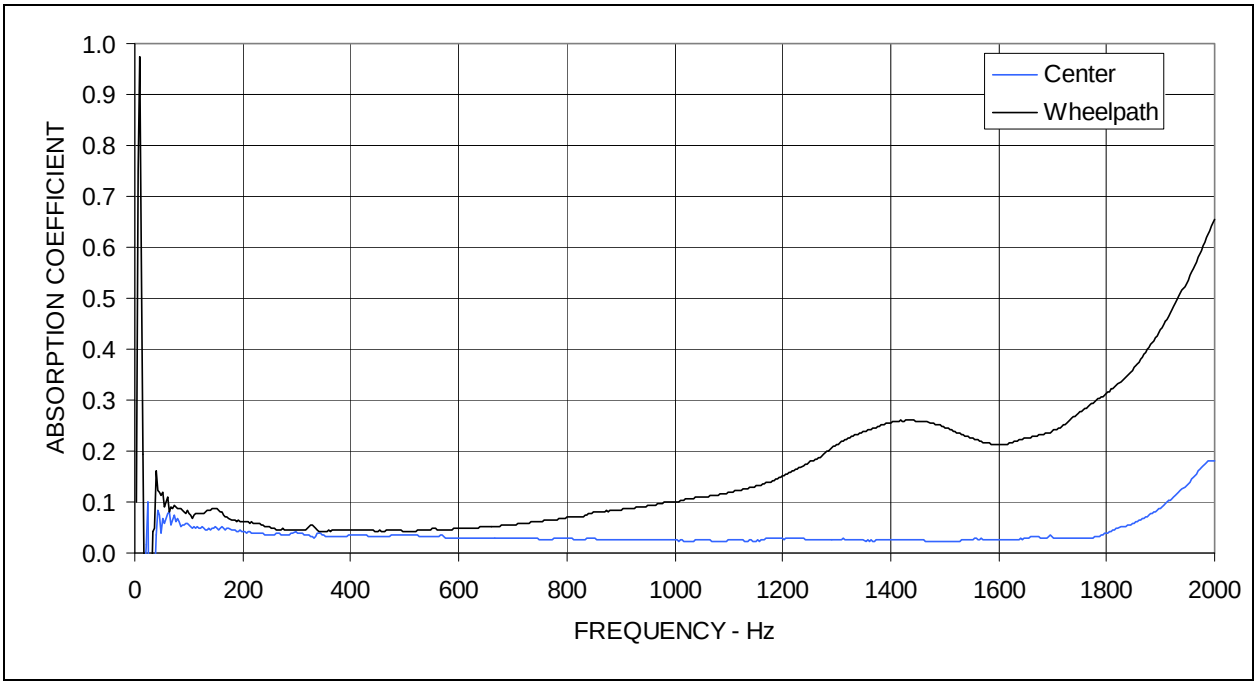

Figure A13: Sound absorption measured on cores from section ES18.

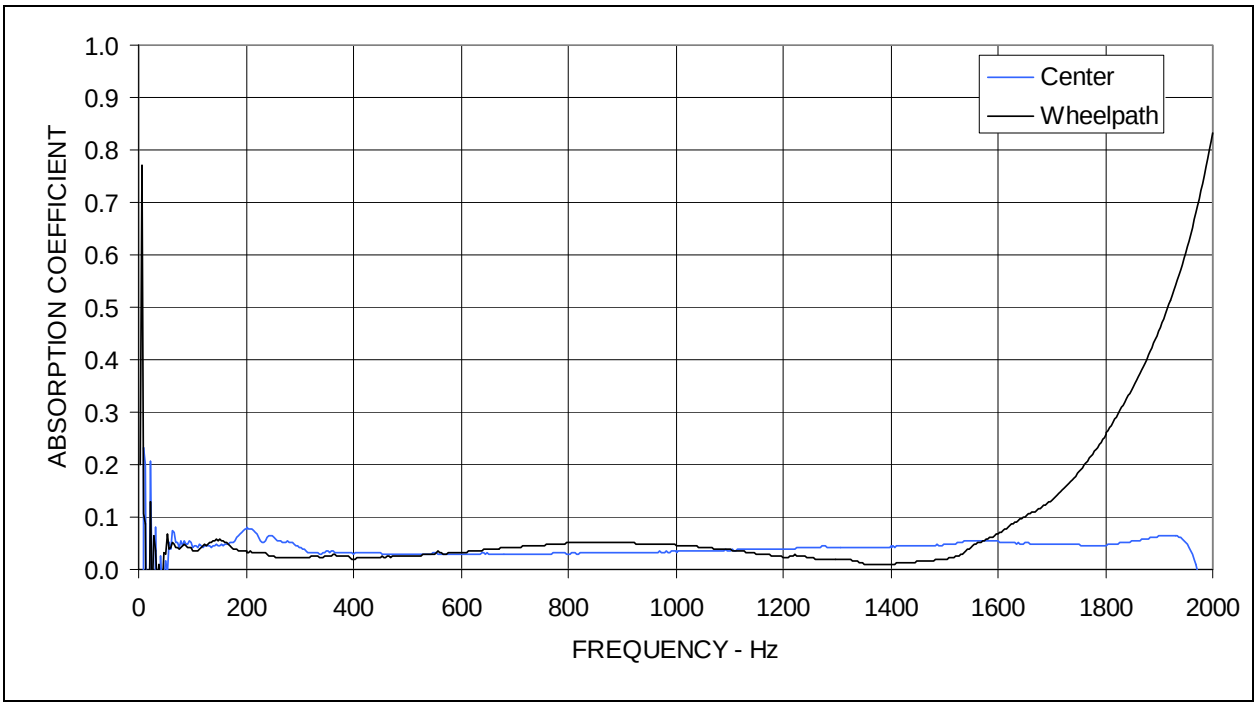

Figure A14: Sound absorption measured on cores from section ES19.

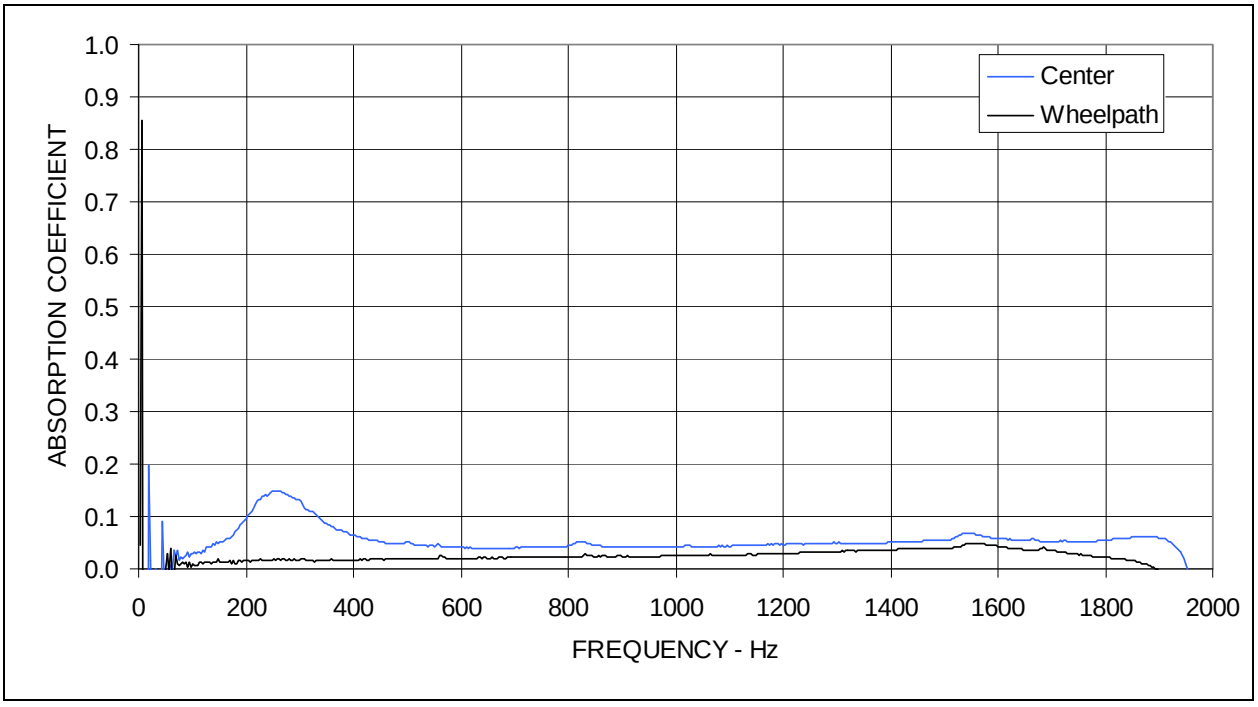

Figure A15: Sound absorption measured on cores from section ES20.

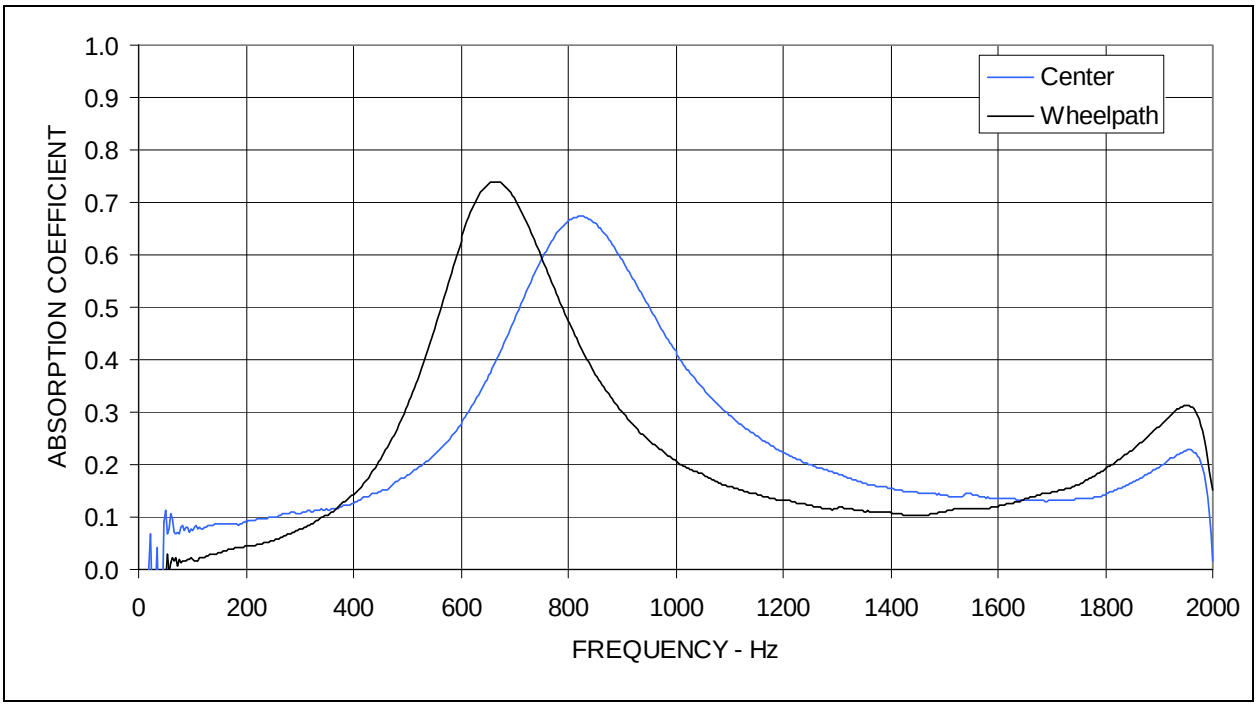

Figure A16: Sound absorption measured on cores from section ES21.

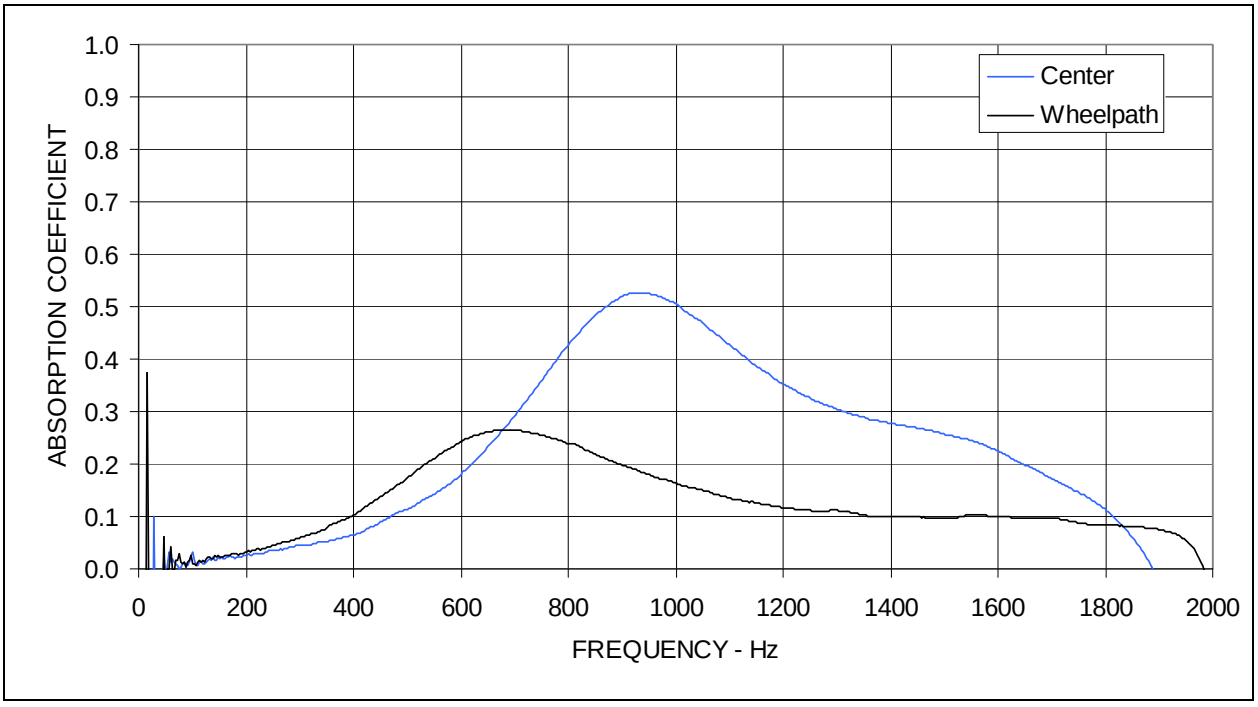

Figure A17: Sound absorption measured on cores from section ES22.

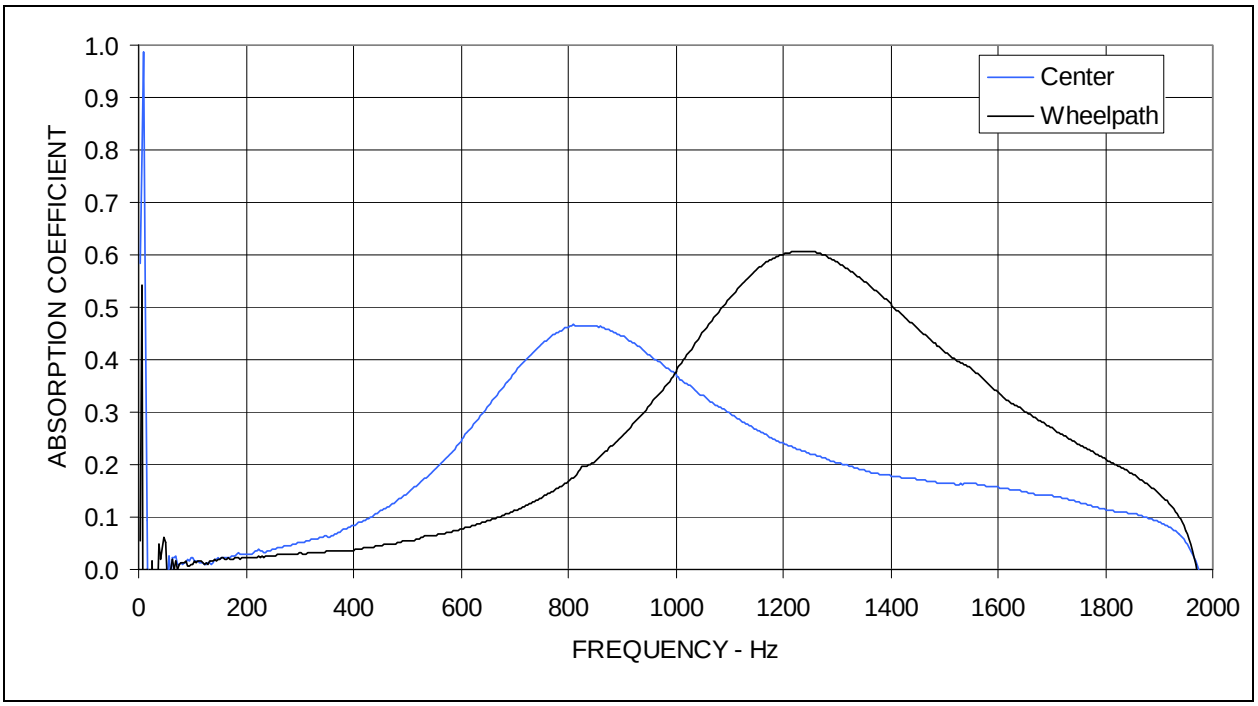

Figure A18: Sound absorption measured on cores from section ES23.

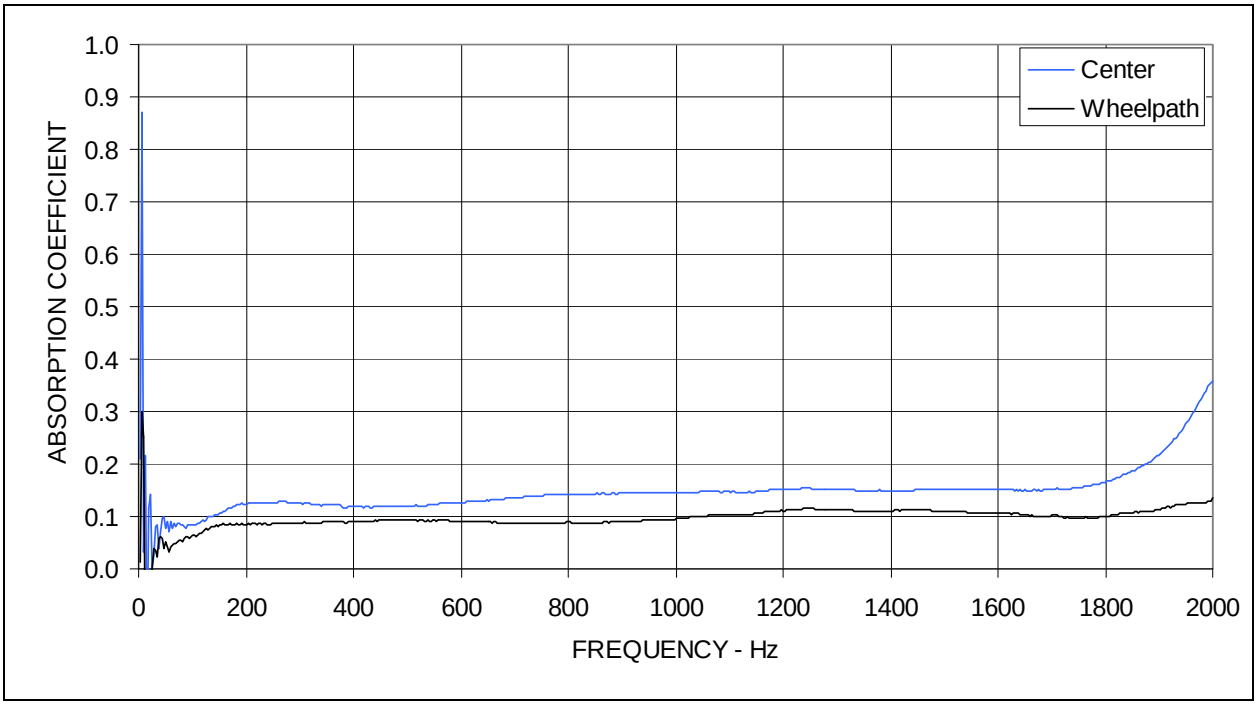

Figure A19: Sound absorption measured on cores from section QP02.

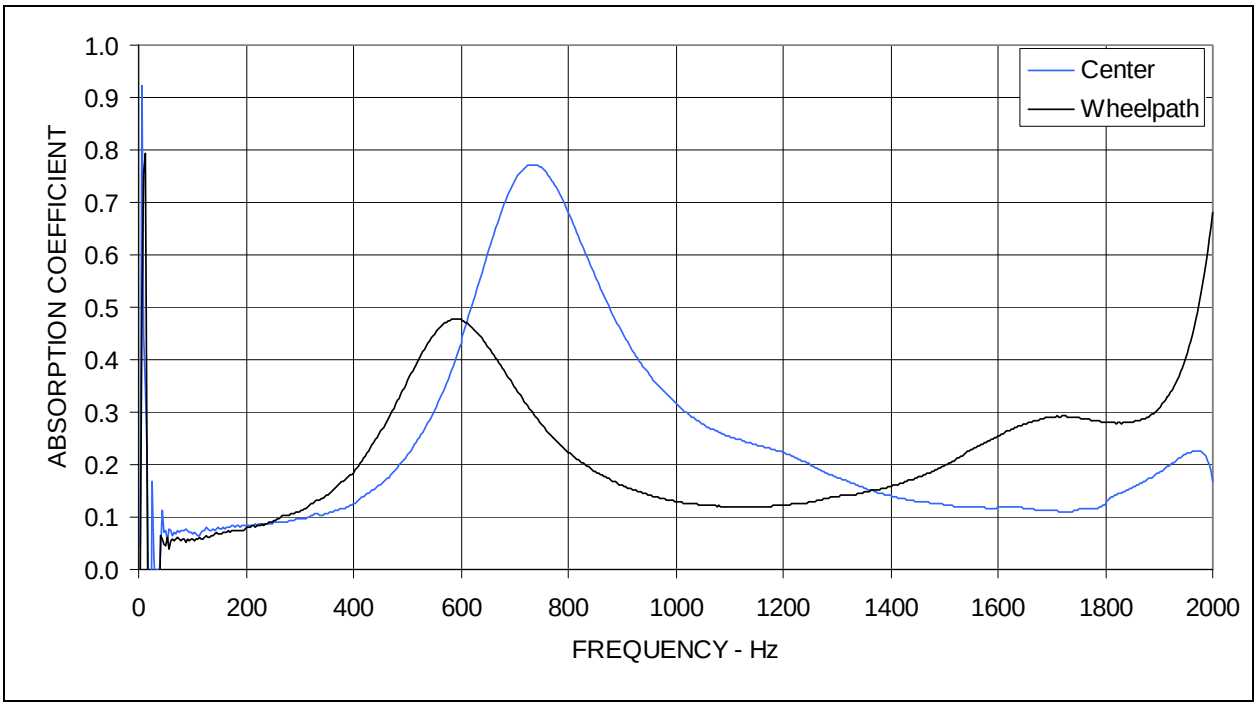

Figure A20: Sound absorption measured on cores from section QP03.

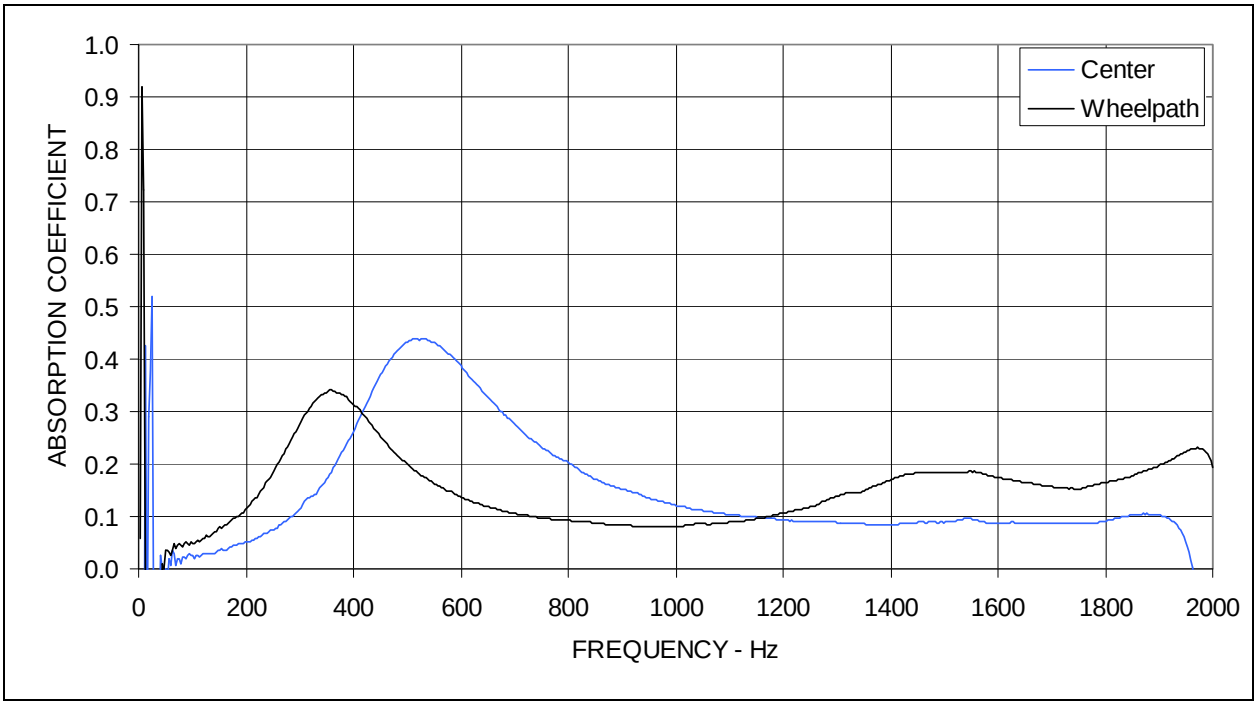

Figure A21: Sound absorption measured on cores from section QP04.

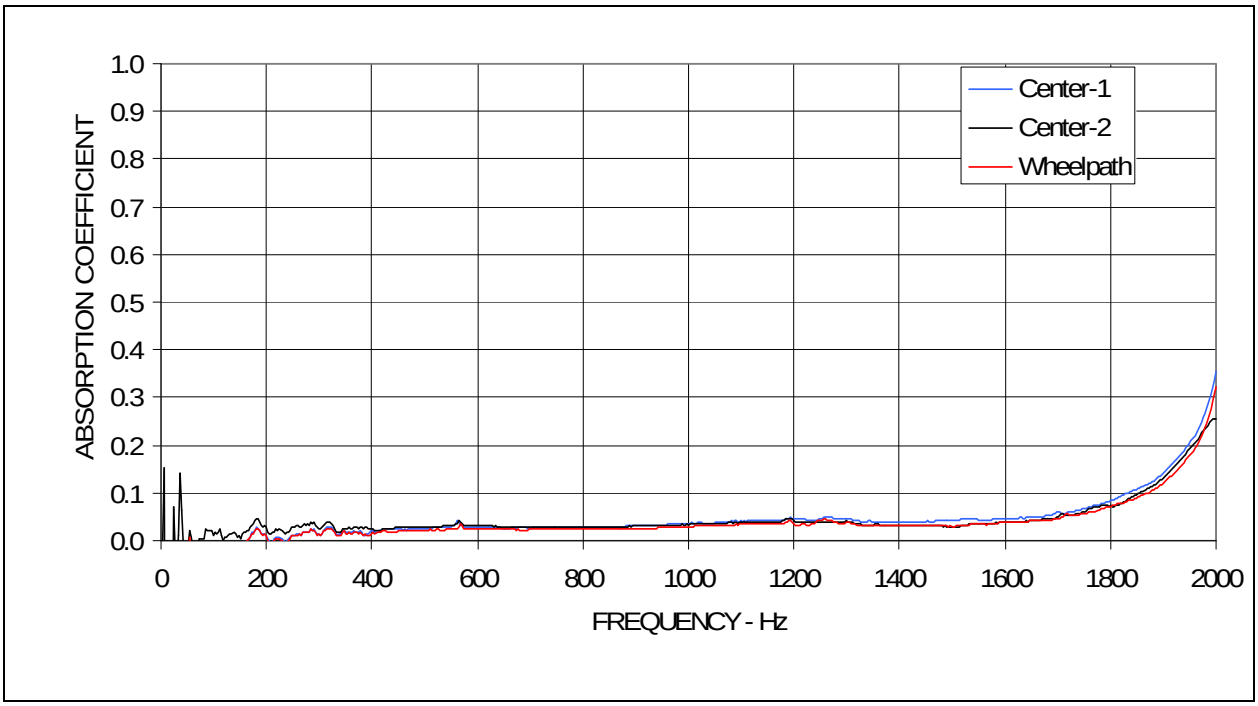

Figure A22: Sound absorption measured on cores from section QP05.

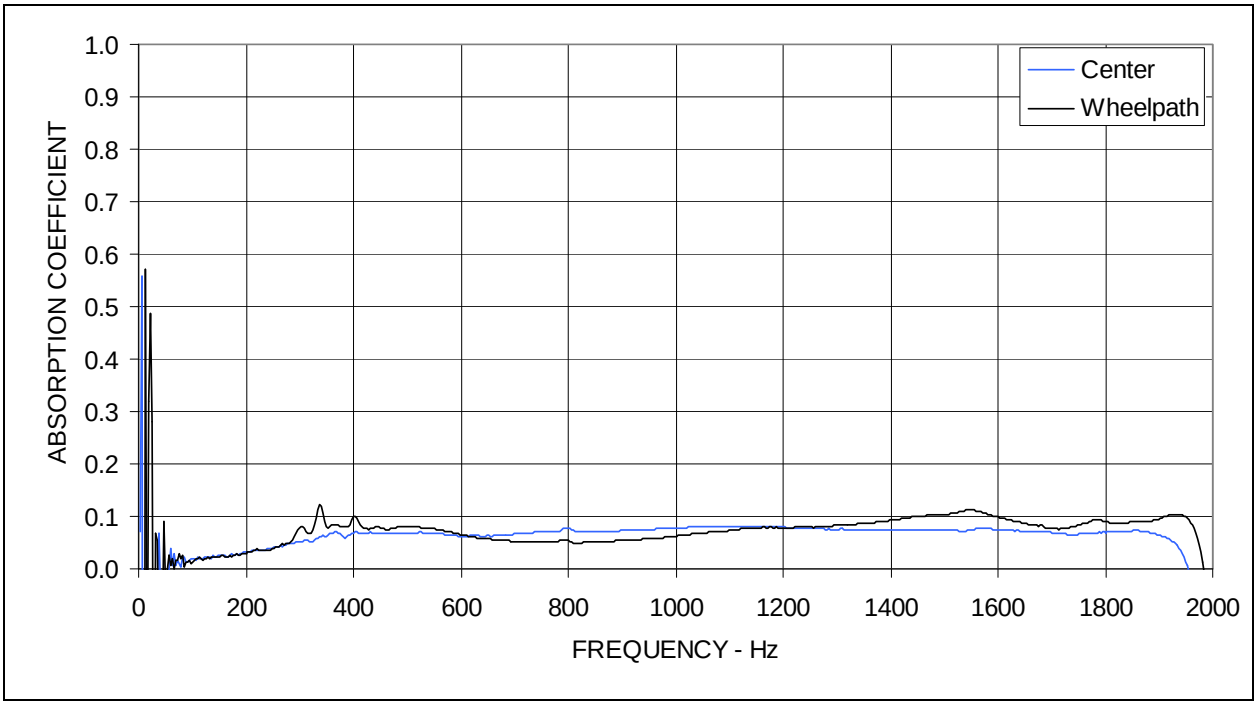

Figure A23: Sound absorption measured on cores from section QP06.

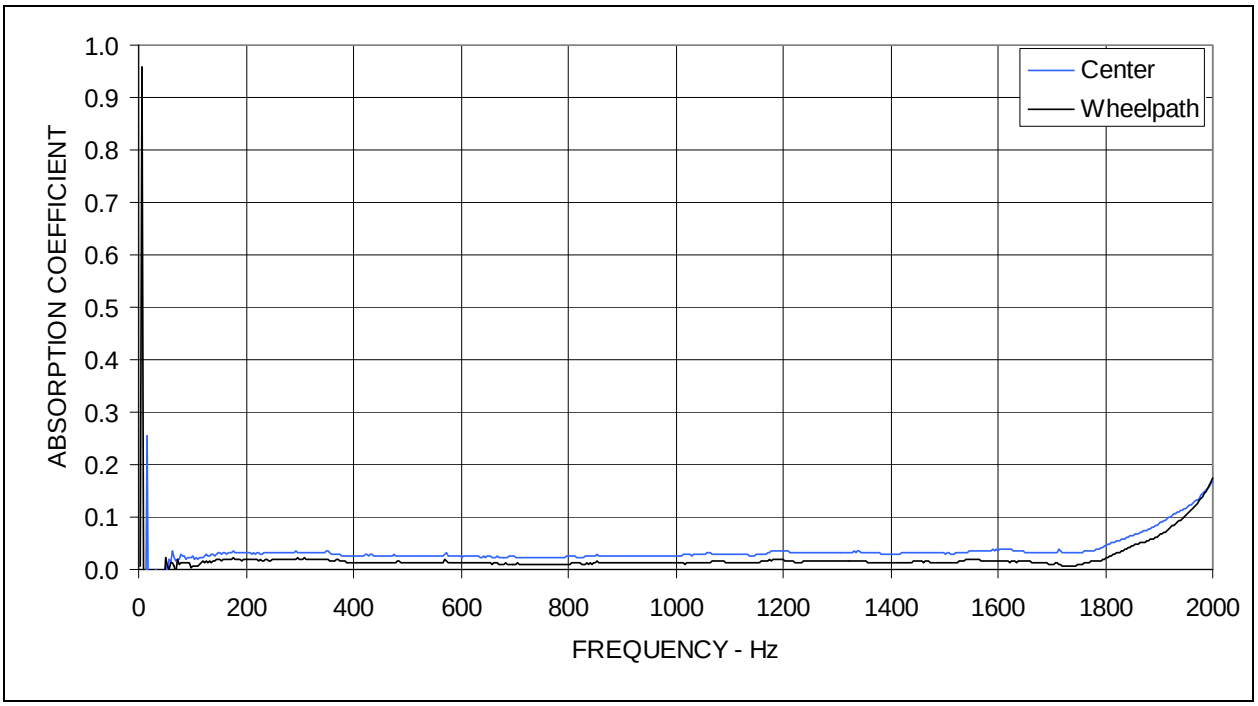

Figure A24: Sound absorption measured on cores from section QP07.

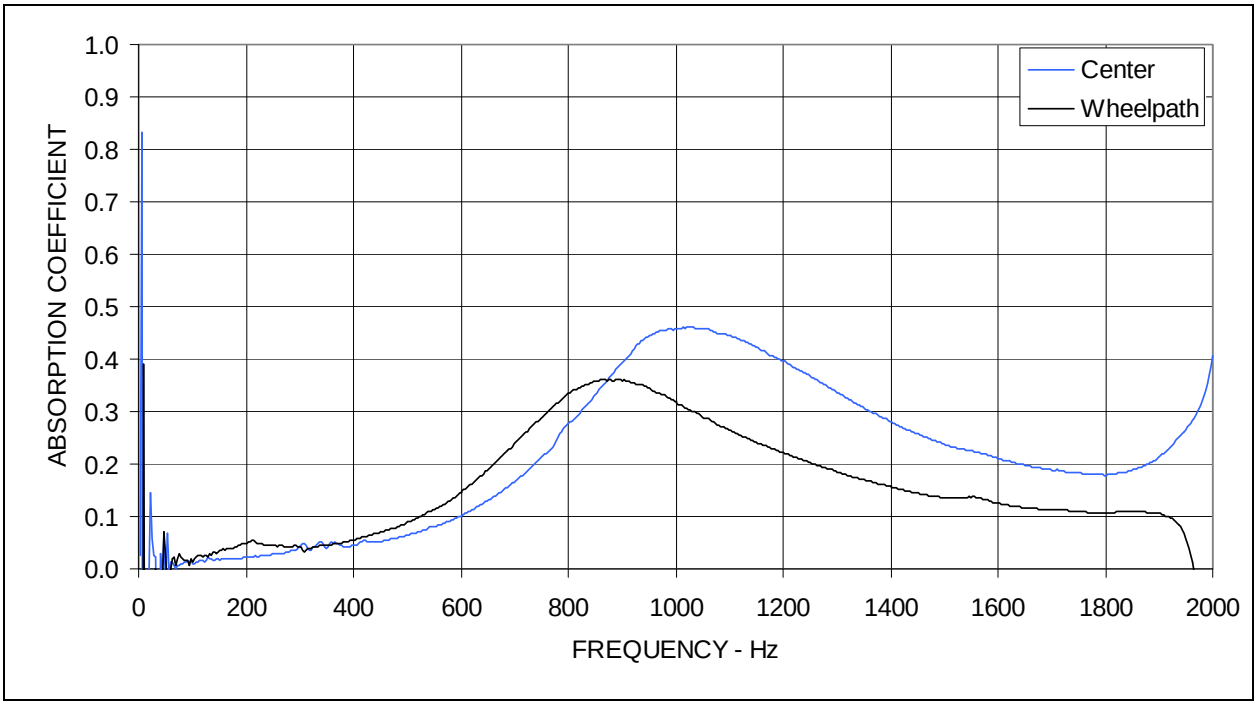

Figure A25: Sound absorption measured on cores from section QP08.

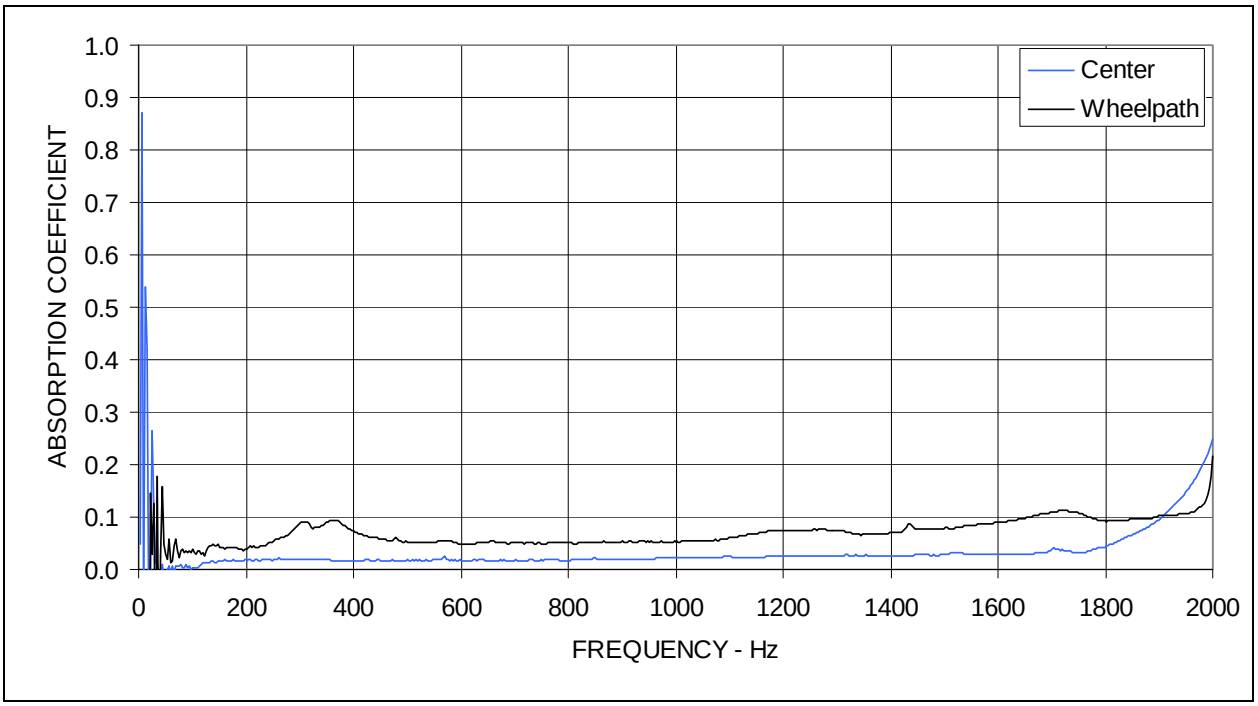

Figure A26: Sound absorption measured on cores from section QP09.

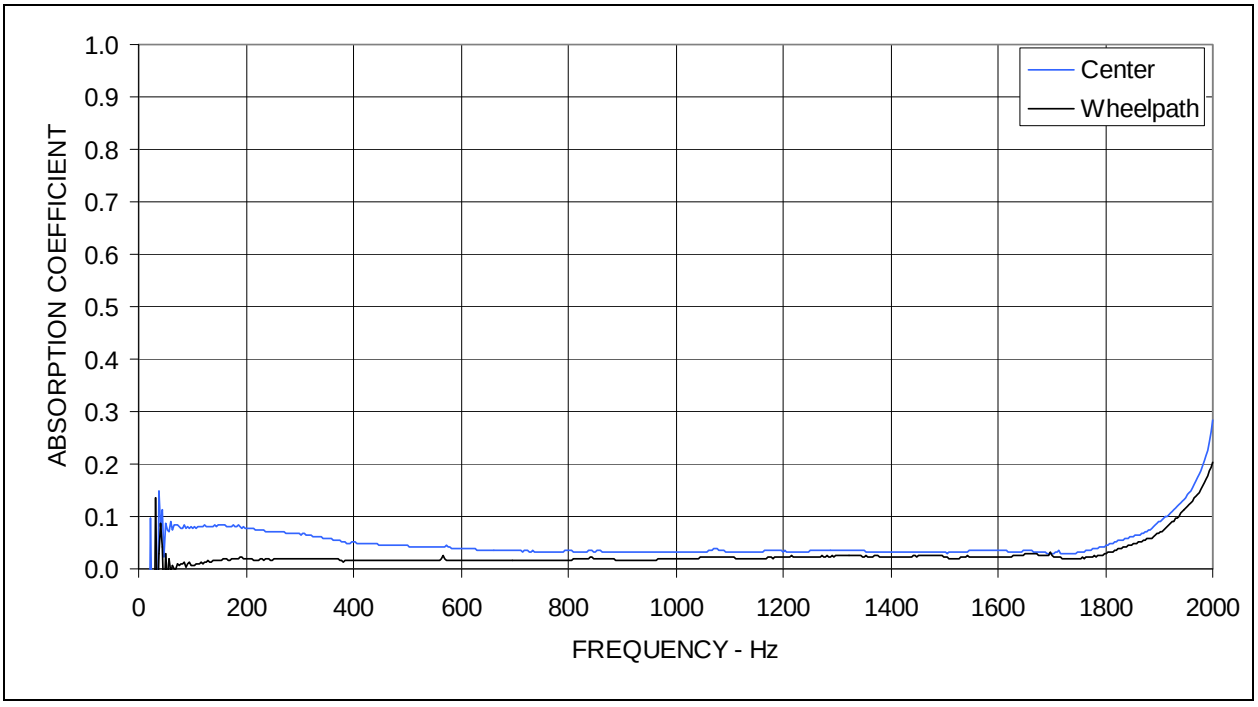

Figure A27: Sound absorption measured on cores from section QP10.

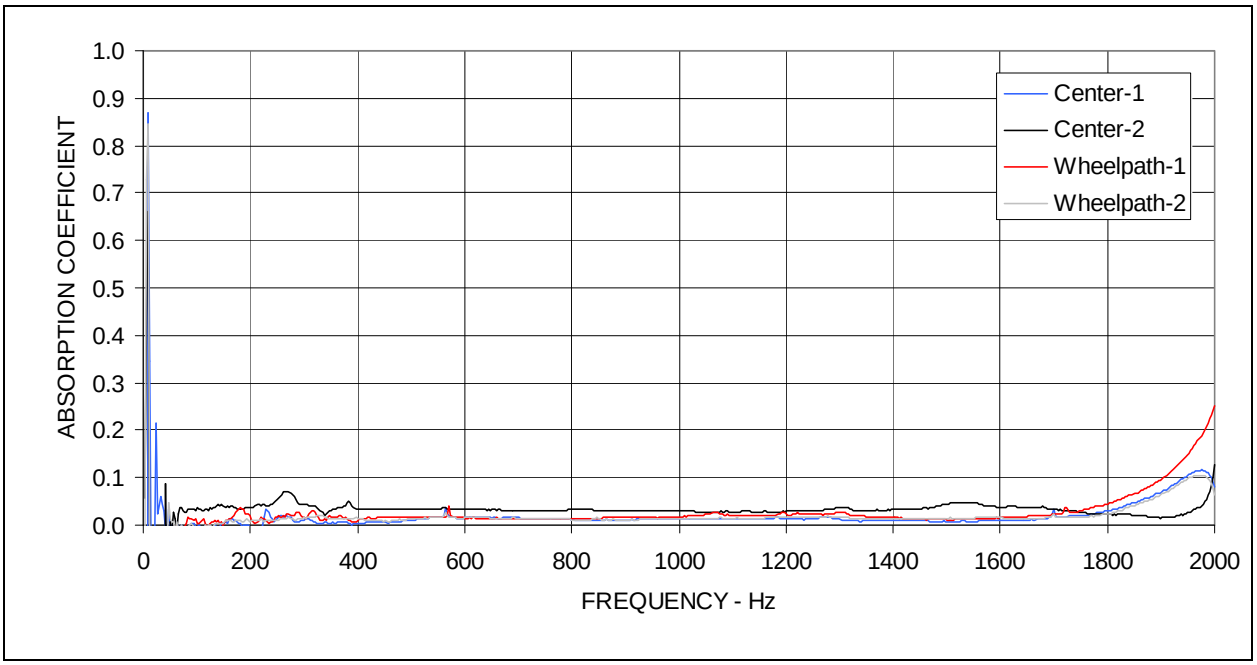

Figure A28: Sound absorption measured on cores from section QP11.

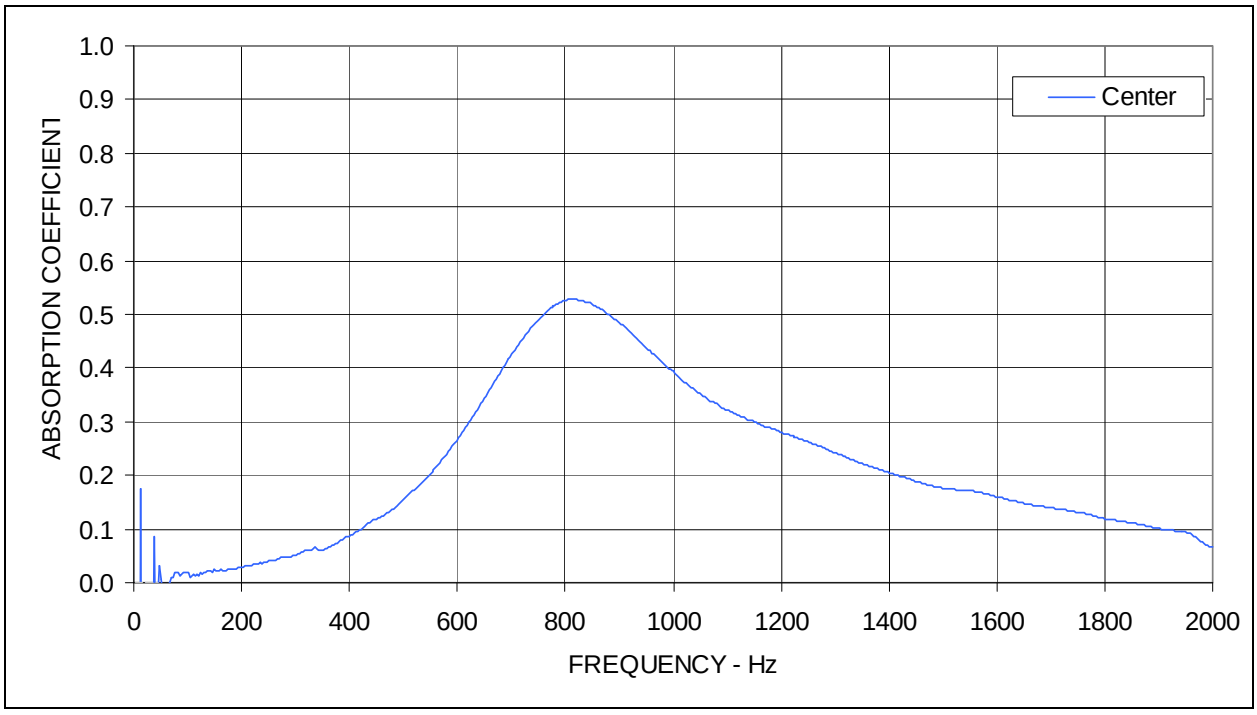

Figure A29: Sound absorption measured on cores from section QP12.

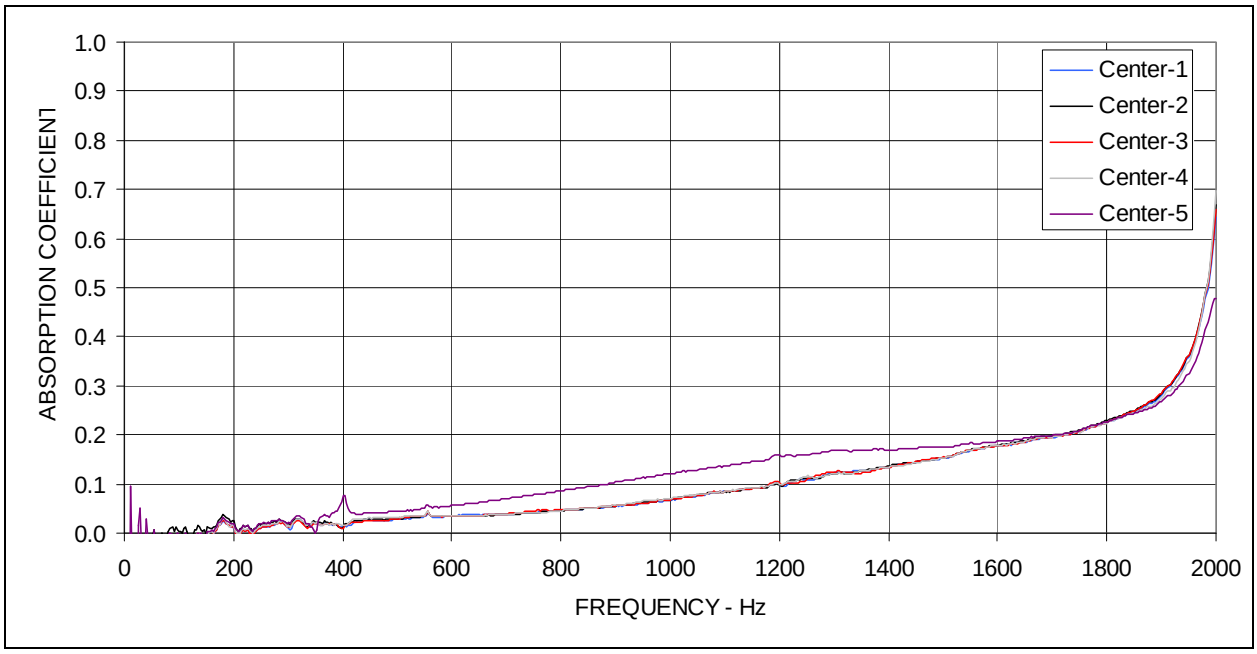

Figure A30: Sound absorption measured on cores from section QP13.

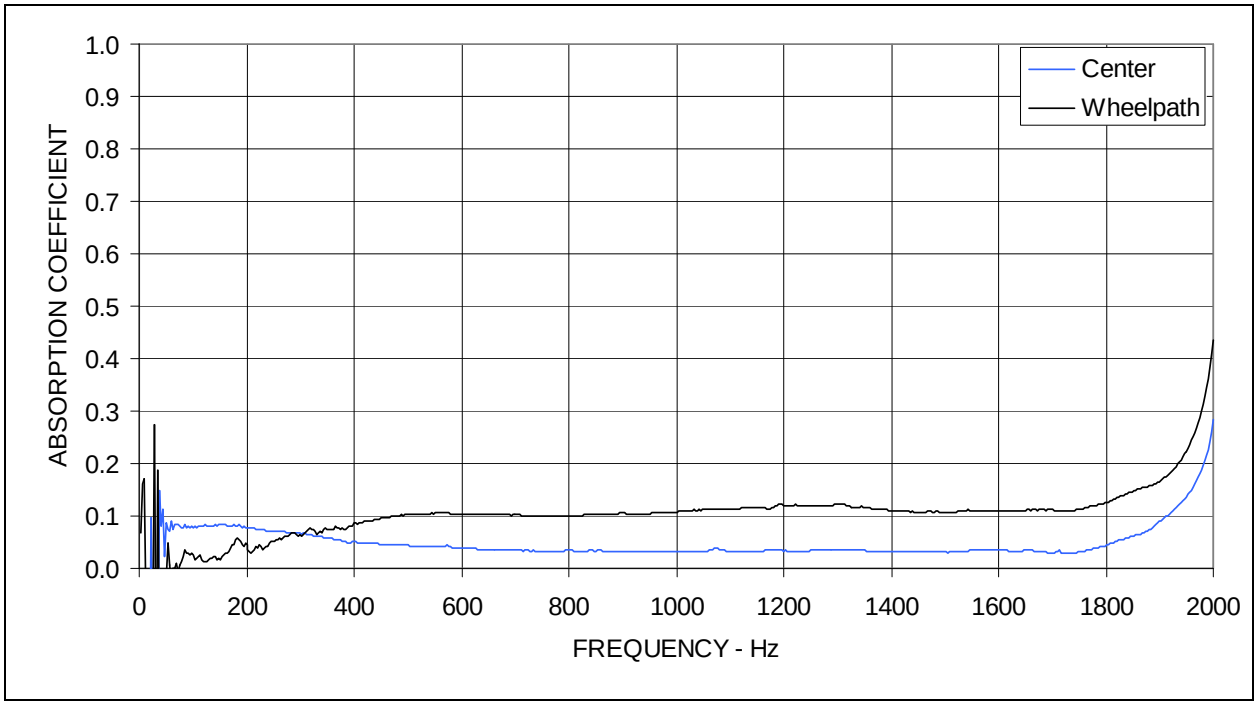

Figure A31: Sound absorption measured on cores from section QP14.

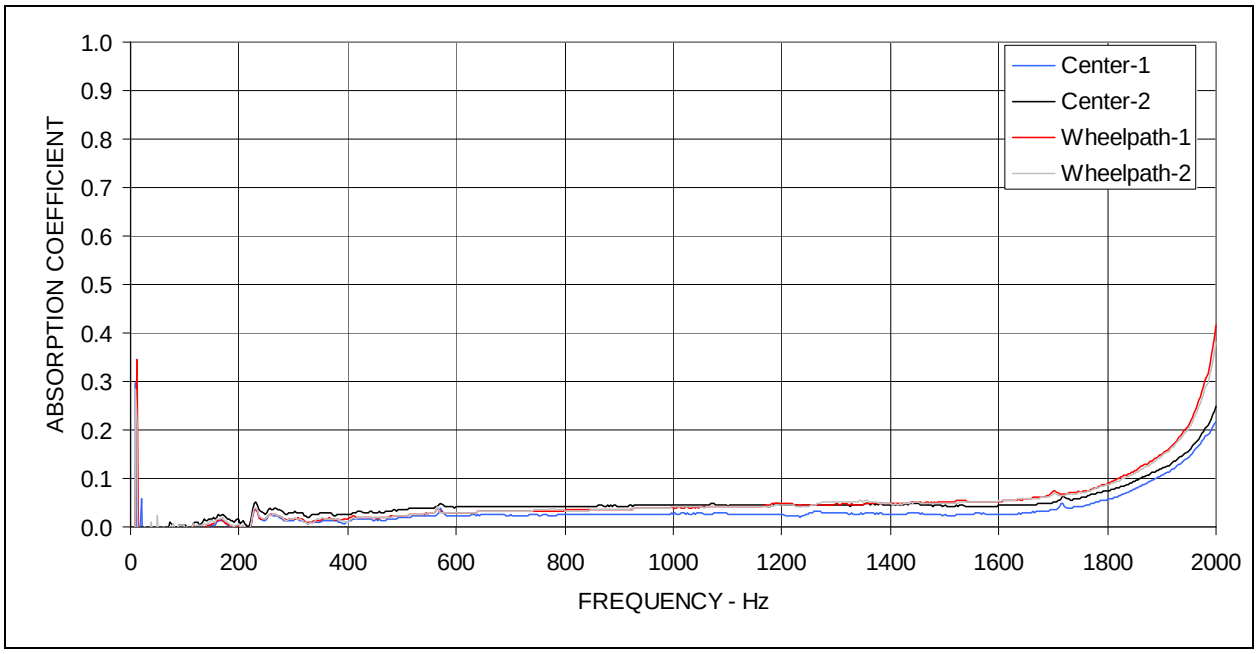

Figure A320: Sound absorption measured on cores from section QP15.

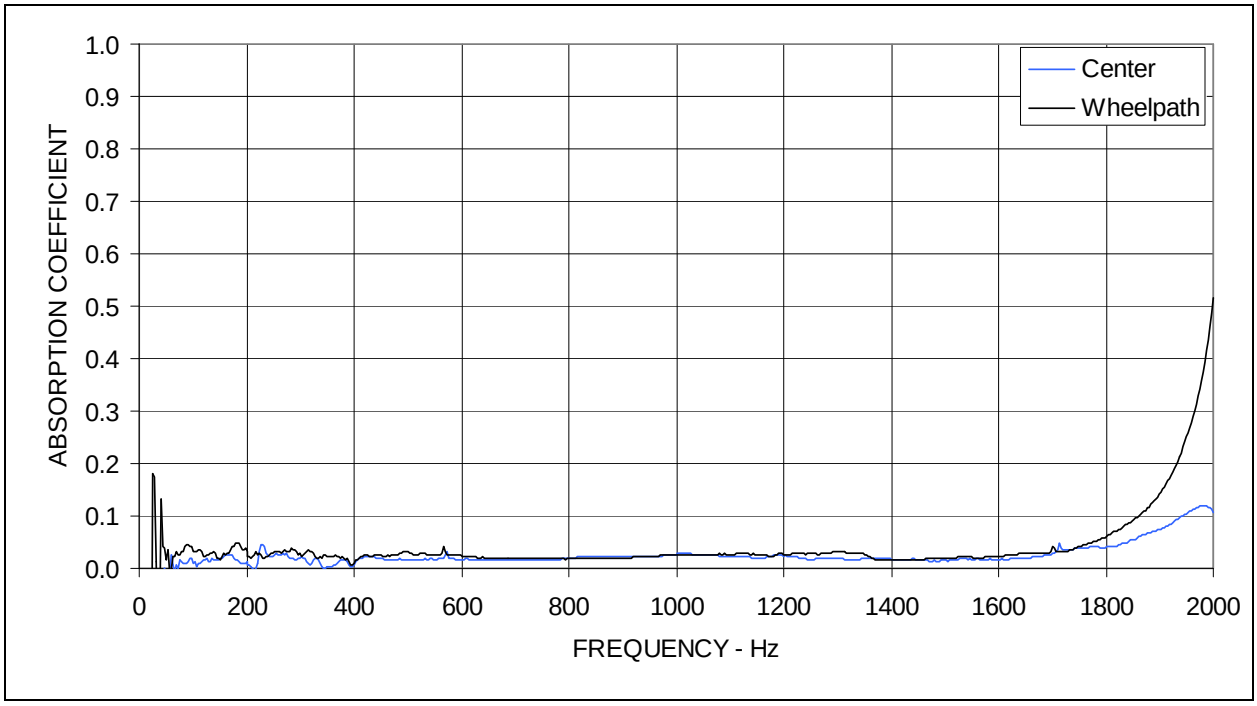

Figure A33: Sound absorption measured on cores from section QP16.

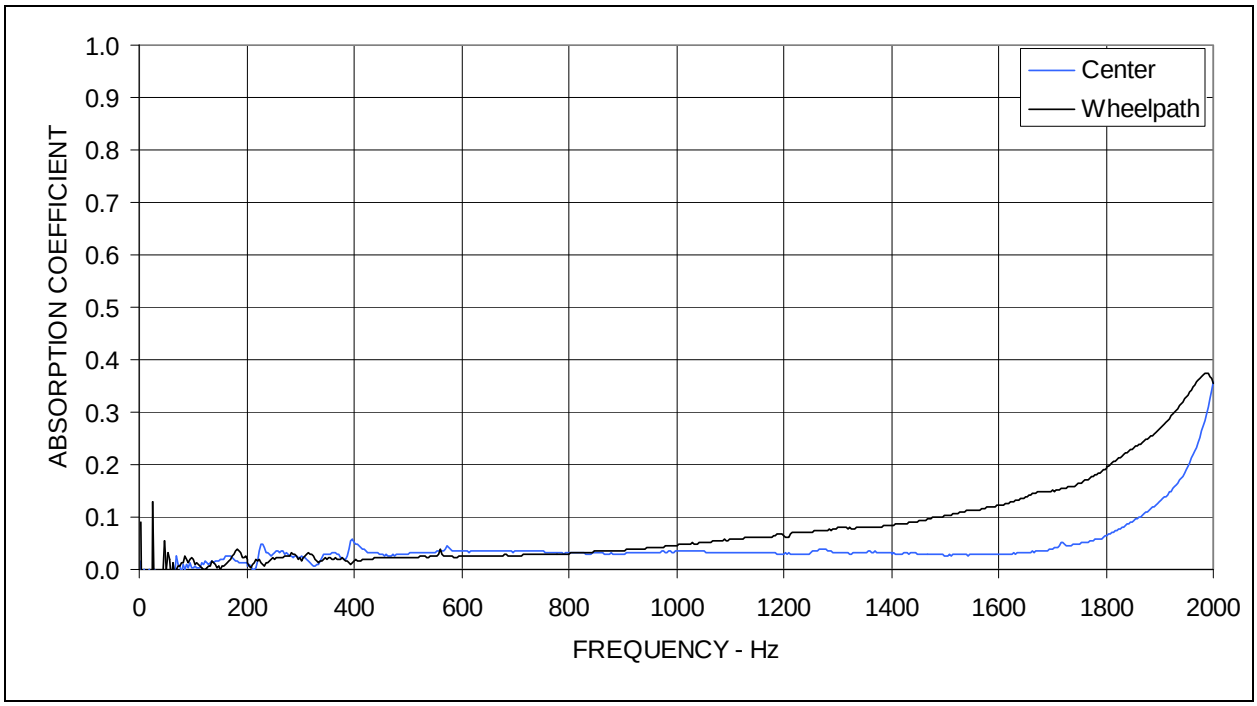

Figure A34: Sound absorption measured on cores from section QP17.

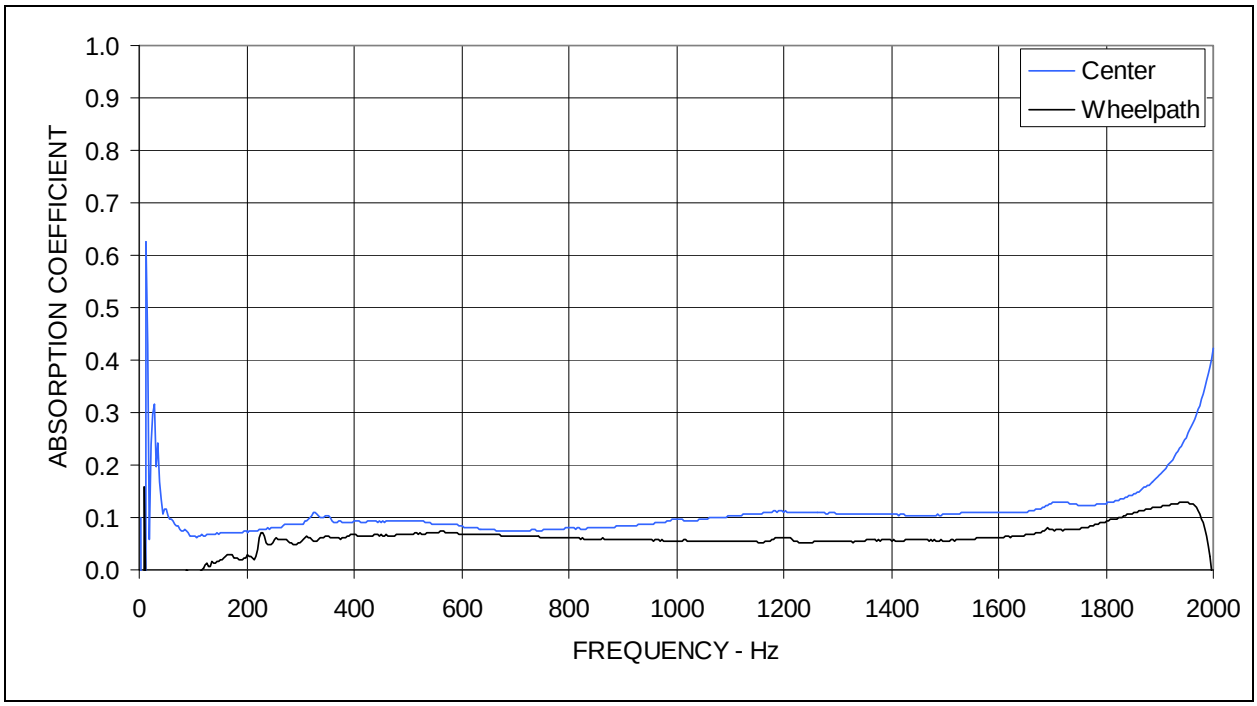

Figure A35: Sound absorption measured on cores from section QP18.

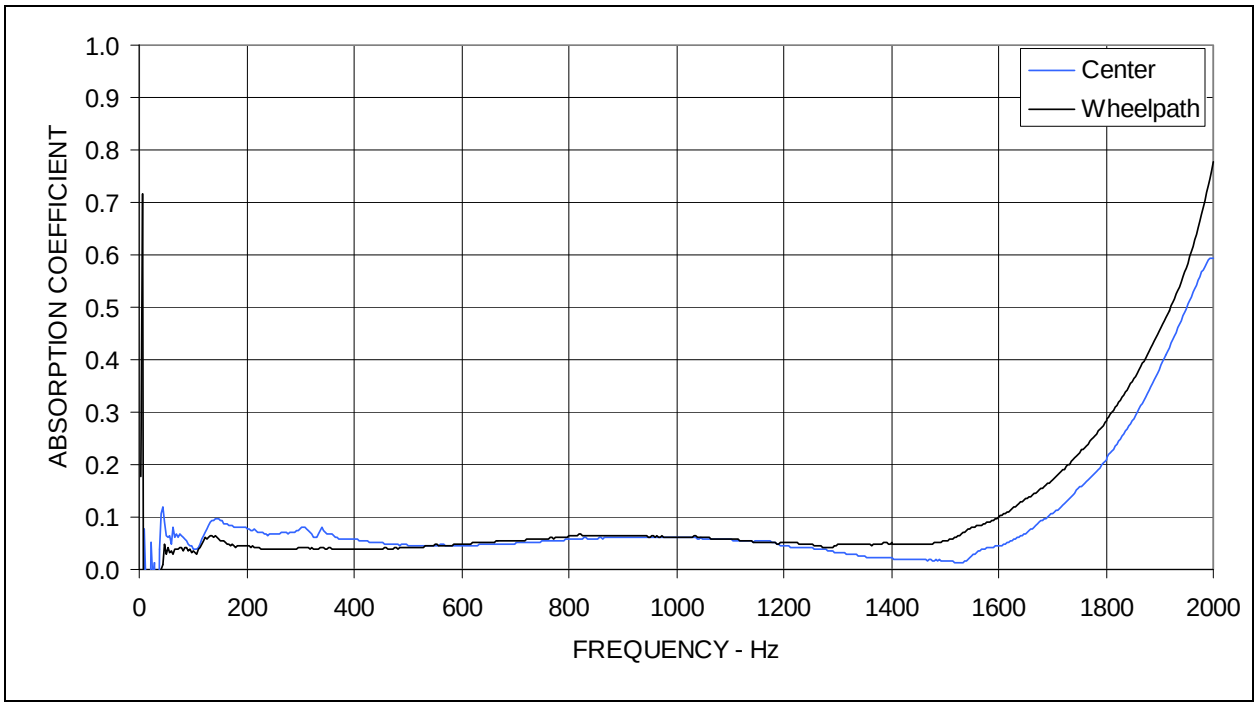

Figure A36: Sound absorption measured on cores from section QP19.

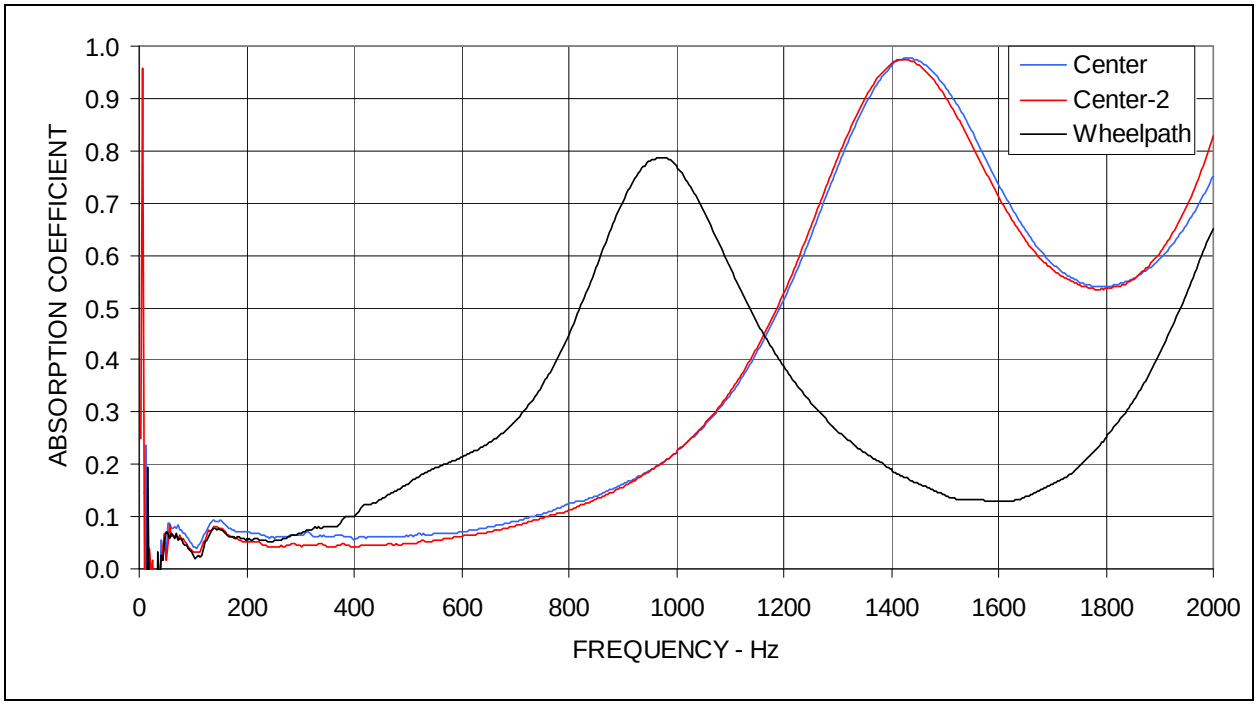

Figure A37: Sound absorption measured on cores from section QP20.

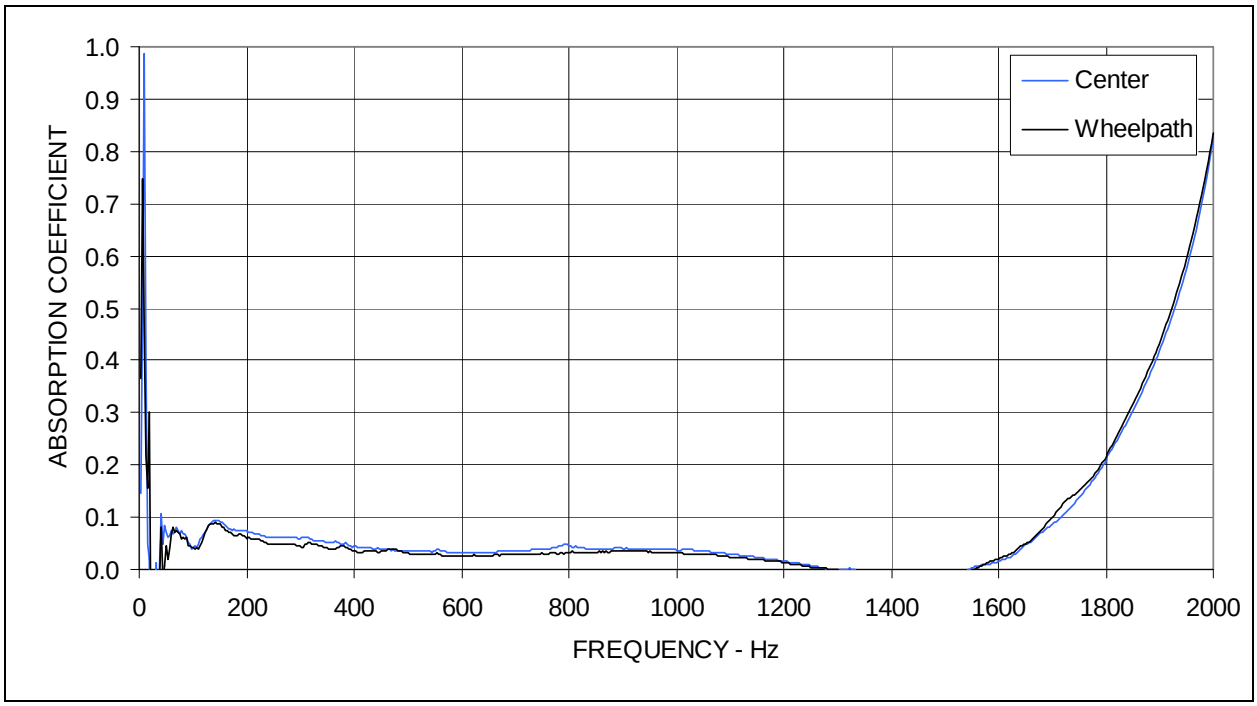

Figure A38: Sound absorption measured on cores from section QP21.

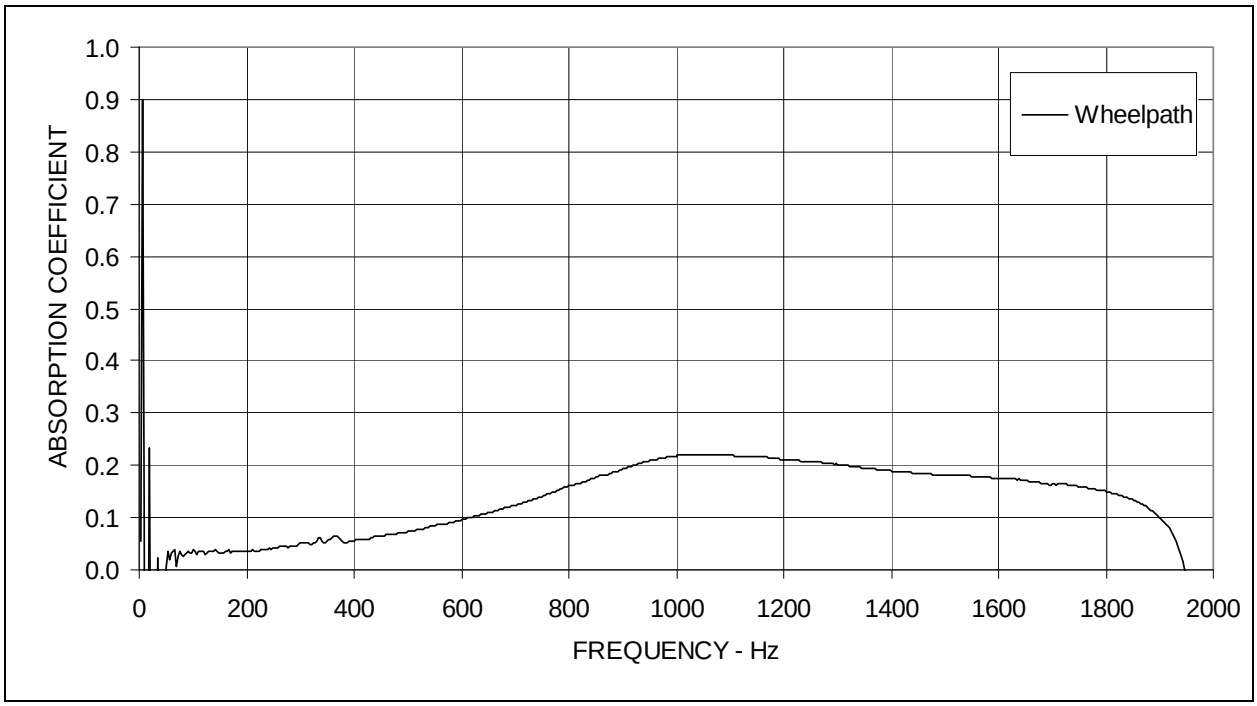

Figure A39: Sound absorption measured on cores from section QP22.

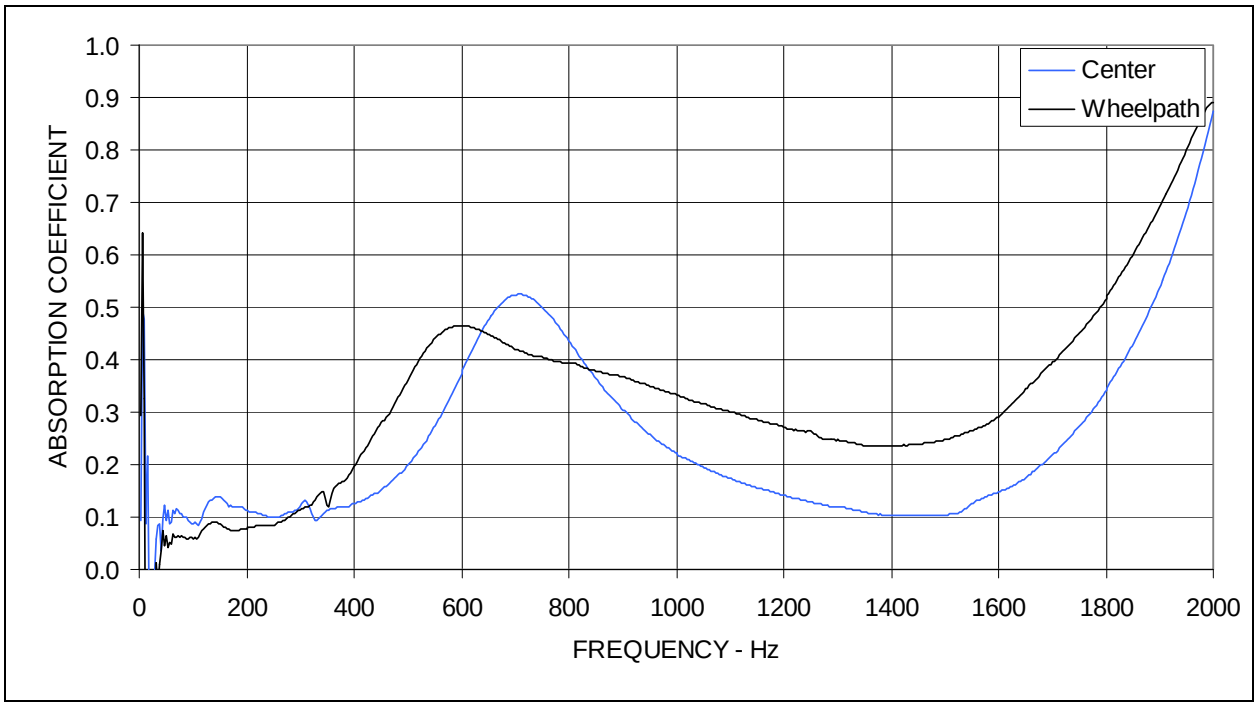

Figure A40: Sound absorption measured on cores from section QP23.

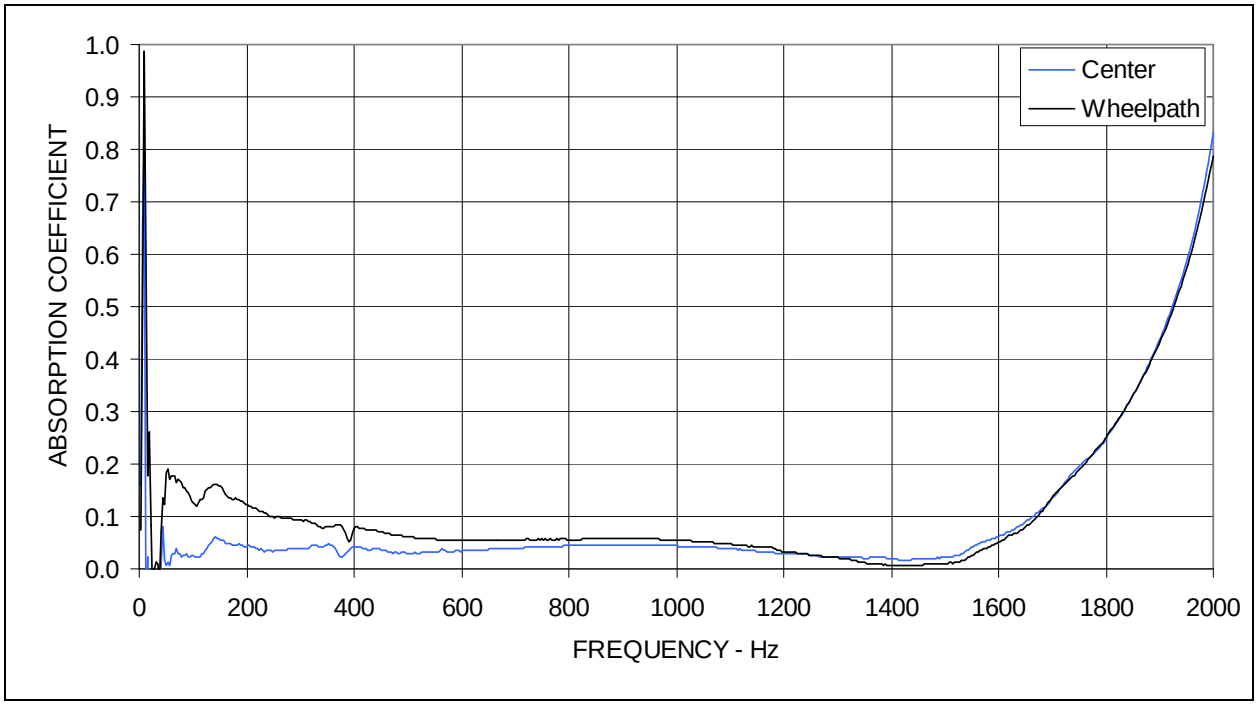

Figure A41: Sound absorption measured on cores from section QP24.

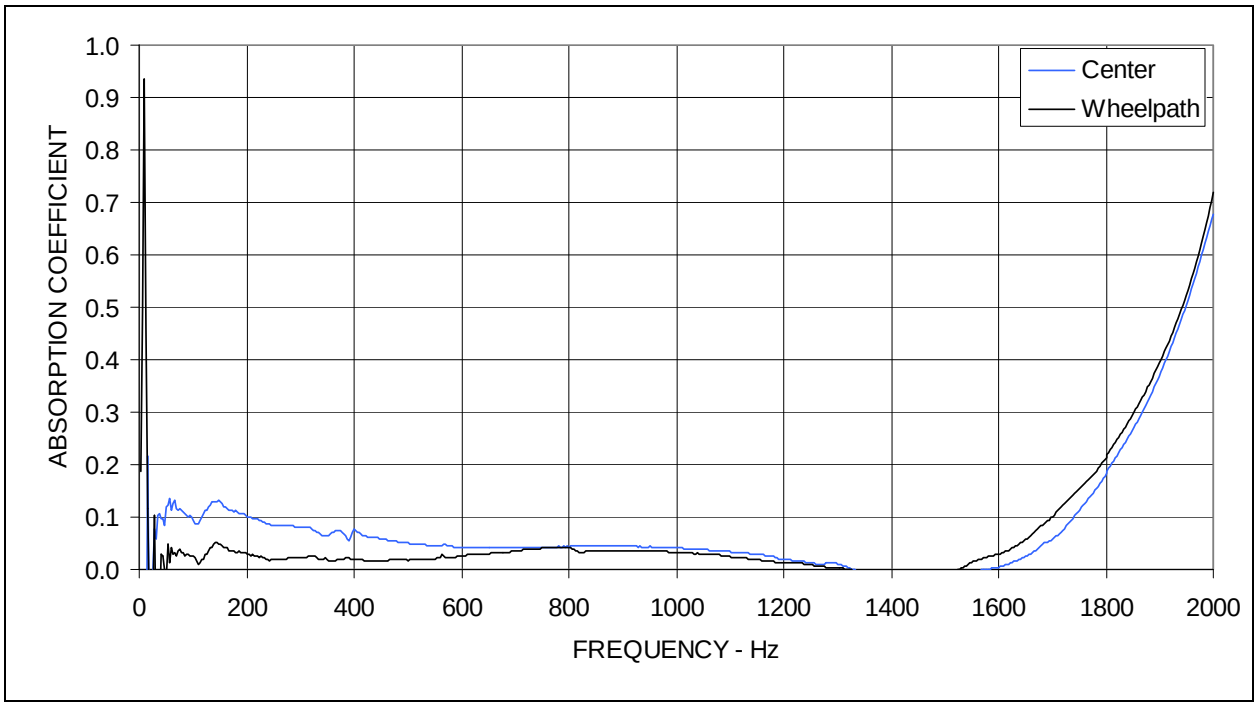

Figure A42: Sound absorption measured on cores from section QP25.

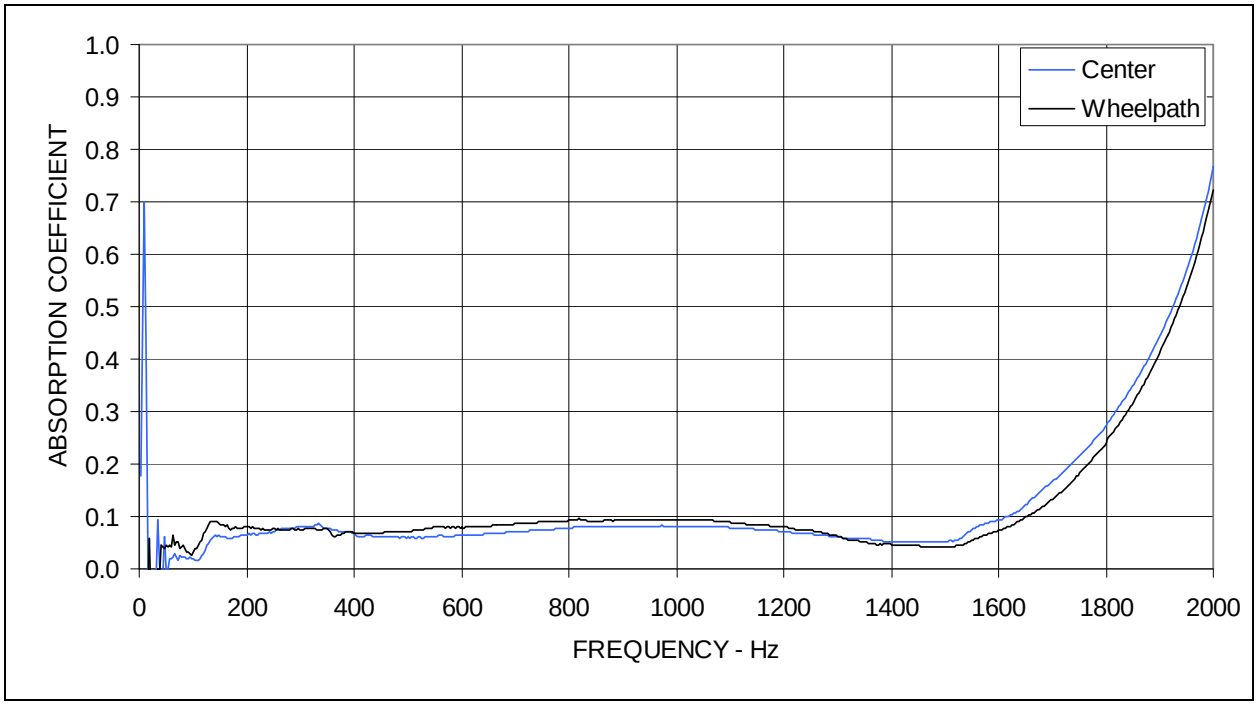

Figure A43: Sound absorption measured on cores from section QP26.

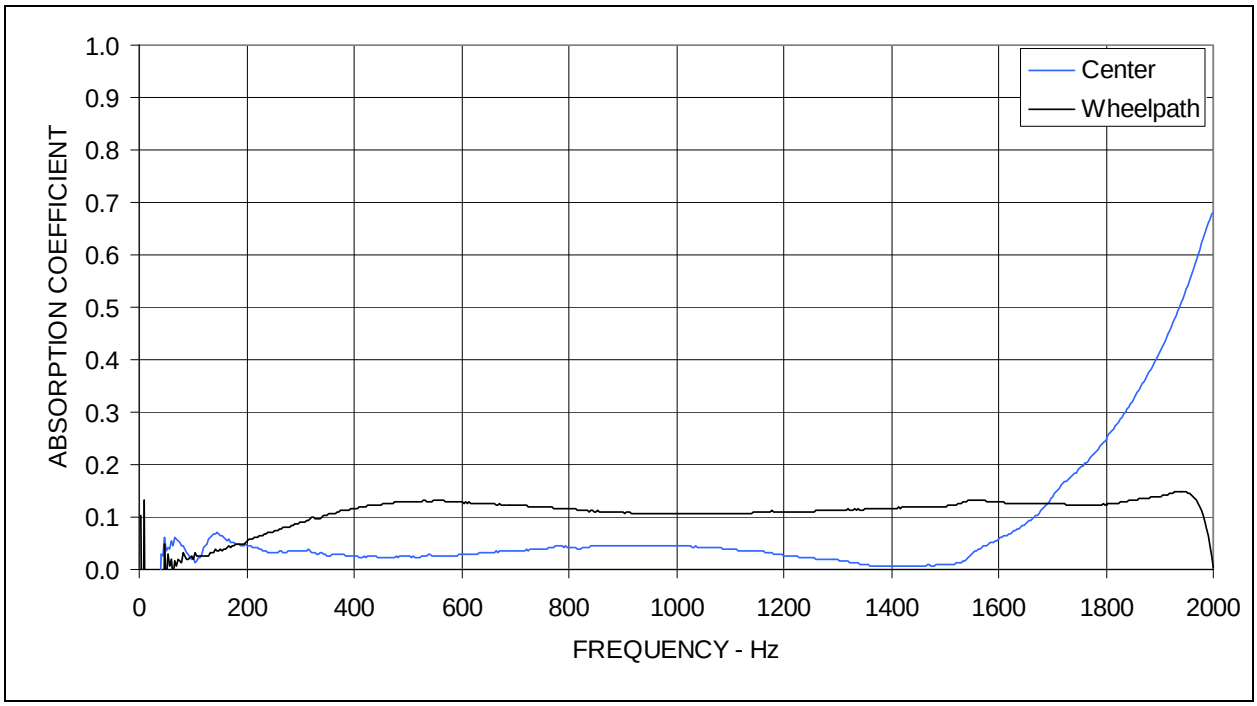

Figure A44: Sound absorption measured on cores from section QP27.

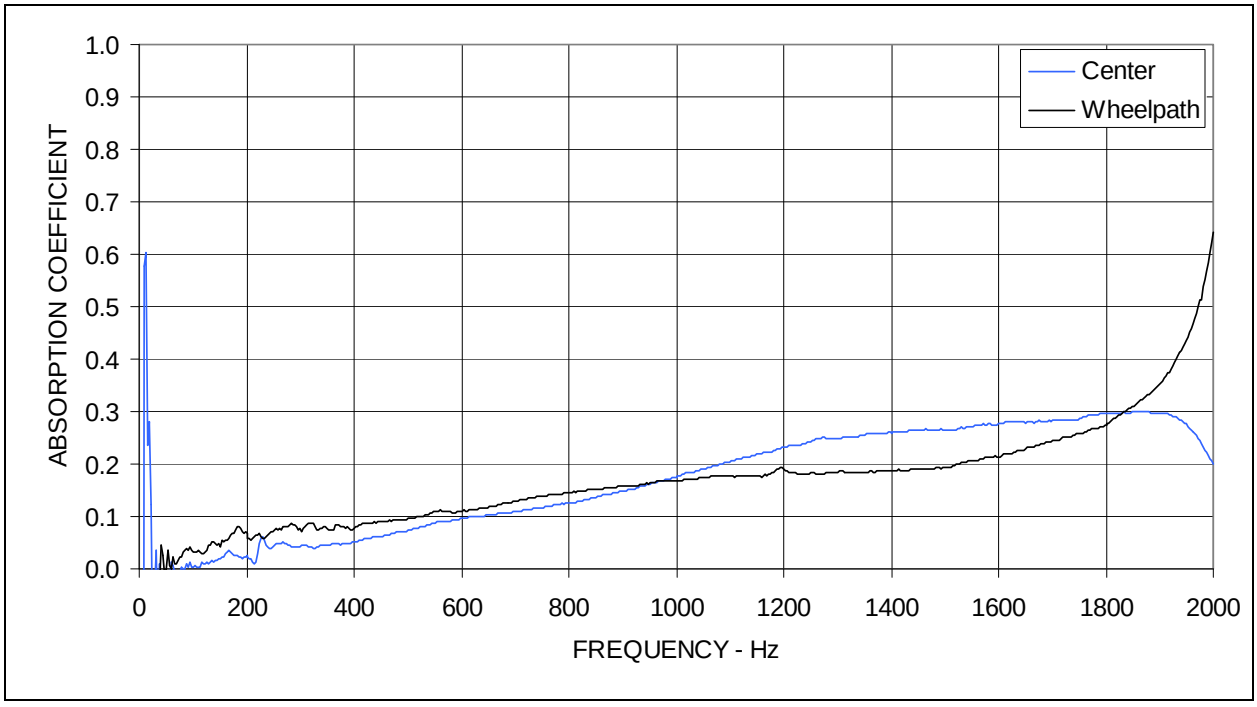

Figure A45: Sound absorption measured on cores from section QP28.

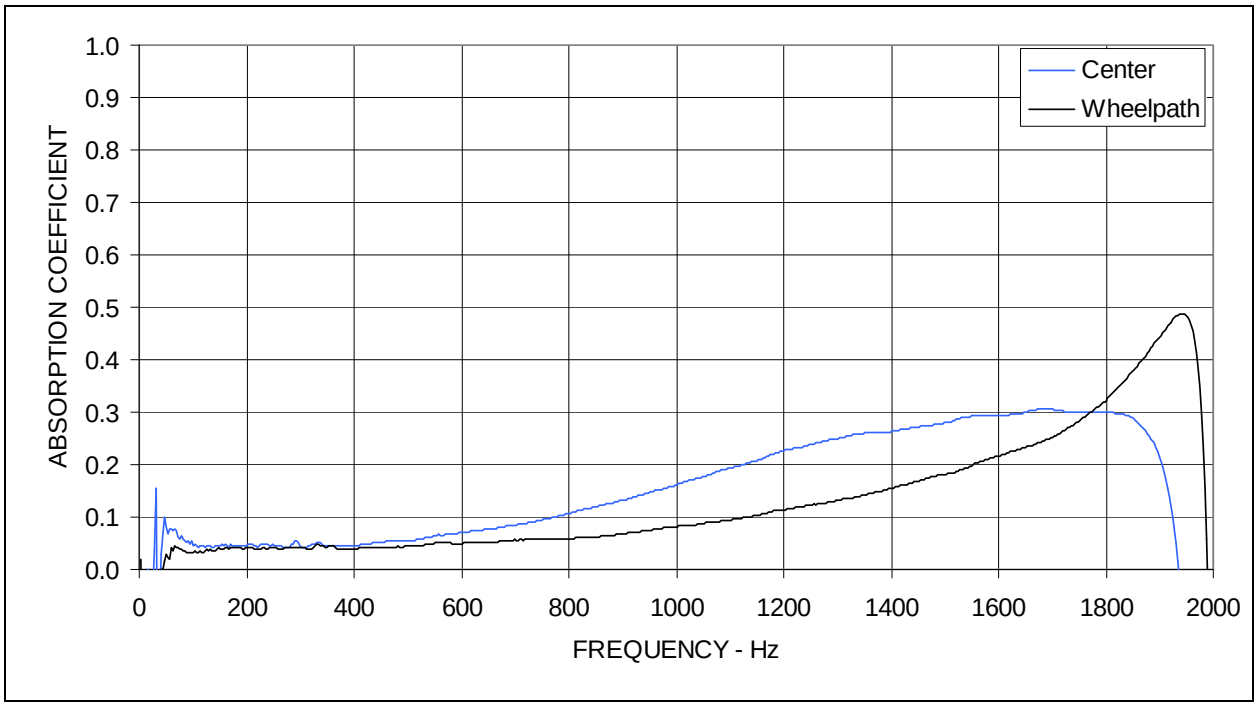

Figure A46: Sound absorption measured on cores from section QP29.

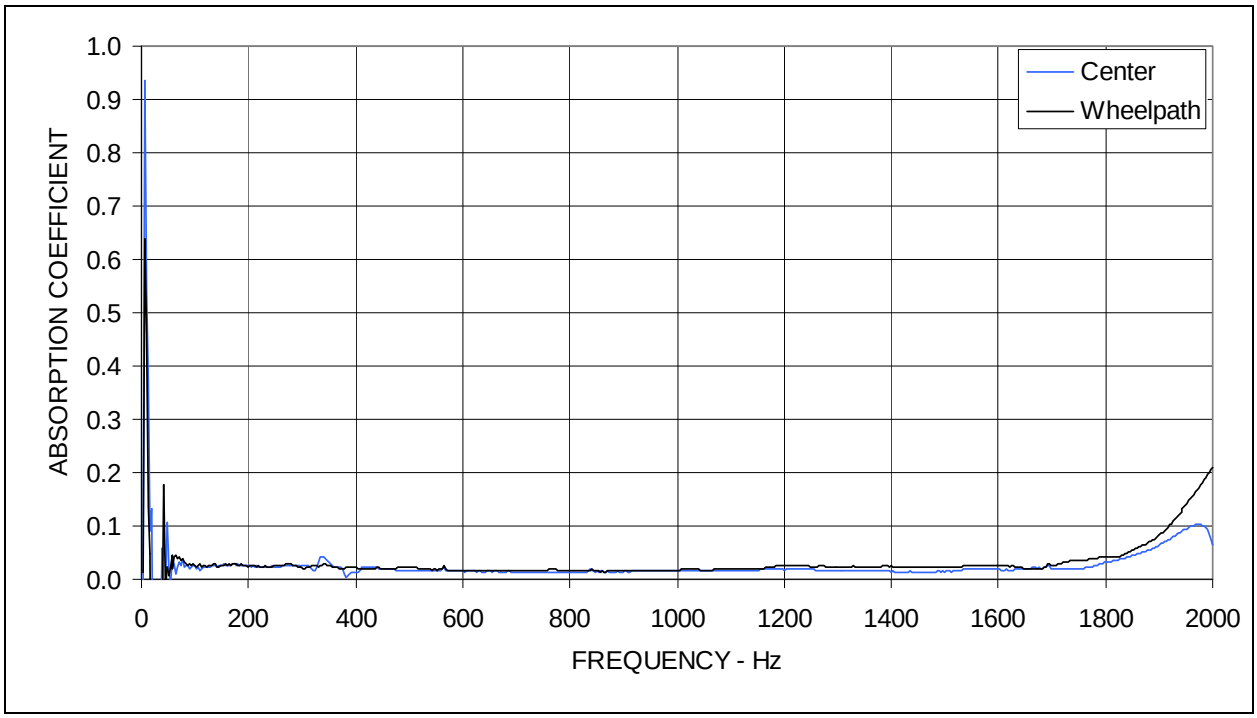

Figure A47: Sound absorption measured on cores from section QP30.

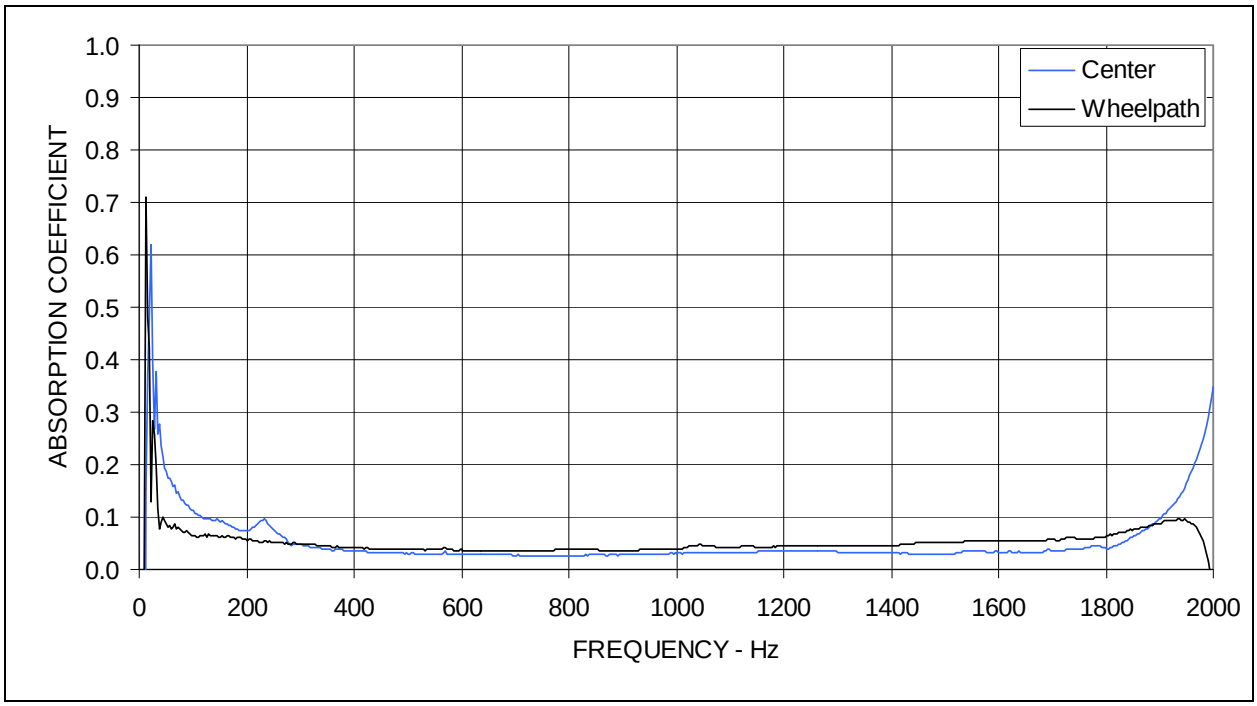

Figure A48: Sound absorption measured on cores from section QP31.

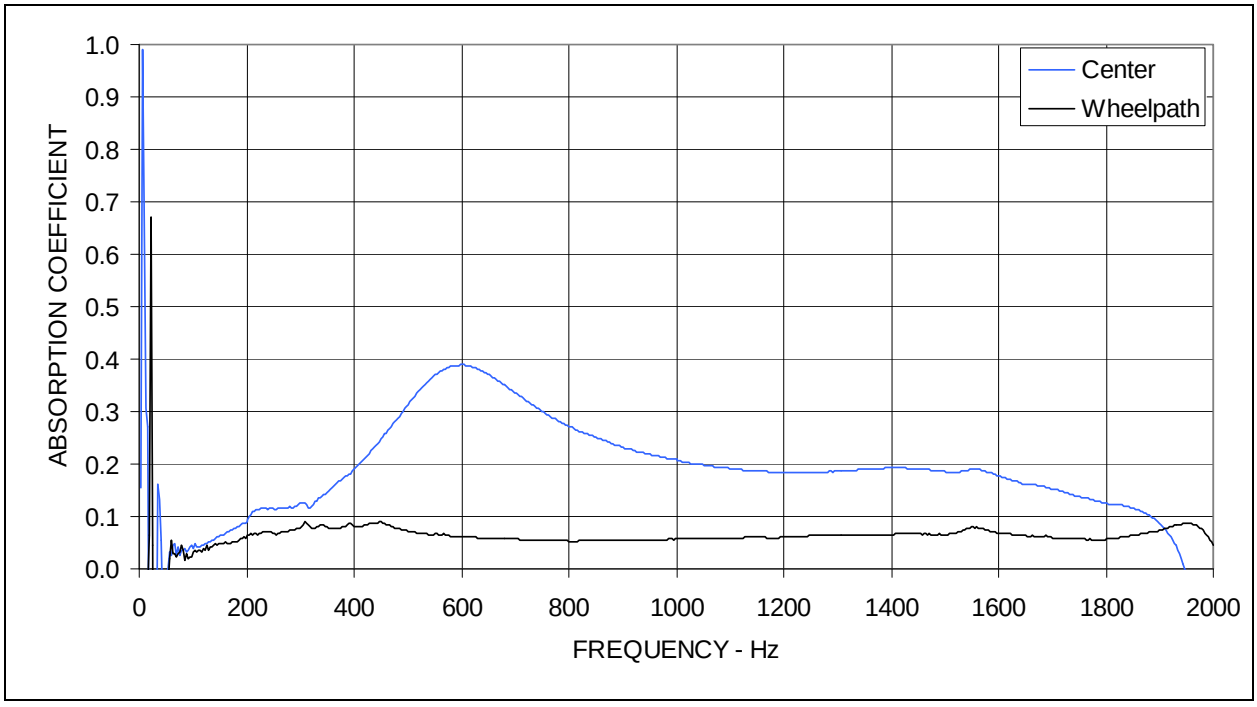

Figure A49: Sound absorption measured on cores from section QP32.

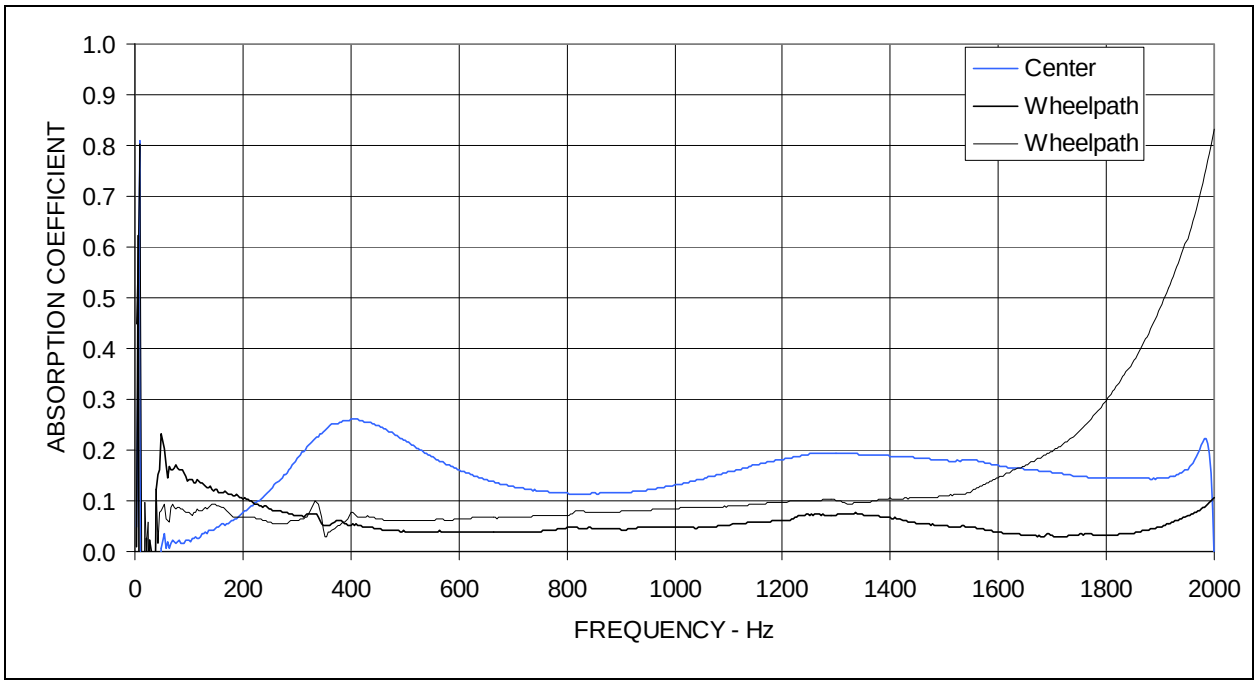

Figure A50: Sound absorption measured on cores from section QP33.

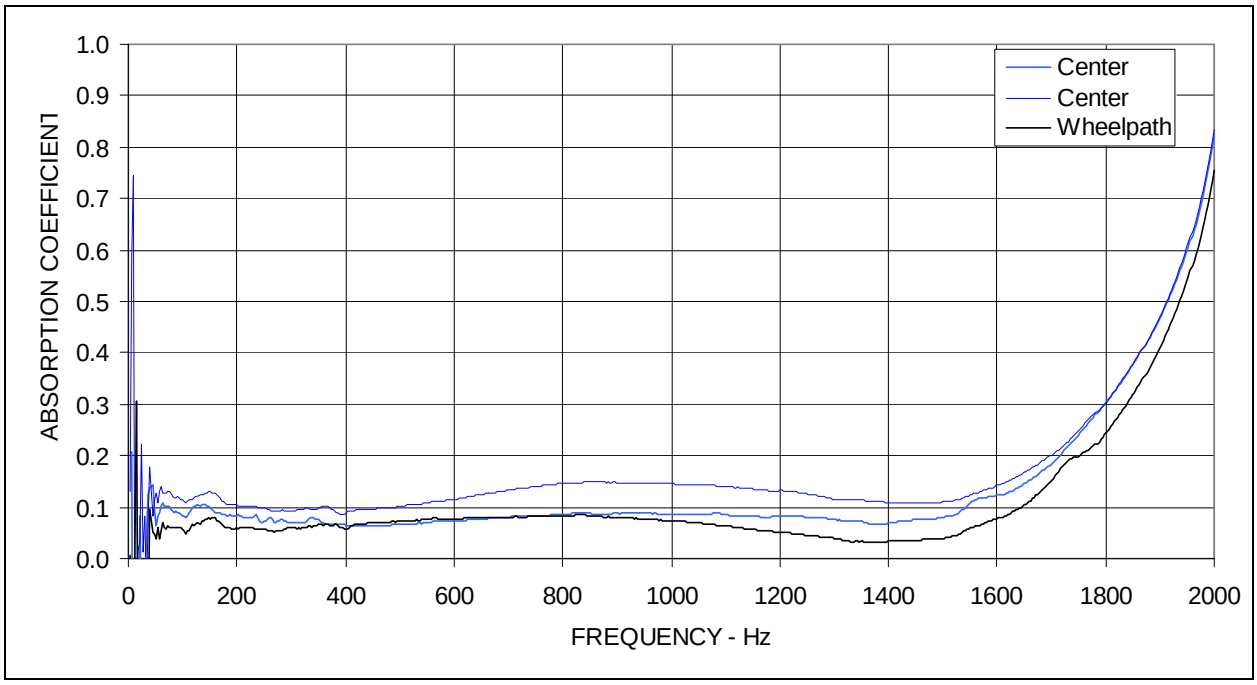

Figure A51: Sound absorption measured on cores from section QP34.

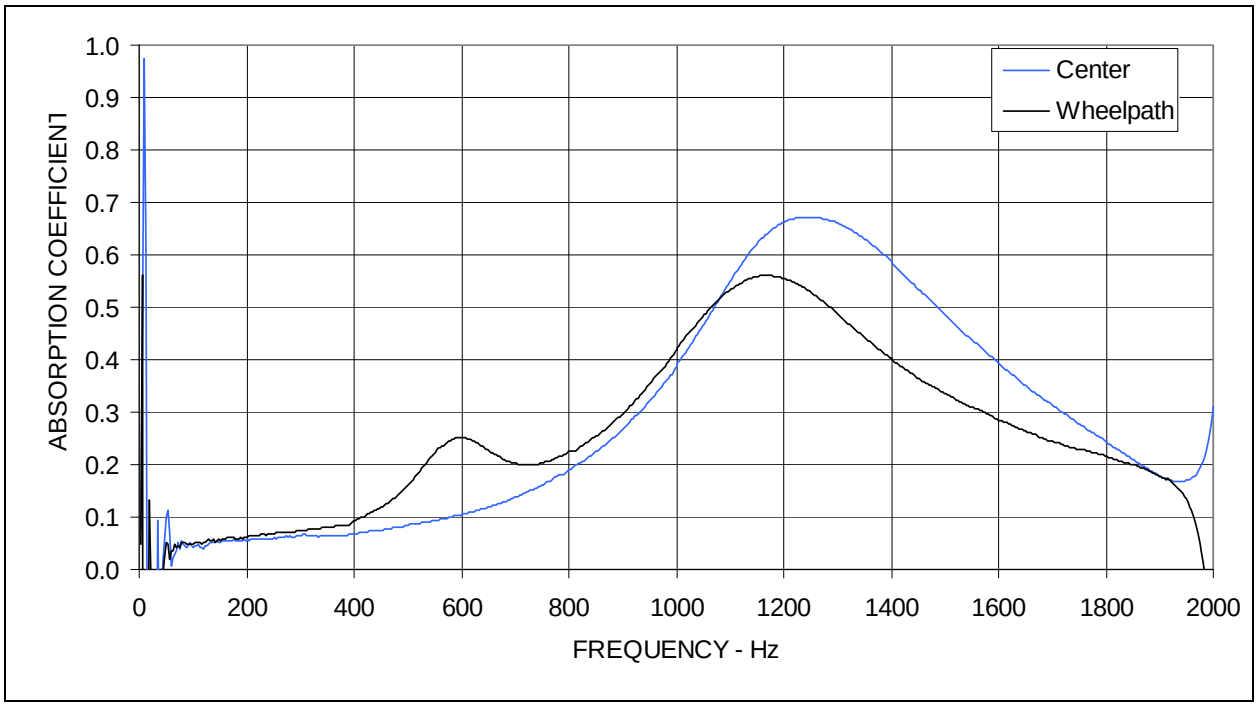

Figure A52: Sound absorption measured on cores from section QP35.

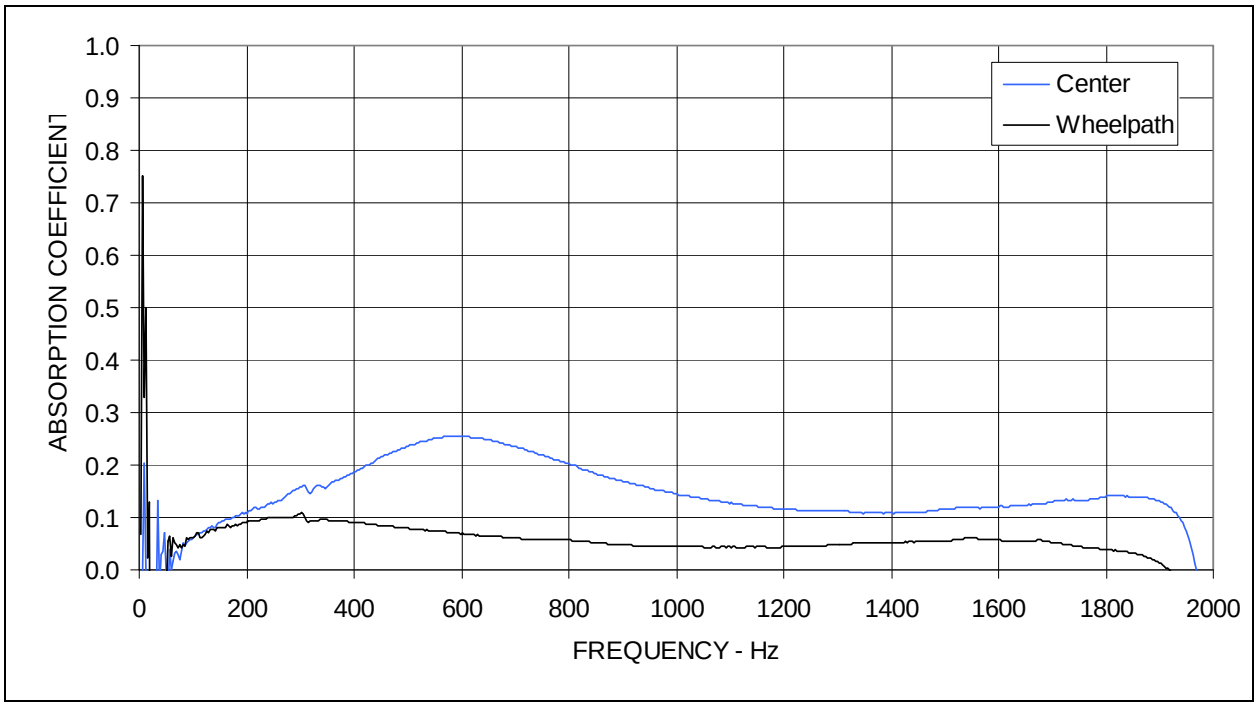

Figure A53: Sound absorption measured on cores from section QP36.

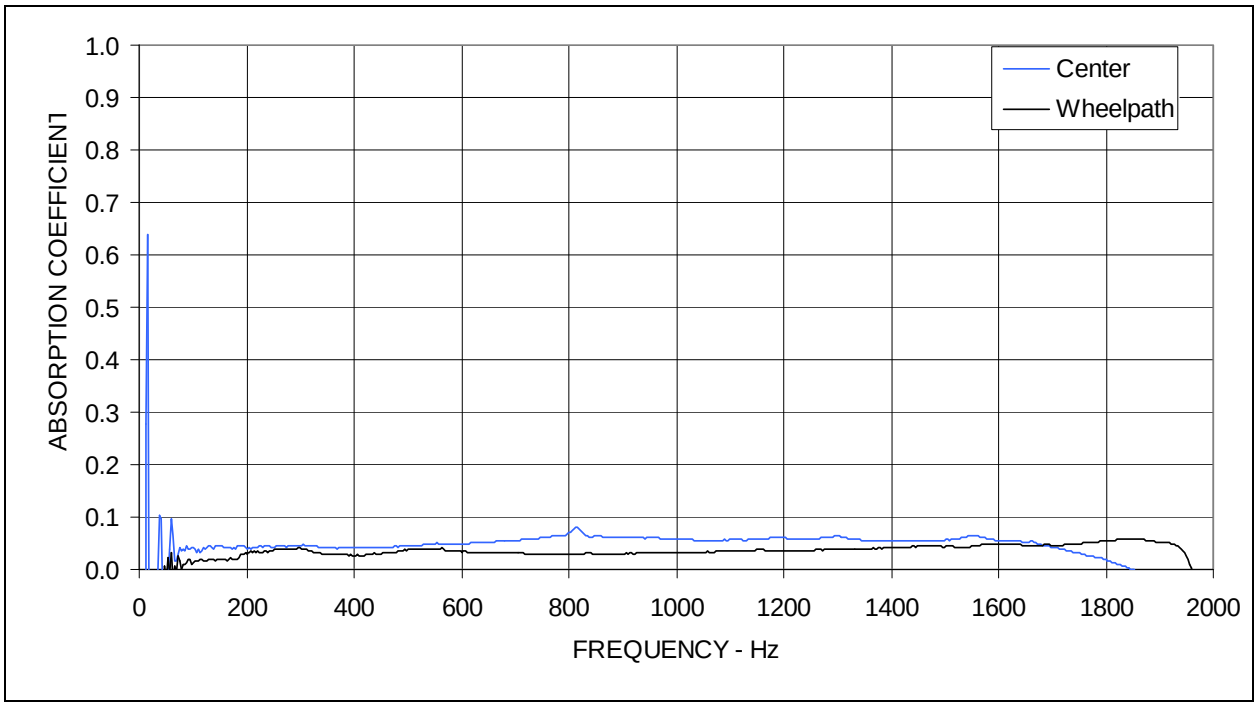

Figure A54: Sound absorption measured on cores from section QP37.

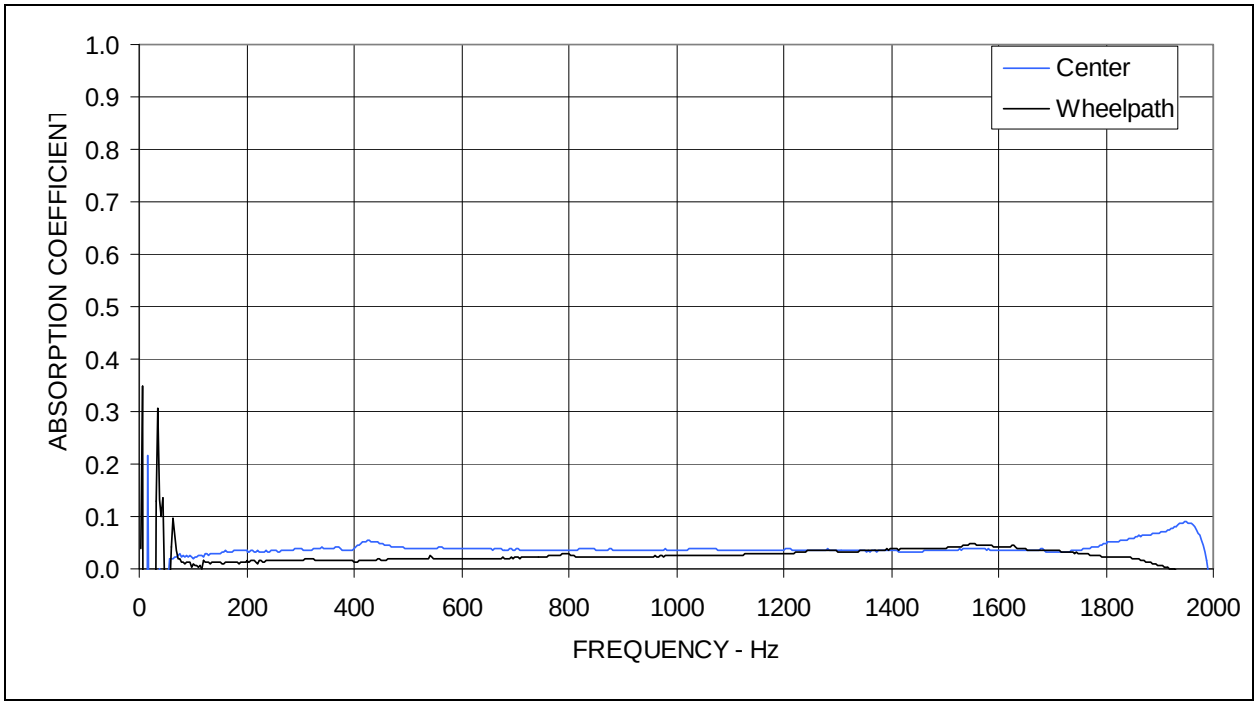

Figure A55: Sound absorption measured on cores from section QP38.

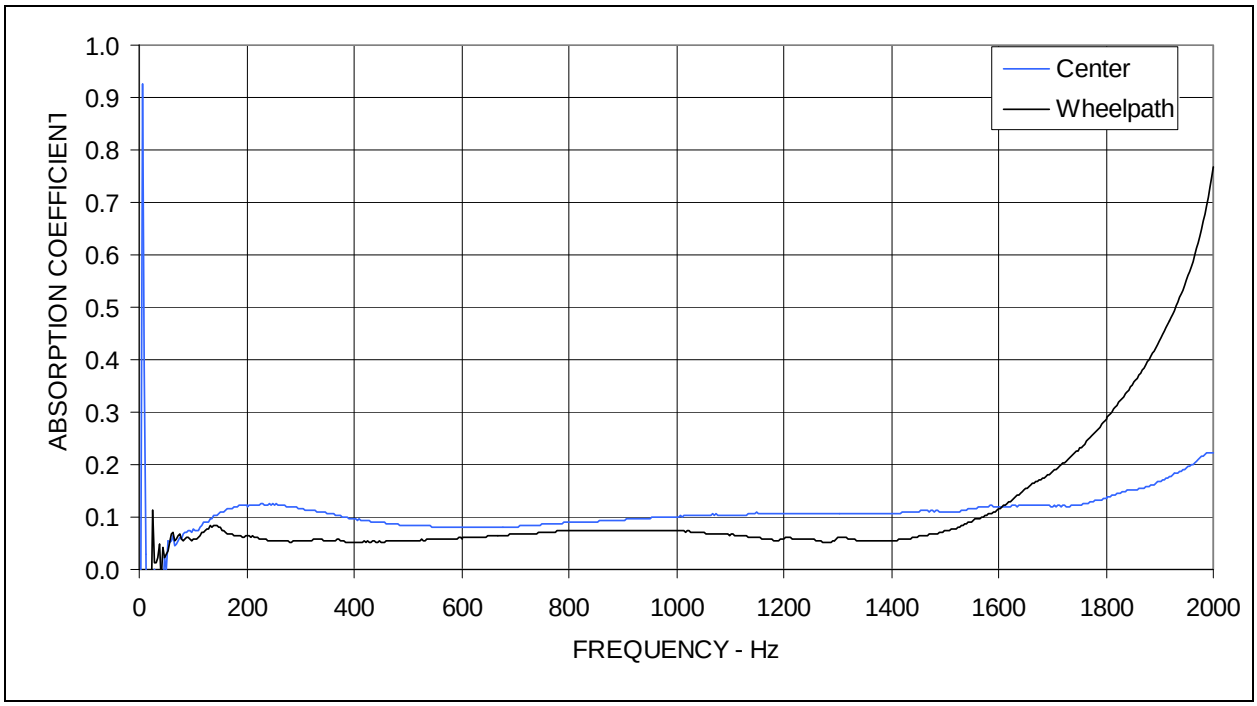

Figure A56: Sound absorption measured on cores from section QP39.

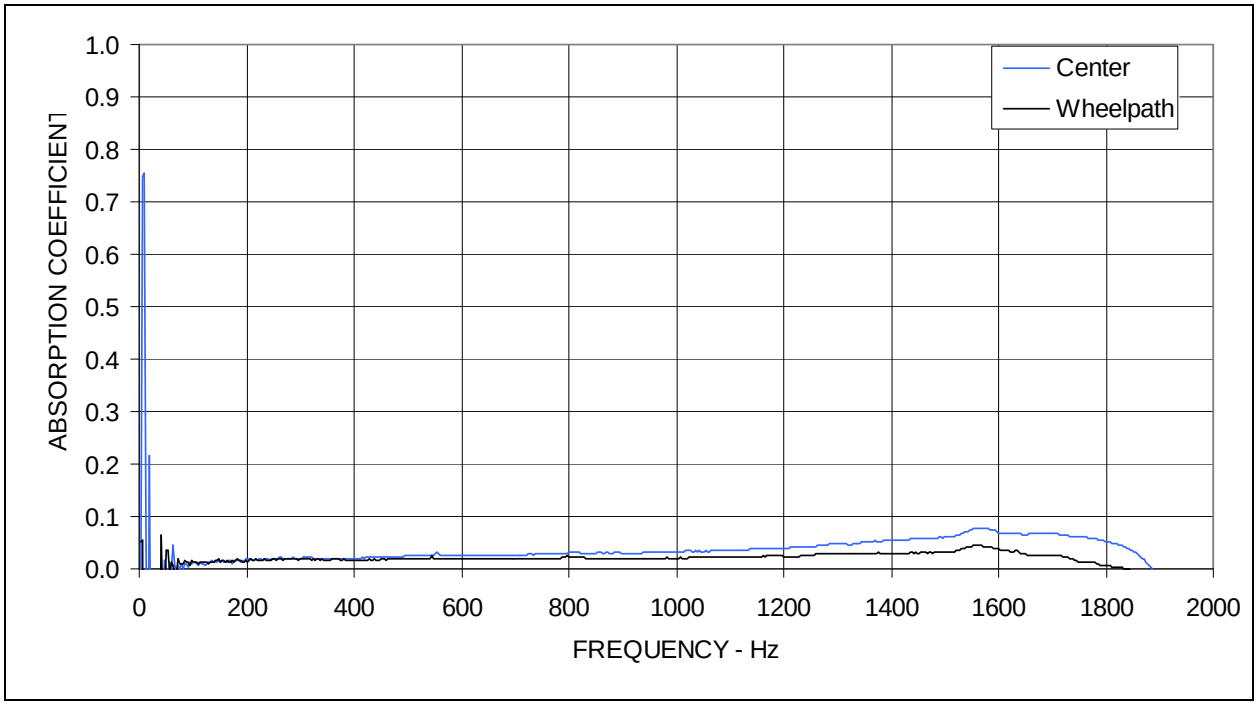

Figure A57: Sound absorption measured on cores from section QP40.

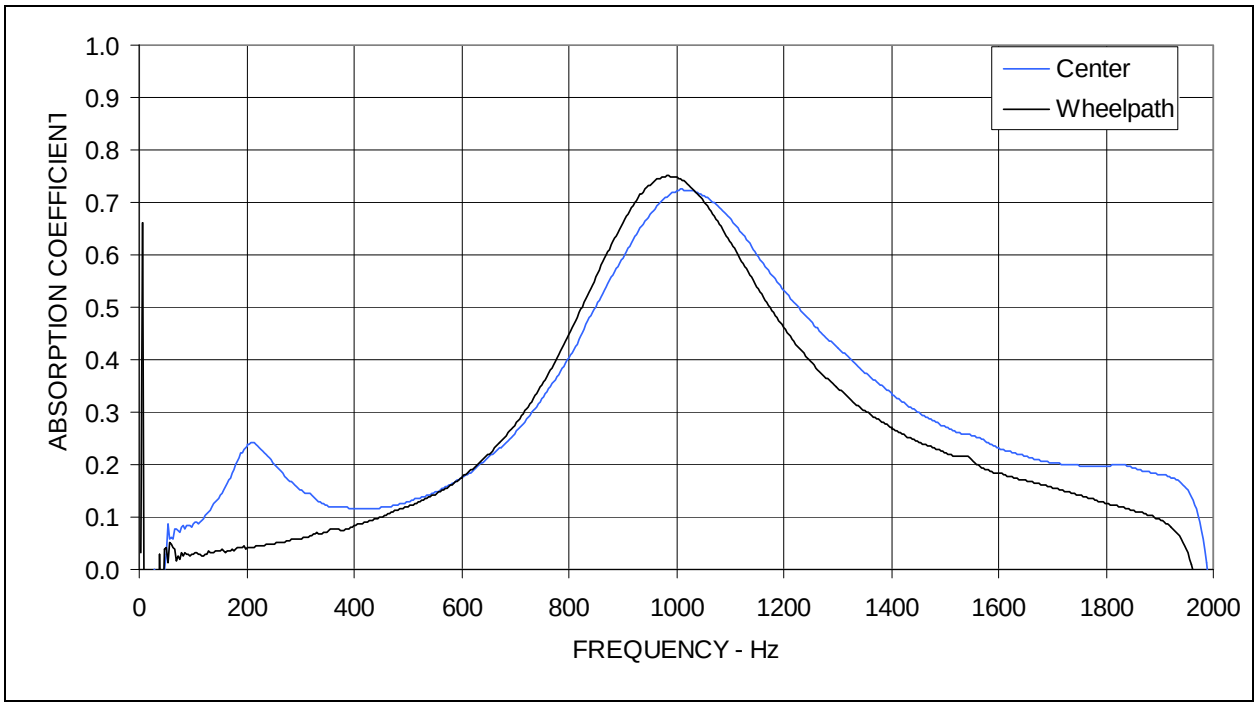

Figure A58: Sound absorption measured on cores from section QP41.

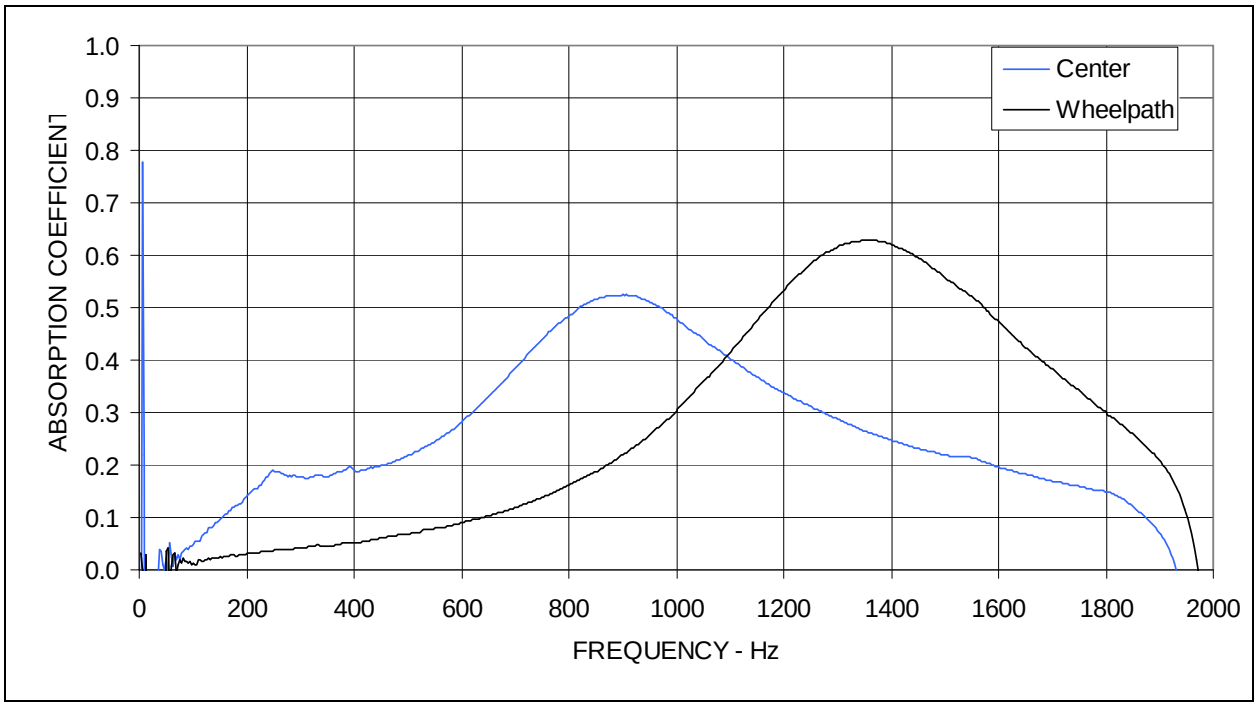

Figure A59: Sound absorption measured on cores from section QP42.

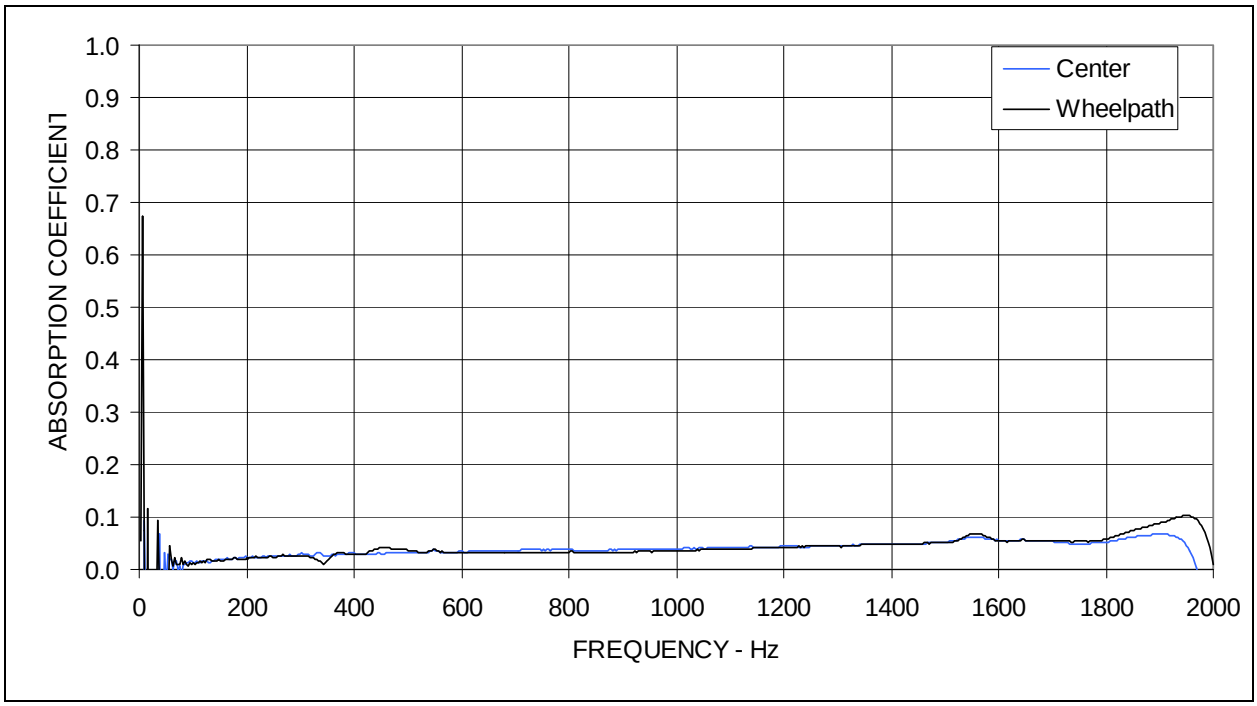

Figure A60: Sound absorption measured on cores from section QP43.

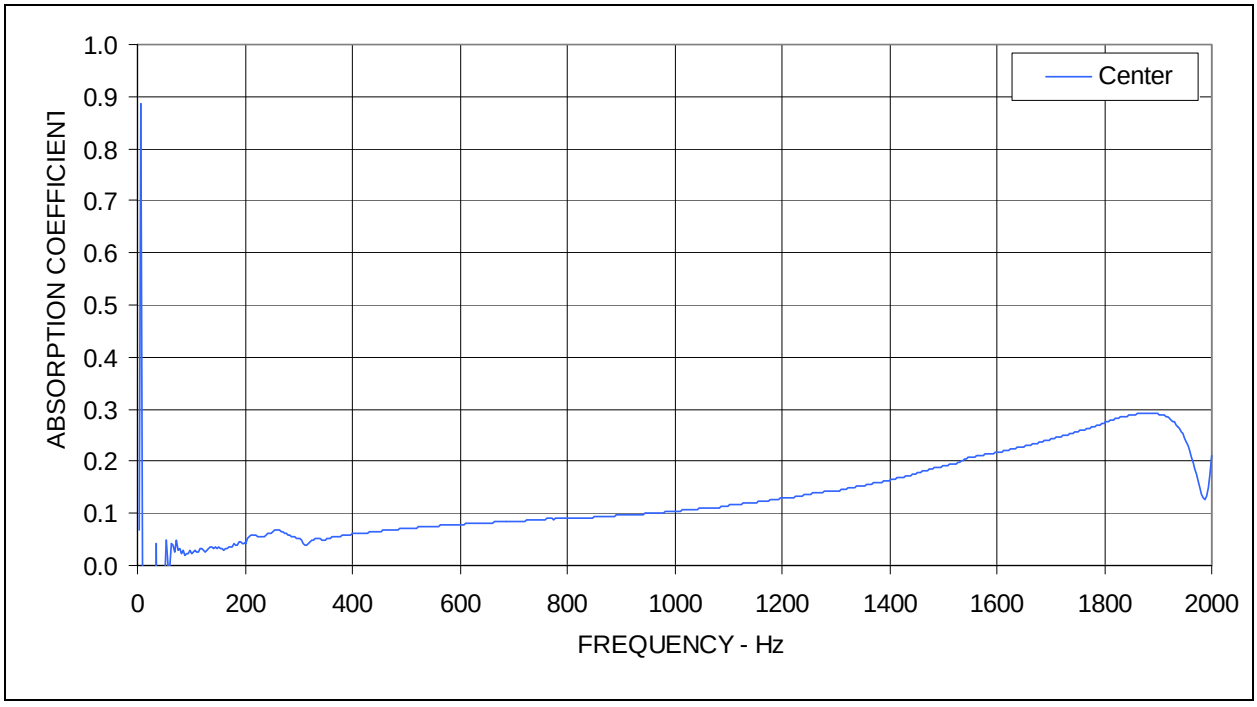

Figure A61: Sound absorption measured on cores from section QP44.

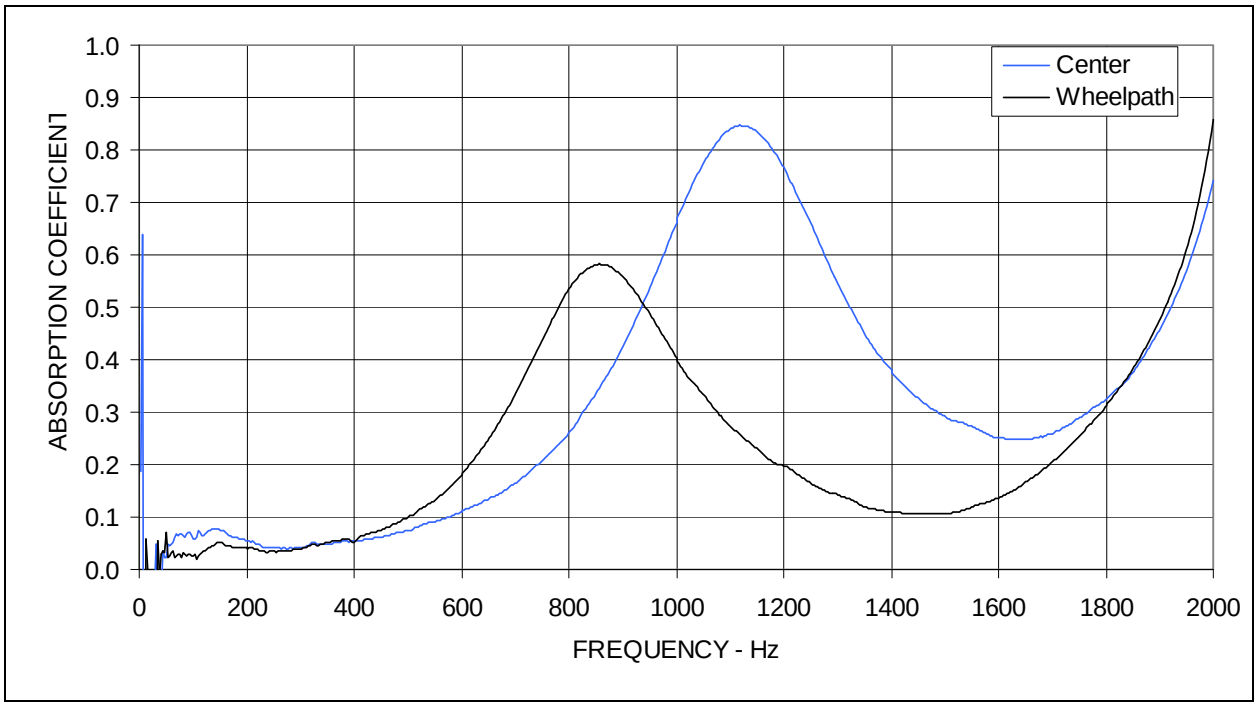

Figure A62: Sound absorption measured on cores from section QP45.

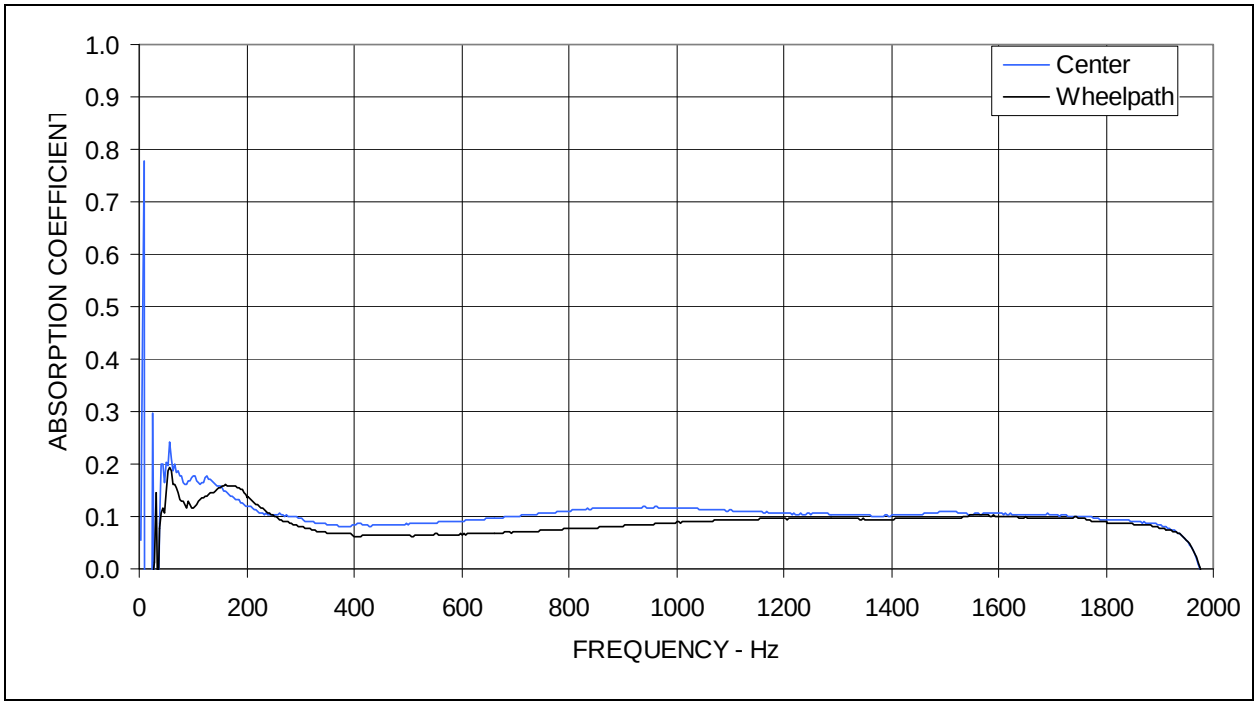

Figure A63: Sound absorption measured on cores from section QP46.

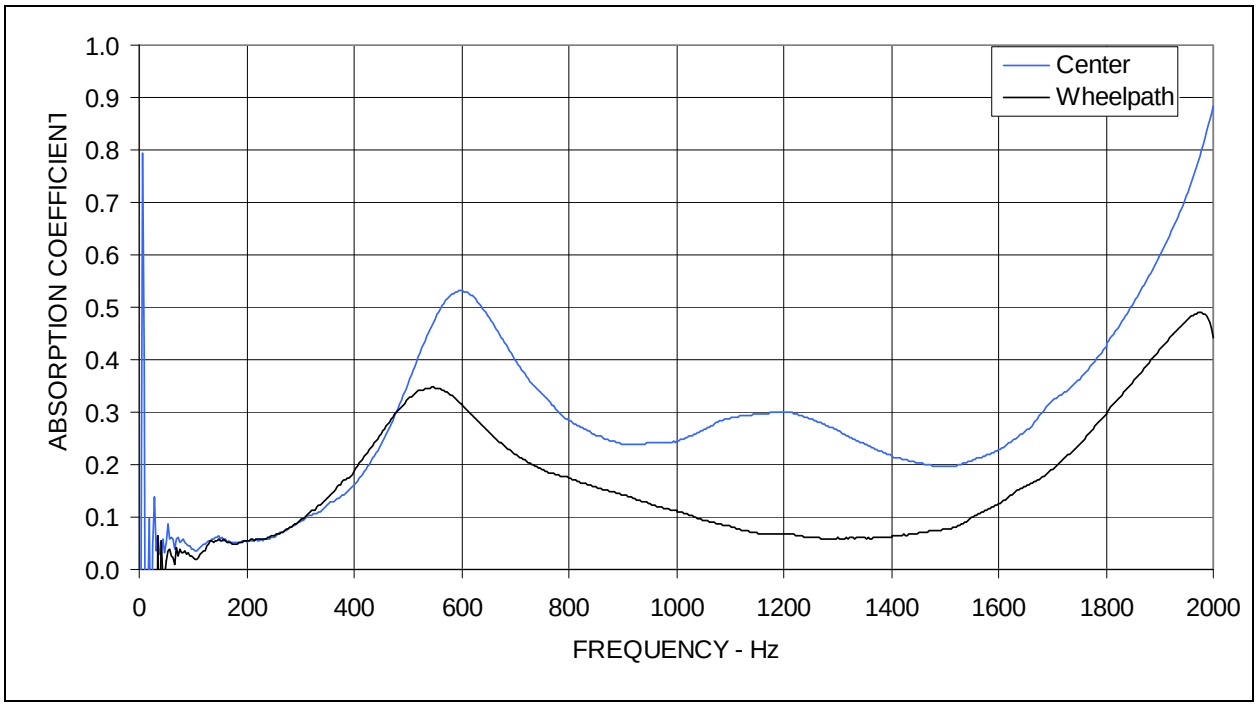

Figure A64: Sound absorption measured on cores from section QP47.

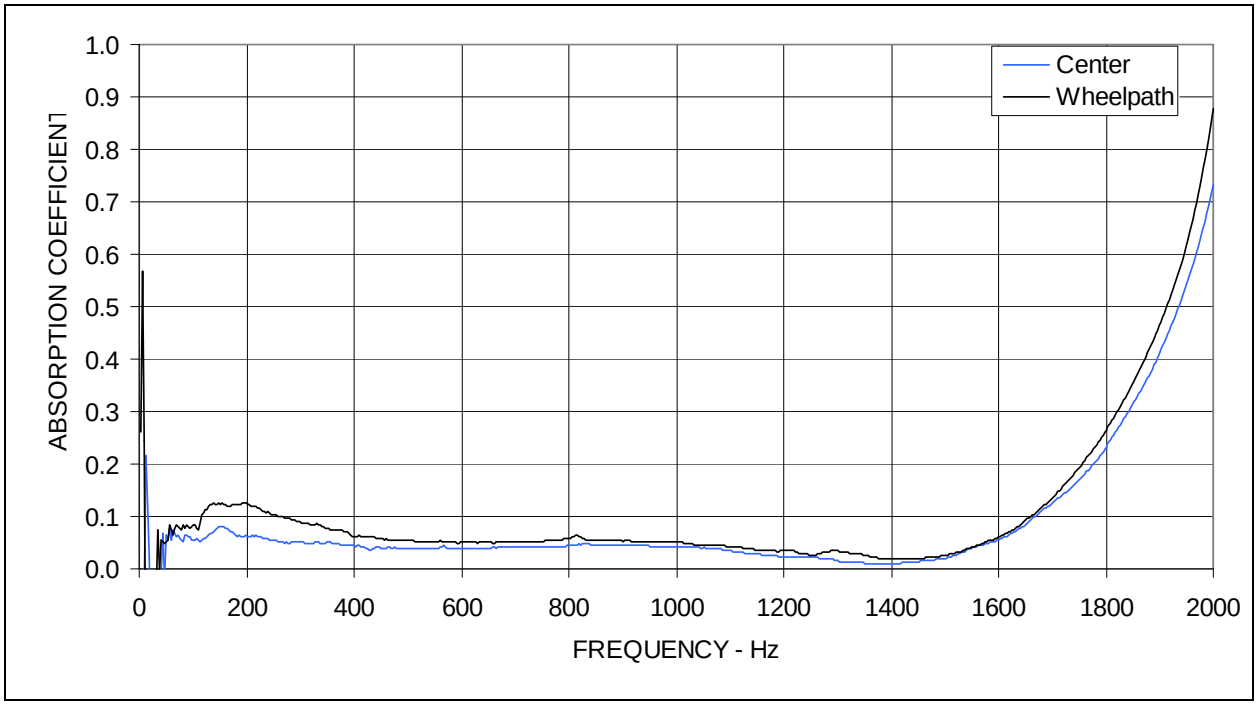

Figure A65: Sound absorption measured on cores from section QP48.

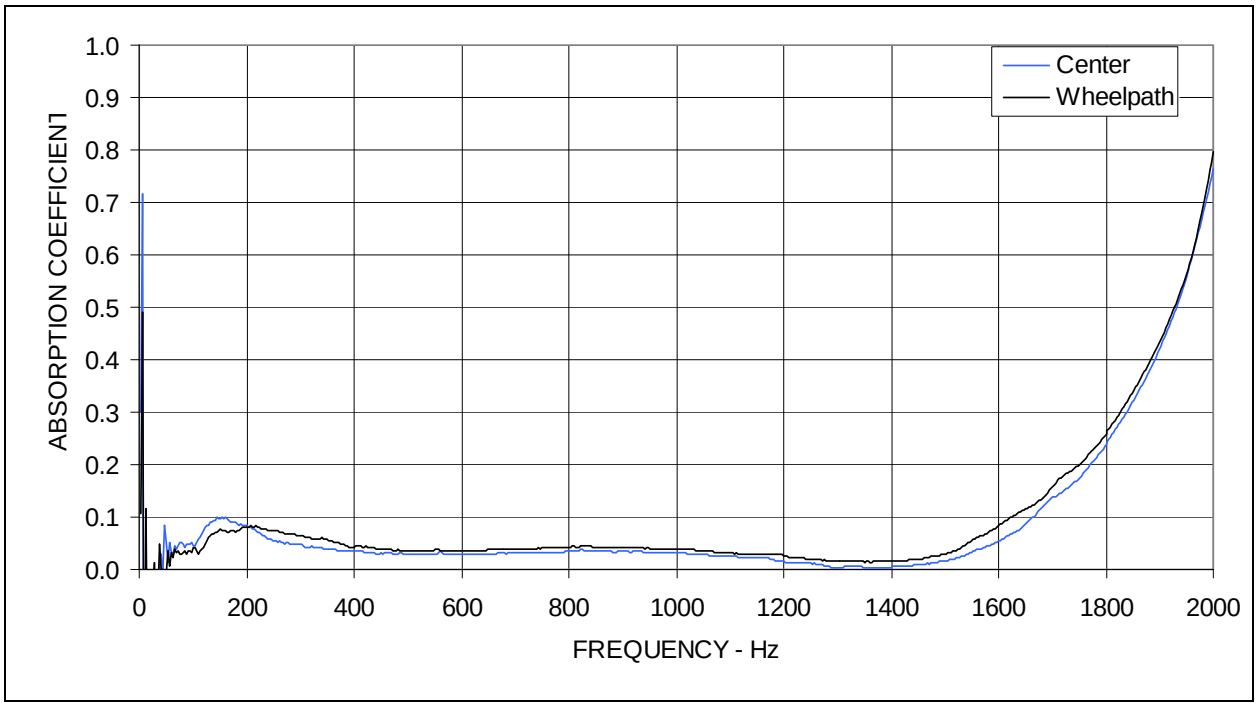

Figure A66: Sound absorption measured on cores from section QP49.

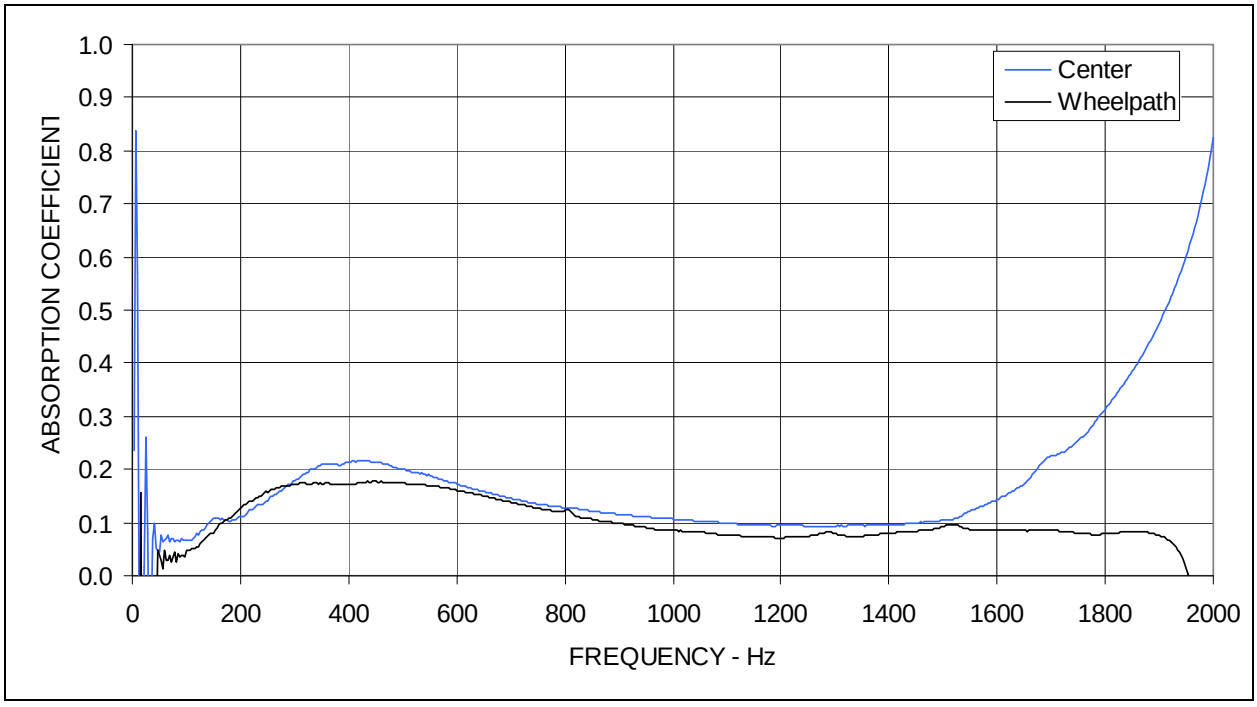

Figure A67: Sound absorption measured on cores from section QP50.

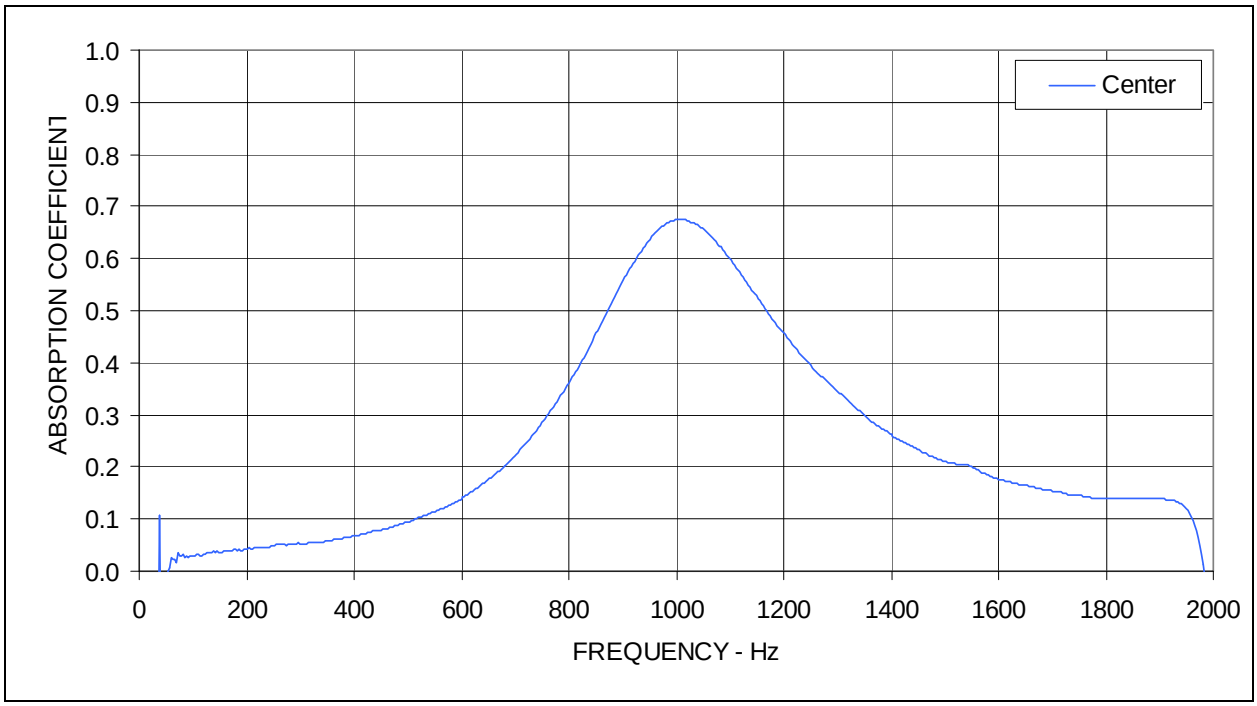

Figure A68: Sound absorption measured on cores from section QP51.

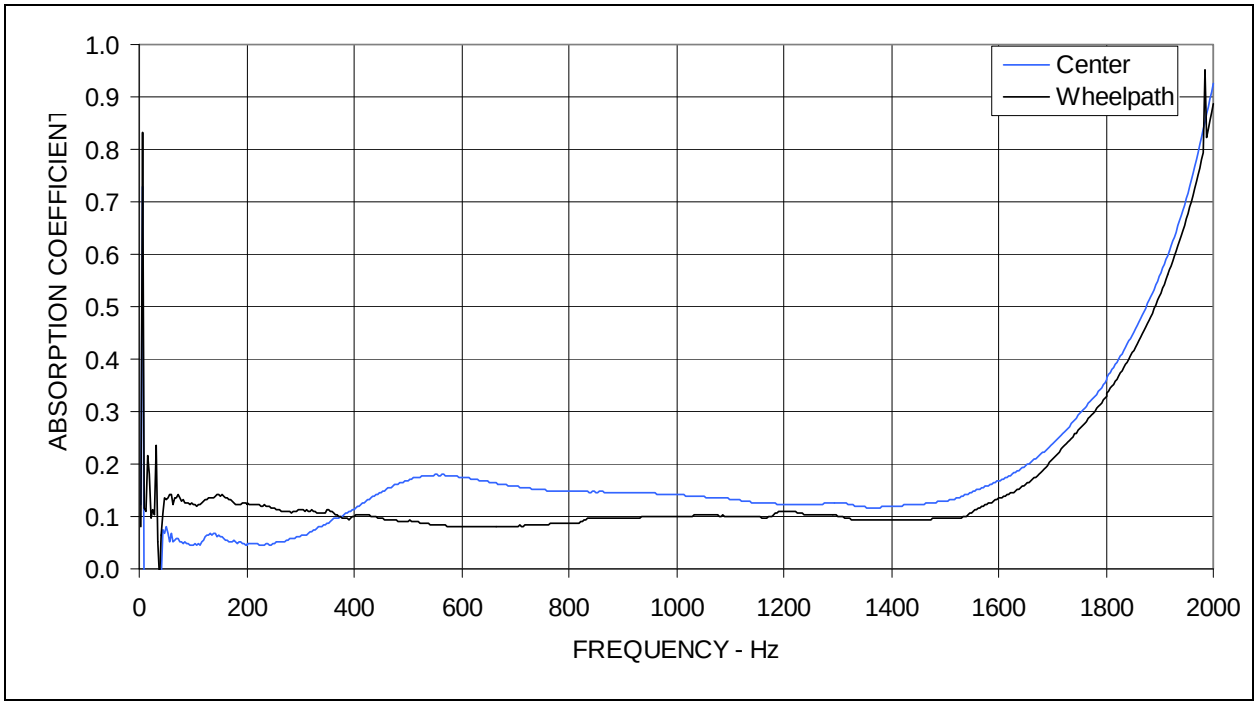

Figure A69: Sound absorption measured on cores from section QP52.

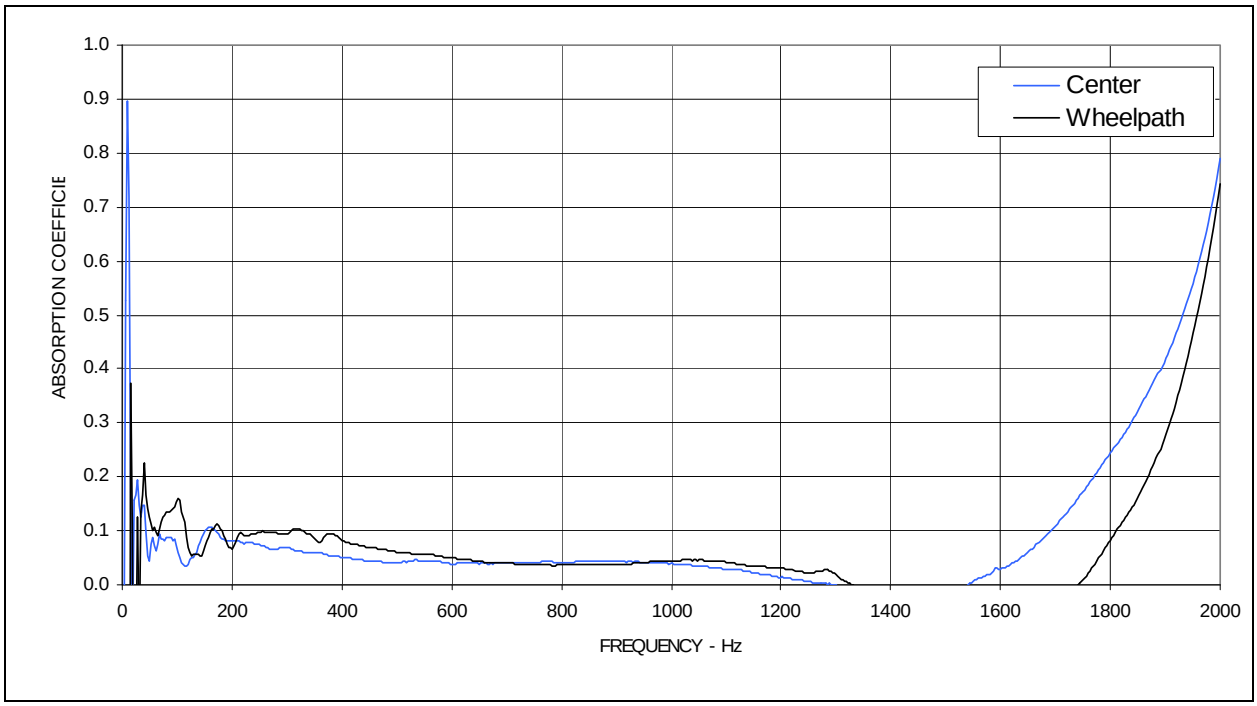

Figure A70: Sound absorption measured on cores from section N103.

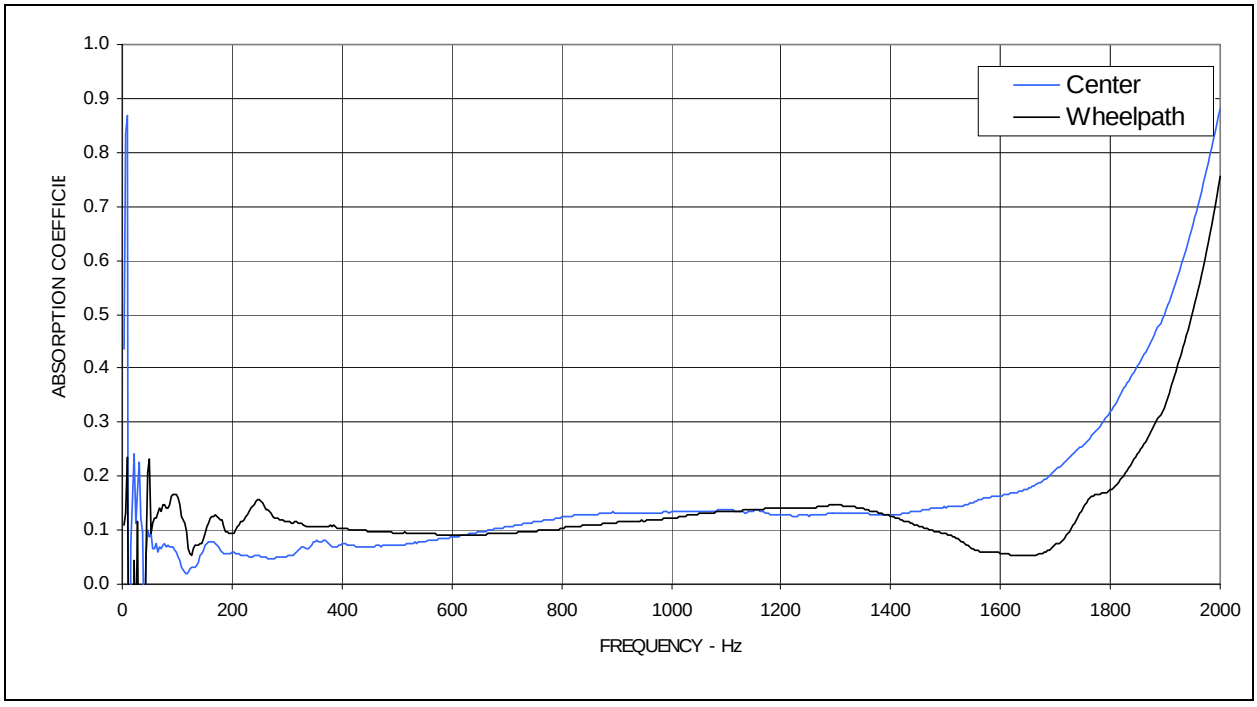

Figure A71: Sound absorption measured on cores from section N104.

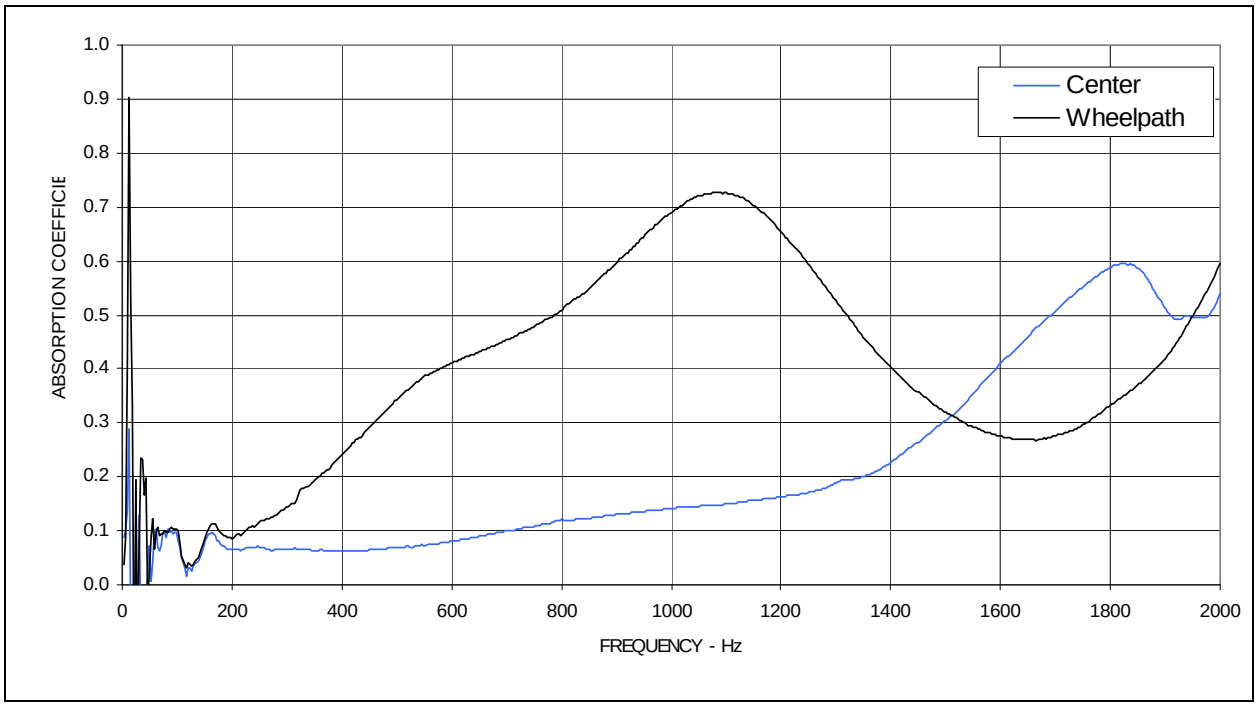

Figure A72: Sound absorption measured on cores from section N105.

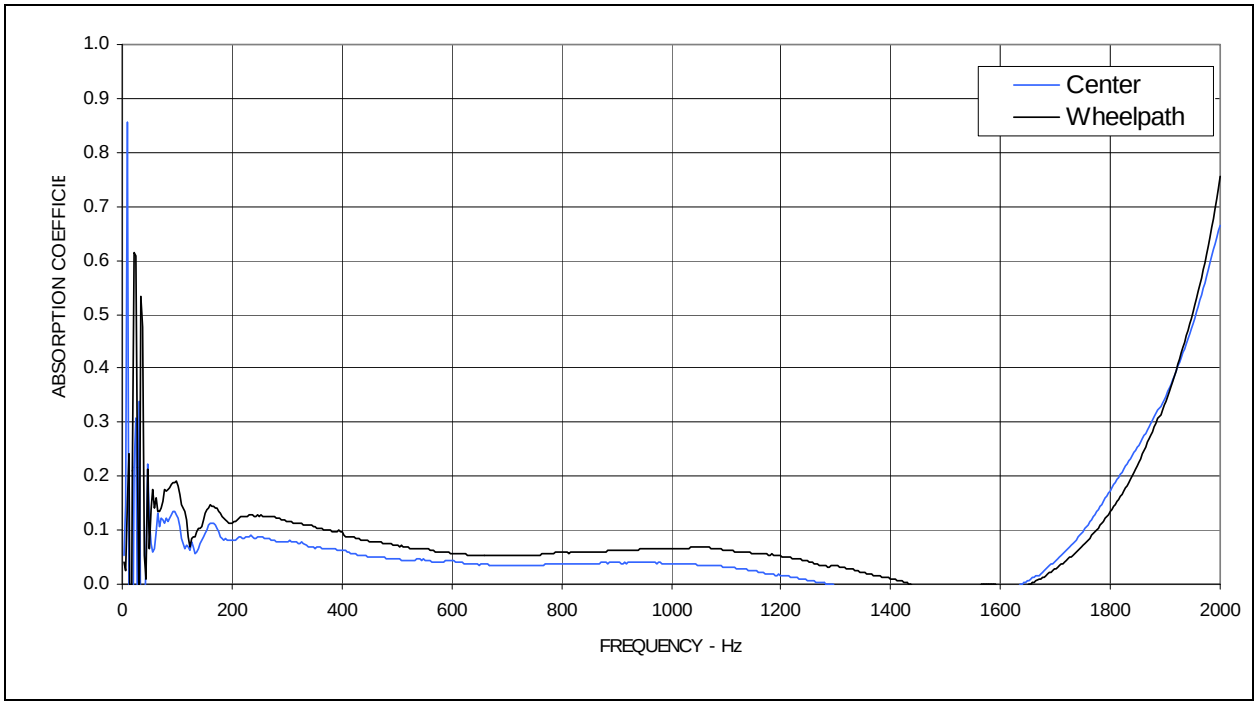

Figure A73: Sound absorption measured on cores from section N121.

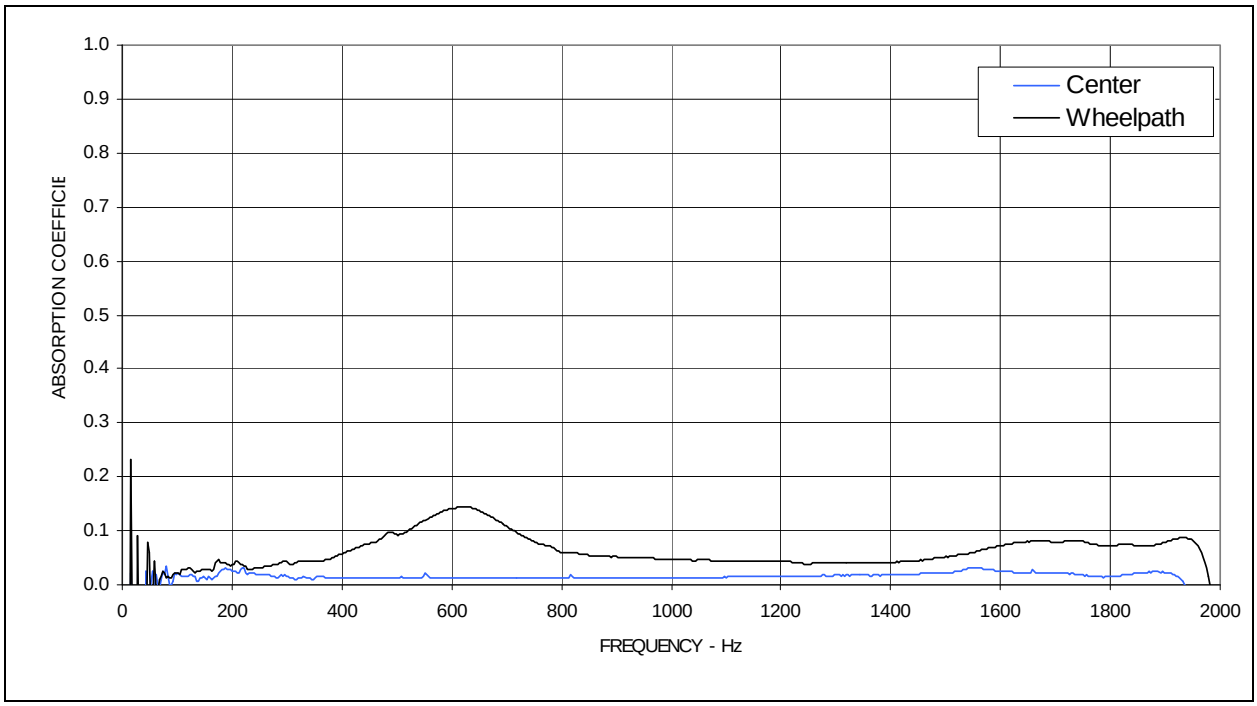

Figure A74: Sound absorption measured on cores from section N434.

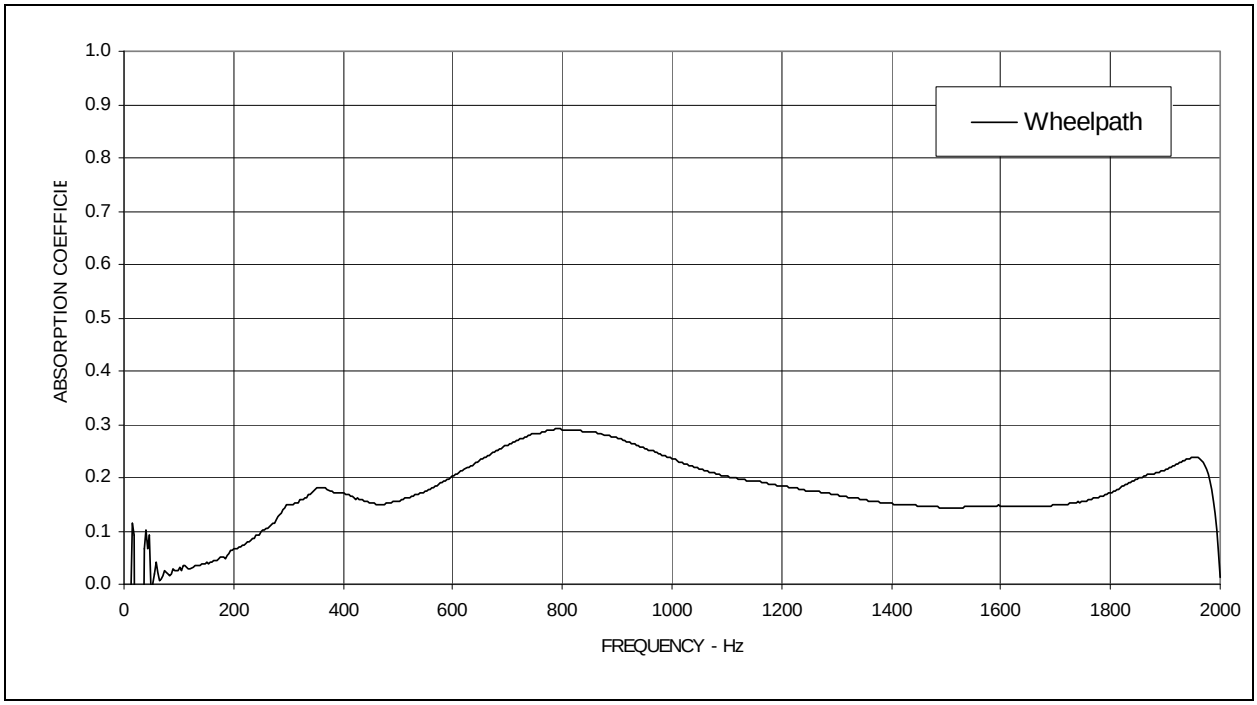

Figure A75: Sound absorption measured on cores from section N467.